DARK MATTER BENCHMARK MODELS FOR EARLY LHC RUN-2 SEARCHES: REPORT OF THE SPRING 2015 ATLAS/CMS DARK MATTER FORUM

Author/contributor list to be added as document is finalized.

Contact editors: lhc-dmf-admin@cern.ch

May 31, 2015

Contents

1

Introduction

Many theories of physics beyond the Standard Model predict the existence of a stable, neutral, weakly-interacting and massive particle that is a putative dark matter candidate. In the following, we refer to such matter as dark matter, even though the observation of such matter at a collider could only establish that it is neutral, weakly-interactive, massive and stable on the distance-scales of 10's of meters. Dark matter has not yet been observed in particle physics experiments, and there is not yet any evidence for non-gravitational interactions between dark matter and Standard Model particles. If such interactions exist, dark matter particles could be produced at the LHC. Since dark matter particles of themselves do not produce signals in the LHC detectors, one way to observe them is when they are produced in association with a visible SM particle $X(=g, q, \gamma, Z, W, \text{or } h)$. Such reactions, which are observed at colliders as particles or jets recoiling against an invisible state, are called "mono-X" or $\not{E}_T$+X reactions [FST06, BHK$^+$10, BFH10]. This type of reaction includes the production of a Higgs boson that decays to pairs of dark matter particles.

To do **CD: why singling out mono-Higgs? (??)**

Early Run-1 searches for $\not{E}_T$+X signatures at ATLAS and CMS employed a basis of contact interaction operators in effective field theories (EFTs) [GIR$^+$11, GIR$^+$10] to calculate the possible signals. These particular EFTs assume that production of dark matter takes place through a contact interaction involving a quark-antiquark pair or two gluons and two dark matter particles. In this case, the missing energy distribution of the signal is determined by the nature and the mass of the dark matter particles and the Lorentz structure of the interaction. Only the overall production rate is a free parameter to be constrained or measured. Both experiments studied a variety of EFTs with different spin structures. Provided that the contact interaction approximation holds, these EFTs can also provide a straightforward way to compare the results from different collider searches with non-collider searches for dark matter. From the time of their proposal however it was clear that, though the contact interactions provide interesting limits, they are not always a good description of dark matter production at the LHC in the regime of interest [GIR$^+$11, SV12].

To do **Check these references here (??)**

The interpretation of Tevatron **??** and Run-1 LHC **??** searches

To do **Add experimental references if not done before (??)**

as constraints on contact interactions provided results that were outside the range of applicability of the EFT description, requiring further study [BFH10, Kop11, FHKT11, FHKT12, SV12, BDSMR14]. Some "simplified models" [AST09, GS11, A$^+$12] of dark matter production were constructed, including particles and interactions beyond the SM. These models can be used consistently at LHC energies, and provide an extension to the EFT approach. Many proposals for such models have emerged (see, for example Refs. [AJW12, AHW13, DNRT13, BDM14, BB13, BB14, AWZ14, A$^+$14a, MMA$^+$14, HKSW15, BFG15, HR15, BT13, CNS$^+$13, BDG$^+$12, PS14, CDM$^+$14]). These model introduce a new particle – a mediator – that allows interactions between SM and DM particles. In the limit of large mediator mass, these simplified models map onto EFT operators. If the mass of the mediator is light, the kinematics of the dark matter production can differ substantially from that due to a contact interaction, modifying limits and possibly requiring new search strategies. Appropriate simplified models can be used both to interpret Dark Matter searches at the LHC, and to guide the design of complementary search signatures.

To do **CD: How are those references chosen? (??)**

1.1   The ATLAS/CMS Dark Matter Forum

To understand what signal models should be used for the upcoming LHC Run 2, groups of experimenters from both ATLAS and CMS collaborations have held separate discussions with small groups of theorists [MMA$^+$14, A$^+$14a]. Another joint discussion was held at the DM@LHC workshop in Oxford, in September 2014 [par]. As discussed at the DM@LHC workshop, ATLAS and CMS organized a forum at the end of 2014, called the *ATLAS-CMS Dark Matter Forum*, to form a consensus on the use of simplified models and EFTs for Run-2 with the participation of experts on theories of dark matter. This is the final report of that forum.

One of the guiding principles of this report is to channel the efforts of the ATLAS and CMS collaborations towards a minimal set of dark matter models that should influence the design of the early Run-2 searches. At the same time, a thorough survey of realistic collider signals of dark matter is a crucial input to the overall design of the search program.

The goal of this report is such a survey, though confined within some broad assumptions and focused on benchmarks for kinematically-distinct signals which are most urgently needed. As far as time and resources have allowed, the assumptions have been carefully motivated by theoretical consensus and comparisons of simulations. But, to achieve a true consensus in only a few months before the start of Run-2, it was important to narrow the scope and timescale to the following:

1. The forum should propose a prioritized, compact set of benchmark simplified models that should be agreed upon by both collaborations for Run-2 searches. The values for the scan on

166 the parameters of the models for which experimental results are
167 provided should be specified, to facilitate theory reinterpretation
168 beyond the necessary model-independent limits that should be
169 provided by all LHC Dark Matter searches.

170 2. The forum should standardize the event generator implemen-
171 tation of the simplified models and harmonize other common
172 technical details as far as practical. It would be desirable to have
173 a common choice of LO/NLO, ME-parton shower matching and
174 merging, factorization and renormalization scales for each of the
175 simplified models. This will also lead to a common set of the-
176 ory uncertainties, which will facilitate the comparison of results
177 between the two collaborations.

178 3. The forum could also discuss how to apply the EFT formalism
179 and present the results of EFT interpretations.

180 4. The forum should prepare a report summarizing these items,
181 suitable both as a reference for the internal ATLAS and CMS
182 audiences and as an explanation of Run-2 benchmarks for theory
183 and non-collider readers. This report represents the views of the
184 participants of the forum.

185 *1.2   Grounding Assumptions*

186 We assume that interactions exist between Standard Model hadrons
187 and whatever the particle that constitutes cosmological dark matter.
188 If this is not the case, then proton collisions will not produce dark
189 matter particles, and dark matter will not scatter off nuclei in direct
190 detection experiments.
191 The Dark Matter itself is assumed to be a single particle, a Dirac
192 fermion WIMP, stable on collider timescales and non-interacting
193 with the detector. The former assumption is reductionistic. The rich
194 particle content of the Standard Model is circumstantial evidence
195 that the dark matter sector, which constitutes five times as much
196 of the mass of the universe, may be more complex than a single
197 particle or a single interaction. But, as was often the case in the
198 discoveries of the SM, here only one mediator and one search chan-
199 nel might play a dominant role in the opening stages of an LHC
200 discovery. The latter assumption focuses our work on early LHC
201 searches, where small kinematic differences between models will
202 not matter in a discovery scenario, and with the imminent re-start
203 of the LHC our report relies heavily on a large body of existing
204 theoretical work which made this assumption. Different types of
205 dark matter particles will typically give similar results. Some ex-
206 ceptions exist: the choice of Dirac fermions forbids some processes
207 that are allowed for Majorana fermions **??**. Aside from this, the
208 cases of Dirac or Majorana fermions or scalars produces only minor
209 changes in the kinematic distributions of the visible particle, espe-
210 cially when considering cut-and-count[1] analysis. Thus the choice of

[1] Cut-and-count refers to an analysis that applies a certain event selection and checks the inclusive number of events which pass. This is to be contrasted with a shape analysis that compares the distribution of events.

Dirac fermion dark matter is deemed sufficient for the benchmarks aiding the design of the upcoming Run-2 searches. Nevertheless, a more complete set of models will certainly be required upon a discovery; see e.g. [CHLR13, HHR14, CHH15] for some studies of observables that may distinguish amongst these models.

Simplified models are considered in depth within this report as a strength of collider experiments lies in the ability to study the mediator, not just the DM. A discovery of an anomalous $\not{E}_T$ signature at the LHC would not uniquely imply discovery of dark matter, while at the same time discovery of an anomalous and annually-modulated signal in a direct-detection experiment would leave unanswered many questions about the nature of the interaction that could be resolved by the simultaneous discovery of a new mediator particle. Collider, direct and indirect detection searches provide complementary ways to approach this problem, and it is in this spirit that our focus is on the mediator. We systematically explore the basic possibilities for mediators of various possible spins and couplings. All models considered are assumed to produce a signature with pairs of dark matter particles. Though more varied and interesting possibilities are added to the literature almost daily, these basic building blocks account for much of the physics studied at hadron colliders in the past three decades.

We also assume that Minimal Flavor Violation (MFV) [CG87, HR90, BGG$^+$01, DGIS02] applies to the models included in this report. This means that the flavor structure of the couplings between dark matter and ordinary particles follows the same structure as the Standard Model. This choice is simple, since no additional theory of flavor is required, beyond what is already present in the SM, and it provides a mechanism to ensure that the models do not violate flavor constraints. As a consequence, spin-0 resonances must have couplings to fermions proportional to the SM Higgs couplings. Flavor-safe models can still be constructed beyond the MFV assumption, for example [ABG14], and deserve further study.

In the parameter scan for the models considered in this report, we make the assumption of a minimal decay width for the particles mediating the interaction between SM and DM. This means that only decays strictly necessary for the self-consistency of the model (e.g. to DM and to quarks) are accounted for in the definition of the mediator width. We forbid any further decays to other invisible particles of the Dark Sector that may increase the width or produce striking, visible signatures. Studies within the Forum show that, for cut-and-count analyses, the kinematic distributions of many models and therefore the sensitivity of the search do not depend significantly on the mediator width, as long as the width remains smaller than the mass of the particle.

The particle content of the models chosen as benchmarks is limited to one single kind of DM whose self-interactions are not relevant for LHC phenomenology, and to one type of SM/DM interaction at a time. These assumptions only add a limited number

260 of new particles to the SM. These simplified models, independently
261 explored by different experimental analyses, can be used as starting
262 points to build more complete theories. Even though this factorized
263 picture does not always lead to full theories and leaves out details
264 that are necessary for the self-consistency of single models (e.g.
265 the mass generation for mediator particles), it is a starting point to
266 prepare a set of distinct but complementary collider searches for
267 Dark Matter, as it leads to benchmarks that are easily comparable
268 across channels.

269 ## 1.3   *Choices of benchmarks considered in this report*

270 Contact interaction operators have been outlined as a complete se-
271 ries of theoretical building blocks representing possible types of
272 interactions between SM and DM particles in [GIR$^+$10]. The ap-
273 proach followed by LHC searches (see e.g. Refs. **??** for the most
274 recent jet+$\not{E}_T$ Run-1 searches with the 8 TeV dataset) so far has been
275 to simulate only a prioritized set of the possible operators with dis-
276 tinct kinematics for the interpretation of the constraints obtained,
277 and provide results to be reinterpreted in terms of the other opera-
278 tors. This report intends to follow this strategy, firstly focusing on
279 simplified models that allow the exploration of scenarios where the
280 mediating scale is not as large. Secondly, this report considers spe-
281 cific EFT benchmarks whenever neither a simplified model comple-
282 tion nor other simplified models yielding similar kinematic distri-
283 butions are available. This is the case for dimension 5 or dimension
284 7 operators with direct Dark Matter-electroweak boson couplings.
285 Considering these models as separate experimental benchmarks
286 will allow to target new signal regions and help validate the contact
287 interaction limit of new simplified models developed to complete
288 these specific operators.

289   In all cases, experimental searches should deliver results that are
290 independent from the specific benchmark tested. Furthermore, it
291 should be possible to map results from simplified models to contact
292 operators, in the high mediator mass limit. Results from EFT bench-
293 marks should include the condition that the momentum transfer
294 does not probe the scale of the interaction; whenever there is no
295 model that allows a direct mapping between these two quantities,
296 various options should be tested to ensure a given fraction of events
297 within the range of applicability of the EFT approach.

298 ## 1.4   *Structure of this report*

299 Chapter 2 of the report is dedicated to simplified models with ra-
300 diation of a hard object either from the initial state or from the
301 mediator. These models produce primarily monojet signatures,
302 but should be considered for all $\not{E}_T$+X searches. Details of the im-
303 plementation of these models in Monte Carlo generators are pro-
304 vided in Appendix A. Chapter 3 contains the benchmark model

recommendations and choices for final states specifically containing
an electroweak boson ($W/Z/\gamma/H$). In this case, both simplified
models leading to mono-boson signatures and contact interaction
operators are considered. Chapter 4 is devoted to the treatment of
the presentation of results for the benchmark models from contact
interaction operators. Chapter 5 prescribes how to estimate theo-
retical uncertainties on the simulation of these models. Chapter **??**
concludes the report. Appendix C contains the necessary elements
that should be included in the results of experimental searches to
allow for further reinterpretation. The technical implementation
and further models that can be studied beyond early searches are
described in Appendix B. For these models, either the implementa-
tion could not be fully developed by the time of this report, or some
of the grounding assumptions were not fully met. Some of these
models have been used in previous ATLAS and CMS analyses and
discussed thoroughly within the Forum. They are therefore worth
considering for further studies and for Run-2 searches, since they
lead to unique $\not{E}_T$+X signatures that are not produced by any other
of the models included in this report.

2

Recommended models for all $\not{E}_T$ +X analyses

In this Chapter we review models that yield $X+\not{E}_T$ signatures, where X is a QCD parton or γ, W, Z or h.

The three main benchmark simplified models suggested in this Chapter for early Run-2 searches

The primary simplified models suggested in this Chapter for Dirac fermion DM comprise spin-0 and spin-1 mediators. Section 2.1 covers the s-channel exchange of a vector mediator [1], while we consider both s-channel and t-channel exchange for scalar mediators in Section 2.2 and 2.3 respectively. Spin-2 mediators are briefly mentioned in Section 2.4. While these models are general and cover a broad set of signatures, the discussion and studies are focused on the monojet final state. Details on final states with EW boson radiation and with heavy flavor quarks from diagrams arising within these models are also discussed in this Chapter.

The simplified model where a vector mediator is exchanged in the s-channel is known to NLO accuracy in the case of DM pair production in association to one parton **??**. All other models are currently known to leading order. Appendix A details the recommended implementation of these models that have been used for the studies in this Chapter. A summary of the recommendation of the generation of this model is provided in Table **??**.

[1] Colored vector mediators can be exchanged in the t-channel, but there are no examples in literature so far.

2.1 Vector and axial vector mediator, s-channel exchange

A simple extension of the Standard Model (SM) is an additional $U(1)$ gauge symmetry, where a dark matter (DM) candidate particle has charges only under this new group. Assuming that some SM particles are also charged under this group, a new gauge boson can mediate interactions between the SM and DM.

We consider the case of a DM particle χ of mass m_{DM} that is a Dirac fermion and where the production proceeds via the exchange of a spin-1 mediator of mass M_{med} in the s-channel, illustrated in Fig. 2.1.

We consider two models with vector and axial-vector couplings between the spin-1 mediator Z' and SM and DM fields, with the corresponding interaction Lagrangians:
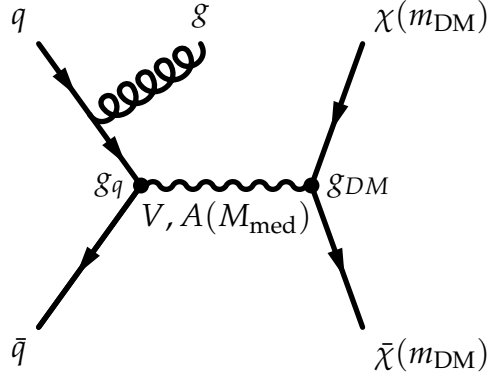
Figure 2.1: Representative Feynman diagram showing the pair production of dark matter particles in association with a parton from the initial state via a vector or axial-vector mediator. The cross section and kinematics depend upon the mediator and dark matter masses, and the mediator couplings to dark matter and quarks respectively: $(M_{\text{med}}, m_{\text{DM}}, g_{\text{DM}}, g_{\text{q}})$.

$$\mathcal{L}_{\text{vector}} = g_{\text{q}} \sum_{q=u,d,s,c,b,t} Z'_\mu \bar{q} \gamma^\mu q + g_{\text{DM}} Z'_\mu \bar{\chi} \gamma^\mu \chi \tag{2.1}$$

$$\mathcal{L}_{\text{axial-vector}} = g_{\text{q}} \sum_{q=u,d,s,c,b,t} Z'_\mu \bar{q} \gamma^\mu \gamma^5 q + g_{\text{DM}} Z'_\mu \bar{\chi} \gamma^\mu \gamma^5 \chi. \tag{2.2}$$

The coupling g_{q} is assumed to be universal to all quarks. As mentioned in the Introduction, when no additional visible or invisible decays contribute to the width of the mediator, the minimal width is fixed by the choices of couplings g_{q} and g_{DM}. The effect of larger widths is discussed on page 41. For the vector and axial-vector models, the minimal width is:

$$\Gamma^V_{\text{min}} = \frac{g^2_{\text{DM}} M_{\text{med}}}{12\pi} \left(1 + \frac{2m^2_{\text{DM}}}{M^2_{\text{med}}} \right) \beta_{DM} \theta(M_{\text{med}} - 2m_{\text{DM}}) \tag{2.3}$$

$$+ \sum_q \frac{3g^2_{\text{q}} M_{\text{med}}}{12\pi} \left(1 + \frac{2m^2_q}{M^2_{\text{med}}} \right) \beta_q \theta(M_{\text{med}} - 2m_q),$$

$$\Gamma^A_{\text{min}} = \frac{g^2_{\text{DM}} M_{\text{med}}}{12\pi} \beta^{3/2}_{DM} \theta(M_{\text{med}} - 2m_{\text{DM}}) \tag{2.4}$$

$$+ \sum_q \frac{3g^2_{\text{q}} M_{\text{med}}}{12\pi} \beta^{3/2}_q \theta(M_{\text{med}} - 2m_q) .$$

$\theta(x)$ denotes the Heaviside step function, and $\beta_f = \sqrt{1 - \frac{4m^2_f}{M^2_{\text{med}}}}$ is the velocity of the fermion f with mass m_f in the mediator rest frame. Note the color factor 3 in the quark terms. Figure 2.2 shows the minimal width as a function of mediator mass for both vector and axial-vector mediators assuming $g_{\text{q}} = g_{\text{DM}} = 1$. With this choice of the couplings, the dominant contribution to the minimal width comes from the quarks, due to the combined quark number and color factor enhancement. We specifically assume that the vector mediator does not couple to leptons. If such a coupling were present, it would have a minor effect in increasing the mediator width, but it would also bring in constraints from measurements of the Drell-Yan process that would unnecessarily restrict the model space.

Therefore, the minimal set of parameters under consideration for these two models is

$$\{ m_{\text{DM}}, M_{\text{med}}, g_{\text{q}}, g_{\text{DM}} \} . \tag{2.5}$$
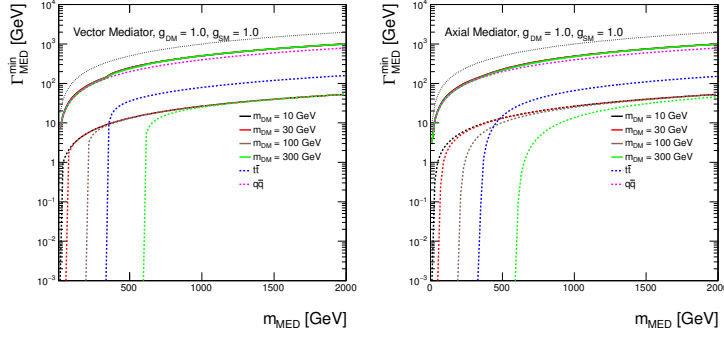
Figure 2.2: Minimal width as a function of mediator mass for vector and axial-vector mediator assuming couplings of 1. The total width is shown as solid lines for Dark Matter masses of 10 GeV, 30 GeV, 100 GeV and 300 GeV in black, red, brown and green, respectively. The individual contributions from Dark Matter are indicated by dotted lines with the same colors. The contribution from all quarks but top is shown as magenta dotted line and the contribution from top quarks only is illustrated by the dotted blue line. The dotted black line shows the extreme case $\Gamma_{\min} = M_{\mathrm{med}}$.

See [BDMM15] for a thorough discussion of these models.

2.1.1 Spin structure of the couplings

In this section, the differences between the vector and axial-vector models are described. Furthermore, it is possible to consider other models in which mixed vector and axial-vector couplings are considered, for instance the couplings to the quarks are axial-vector whereas those to DM are vector. Such comparisons are also presented.

The samples with pure vector and pure axial-vector couplings are compared for $M_{\mathrm{med}} = 100$ GeV and different Dark Matter masses in Fig. 2.3. No differences in the shape of the $\not{E}_T$ distributions are observed between the samples with coincident masses. In the case of the on-shell Dark Matter pair production where $2m_{\mathrm{DM}} \ll M_{\mathrm{med}}$, the cross sections of the pure vector and pure axial-vector models are similar. With increasing Dark Matter mass towards the $2m_{\mathrm{DM}} = M_{\mathrm{med}}$ transition and beyond into the off-shell production regime, the relative difference between the cross sections of the two samples is increasing, with the vector samples having larger cross sections.

To do **Do we want to propose to generate one model only and refer to the cross section tables in HEPData repository for the other? (??)**
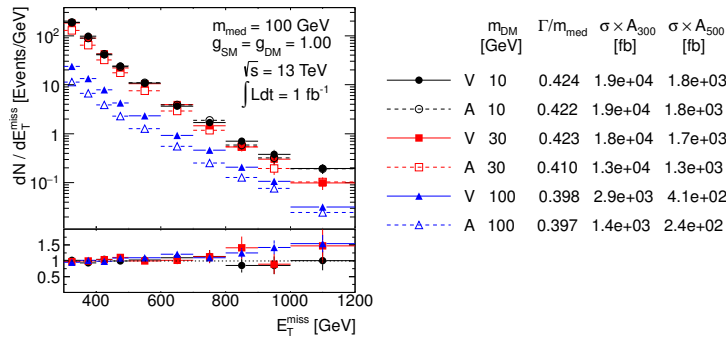
To do **This can be understood in the eikonal approximation since the A terms have an additional v^2 in front. (??)**

Figure 2.3: Comparison of the pure vector and pure axial-vector couplings. The $\not{E}_T$ distribution is shown for the samples generated with $M_{\mathrm{med}} = 100$ GeV and different Dark Matter masses. Ratios of the normalized distributions are shown for between the samples with coincident masses. A_{300} and A_{500} in the table denote the acceptance of the $\not{E}_T > 300$ GeV and $\not{E}_T > 500$ GeV cut, respectively.

Figure 2.4 shows the samples generated with pure and mixed couplings for $m_{\mathrm{DM}} = 100$ GeV and $M_{\mathrm{med}} = 1$ TeV, i.e. where the Dark Matter pair is produced on-shell. The mediator width between the pure vector and pure axial-vector couplings differ only by 2% in this case, and $< 10\%$ agreement between the cross sections is found. The mediator widths for the samples with the same

type coupling to quarks agree at better than 1% since the width is
dominated by the quark contribution, as expected from Eq. 2.3. No
significant differences between the samples with same type Dark
Matter coupling are seen, given the statistical precision of the gen-
erated samples. This is expected since the mediator is produced
on-shell, and the details of the invisible decay are unimportant in
cut-and-count searches.

For the off-shell Dark Matter pair production, shown in Fig. 2.5
for $m_{DM} = 100$ GeV and $M_{med} = 100$ GeV, there is approximately
a factor 2 difference between the cross-sections of the samples with
pure couplings is observed. As in the previous case, the samples
with the same type coupling to Dark Matter are similar both in
terms of cross sections and $\not{E}_T$ shape. Since the contribution to the
mediator width from Dark Matter is closed in this case, only the
quark couplings define the width. Only couplings to light quarks
are opened in the case of $M_{med} = 100$ GeV for which the differ-
ences between the partial widths of vector and axial-vector cou-
plings are marginal. This explains the similar minimal widths for
all four samples stated in Fig. 2.5.

In general, the coupling to quarks is not expected to play an im-
portant role as it is only needed to produce the mediator which
is confirmed by the observations above. On the contrary, the cou-
pling to Dark Matter determines the form of the matrix element
which explains the similarity of the samples with the same type
Dark Matter couplings. Based on these arguments, we recommend
to consider only the models with pure vector couplings or pure
axial-vector couplings.
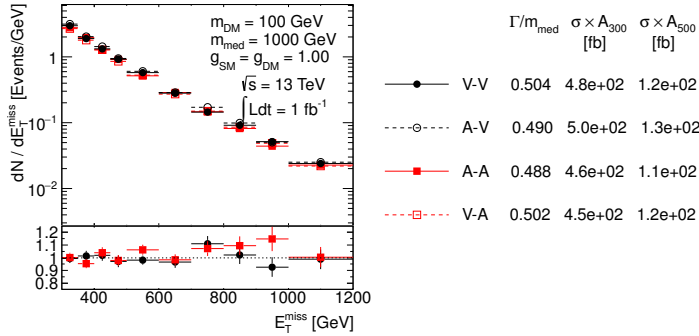
Figure 2.4: Comparison of the pure
vector, V-V, and pure axial-vector, A-A,
couplings with mixed couplings, A-V
and V-A where the first (second) letter
indicates the Standard Model (Dark
Sector) vertex. The $\not{E}_T$ distribution is
shown for the samples generated with
$m_{DM} = 100$ GeV and $M_{med} = 1$ TeV.
Ratios of the normalized distributions
are shown for A-V over V-V and for
V-A over A-A. A_{300} and A_{500} in the
table denote the acceptance of the
$\not{E}_T > 300$ GeV and $\not{E}_T > 500$ GeV cut,
respectively.
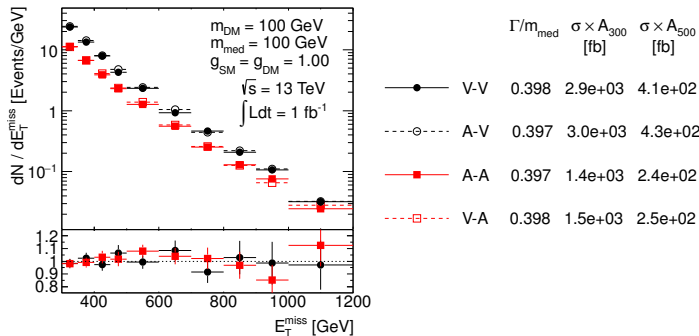
Figure 2.5: Comparison of the pure
vector, V-V, and pure axial-vector, A-A,
couplings with mixed couplings, A-V
and V-A where the first (second) letter
indicates the Standard Model (Dark
Sector) vertex. The $\not{E}_T$ distribution
is shown for the samples generated
with $m_{DM} = 100$ GeV and $M_{med} =$
100 GeV. Ratios of the normalized
distributions are shown for A-V
over V-V and for V-A over A-A. A_{300}
and A_{500} in the table denote the
acceptance of the $\not{E}_T > 300$ GeV and
$\not{E}_T > 500$ GeV cut, respectively.

2.1.2   *Parameter scan*

In order to determine an optimal choice of the parameter grid for the simulation of early Run-2 benchmark models, dependencies of the kinematic quantities and cross sections on the model parameters have been studied. The following paragraphs list the main observations from the scans over the parameters that support the final proposal for the benchmark signal grid.

Scan over the couplings   To study the dependence of kinematic distributions on the coupling strength, samples were generated where a pair of $m_{\mathrm{DM}} = 10$ GeV Dark Matter particles is produced on-shell from the mediator of $M_{\mathrm{med}} = 1$ TeV. Figure 2.6 compares the shapes of the $\not{E}_T$ distribution for the different choices of the coupling strength. This is a generator-level prediction with no kinematic selections or detector simulation. Coupling values in the scan range 0.1–1.45, fixing $g_{\mathrm{q}} = g_{\mathrm{DM}}$, correspond to a rough estimate of the lower sensitivity of mono-jet analyses and a maximum coupling value such that $\Gamma_{\mathrm{min}} < M_{\mathrm{med}}$. We observe that the shapes of the $\not{E}_T$ or jet p_T distributions do not depend on the couplings (and consequently the width) in the ranges considered. A large width of the mediator implies a broad integral over the contributing parton distributions, which might not be well approximated by the midpoint of this integral. This study shows that the effect, in the p_T distribution of the observed gluon, is not important.

Based on similar findings for different choices of M_{med} and m_{DM}, we conclude that the shapes of kinematic distributions are not altered by coupling variations, neither for the on-shell Dark Matter production where $M_{\mathrm{med}} > 2m_{\mathrm{DM}}$, nor for the off-shell Dark Matter production where $M_{\mathrm{med}} < 2m_{\mathrm{DM}}$. Only the production cross sections change. Differences in kinematic distributions are expected only close to the transition region where both on-shell and off-shell decays occur.

Figure 2.6: Scan over couplings. The $\not{E}_T$ distribution is compared for the vector mediator models using the parameters as indicated. Ratios of the normalized distributions with respect to the first one are shown. A_{300} and A_{500} in the table denote the acceptance of the $\not{E}_T > 300$ GeV and $\not{E}_T > 500$ GeV cut, respectively.

When small coupling strengths are combined with extremely heavy mediators, one must take particular care to integrate over all values of the dark matter pair invariant mass, down to the lowest values for which the $\not{E}_T$ satisfies threshold requirements. See the Appendix A.1.1 page 80 for details.

To do **Now these figures seem out of place. The point of the first plot seems to be that the EFT limit is only recovered for** $g = 1$. **(??)**
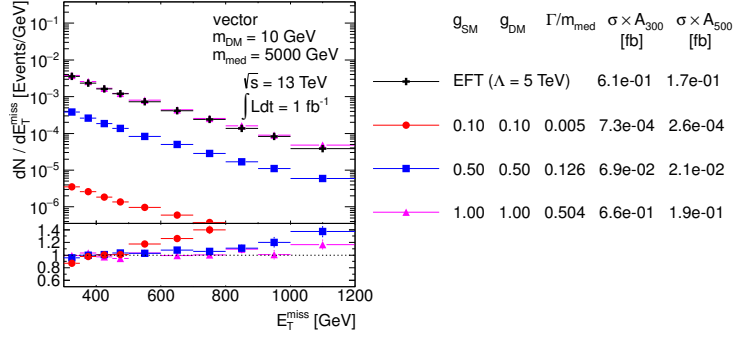
Figure 2.7: Comparison of the $\not{E}_T$ distributions from the D5 EFT sample and the vector models with 5 TeV heavy mediator of various widths. Ratios of the normalized distributions with respect to the first one are shown. A_{300} and A_{500} in the table denote the acceptance of the $\not{E}_T > 300$ GeV and $\not{E}_T > 500$ GeV cut, respectively.
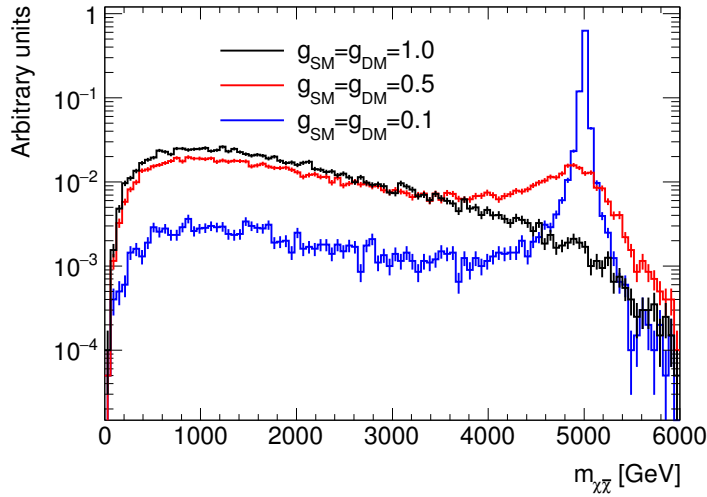
Figure 2.8: Invariant mass of the Dark Matter pair in the vector mediator samples with $m_{DM} = 10$ GeV, $M_{med} = 5$ TeV and different coupling strengths. The distributions are normalised to unit area.

469 Since kinematic distributions are robust to changes in the specific
470 values of coupling as long as heavy narrow mediators are avoided,
471 the choice of $g_q = g_{DM}$ is reasonable to reduce the parameter space
472 to be scanned. There are no complications associated with small
473 couplings, but, also, the early part of Run 2 will not be sensitive to
474 them. The range of couplings we recommend limit the calculated
475 width of the mediator to be near or below M_{med}.

476 For direct mediator searches, such as $q\bar{q} \to Z' \to q\bar{q}$, asymmetric
477 couplings ($g_q \neq g_{DM}$) might also be considered. A scan in g_{DM} vs
478 g_q can then be performed for a fixed mediator mass. Such searches
479 may restrict g_q to a greater degree than g_{DM}.

480 *Scan over m_{DM}* For a fixed mediator mass M_{med} and couplings, the
481 Dark Matter mass falls into three regimes:

482 On-shell When $M_{med} \gg 2m_{DM}$, most mediators are produced on-
483   shell. The hardness of the ISR is set by M_{med}, and the kinematic
484   distributions do not strongly depend on m_{DM}. This is illustrated
485   in Fig. 2.9 for an example of M_{med} =1 TeV 10 GeV $< m_{DM} <$
486   300 GeV. The cross section decreases as the m_{DM} approaches
487   $M_{med}/2$. A coarse binning along m_{DM} is sufficient.

488 Threshold When $M_{med} \approx 2m_{DM}$, the production is resonantly
489   enhanced, and both the cross section and kinematic distributions
490   change more rapidly as a function of the two masses, and finer
491   binning is needed in order to capture the changes.

492 Off-shell When $M_{med} ll 2m_{DM}$, the Dark Matter pair is produced
493   off-shell. The mediator propagator gives an explicit suppression
494   of $(M_{med}/Q)^4$ that suppresses hard ISR. The $m_{DM} = 1$ TeV
495   case, shown in Fig. 2.9, and Figure 2.10 demonstrates that the
496   $\not{E}_T$ spectrum hardens with increasing m_{DM}, accompanied by
497   the gradual decrease of the cross section. Due to the significant
498   cross section suppression, it is not necessary to fully populate the
499   parameter space. Imminent LHC searches are not expected to be
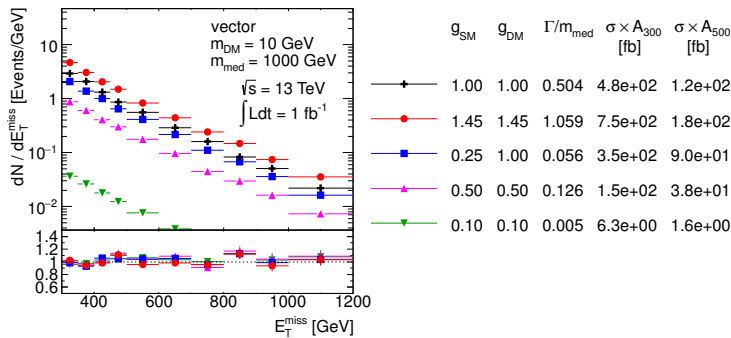500   sensitive to these signals.
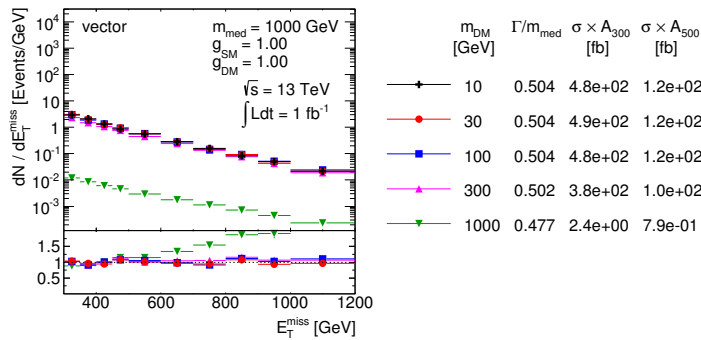
Figure 2.9: Scan over Dark Matter mass. The $\not{E}_T$ distribution is compared for the vector mediator models using the parameters as indicated. Ratios of the normalized distributions with respect to the first one are shown. A_{300} and A_{500} in the table denote the acceptance of the $\not{E}_T > 300$ GeV and $\not{E}_T > 500$ GeV cut, respectively.

501 *Scan over the mediator mass* Changing the mediator mass for fixed
502 Dark Matter mass and couplings leads to significant differences
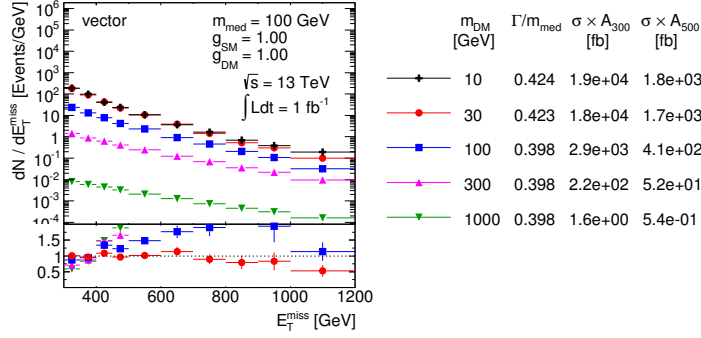
Figure 2.10: Scan over Dark Matter mass. The $\not{E}_T$ distribution is compared for the vector mediator models using the parameters as indicated. Ratios of the normalized distributions with respect to the first one are shown. A_{300} and A_{500} in the table denote the acceptance of the $\not{E}_T > 300$ GeV and $\not{E}_T > 500$ GeV cut, respectively.

in cross section and shapes of the kinematic variables for on-shell production, as shown in Fig. 2.11. As expected, higher mediator masses lead to harder $\not{E}_T$ spectra. On the other hand, the $\not{E}_T$ shapes are similar in the off-shell Dark Matter production regime. This is illustrated in Fig. 2.12. Therefore, a coarse binning in M_{med} is sufficient in the off-shell regime.
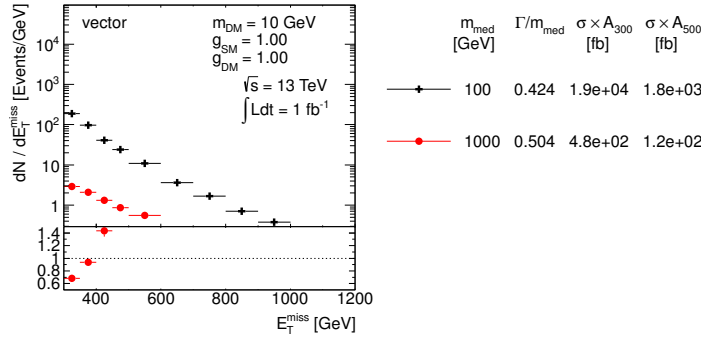
Figure 2.11: Scan over mediator mass. The $\not{E}_T$ distribution is compared for the vector mediator models using the parameters as indicated. Ratios of the normalized distributions with respect to the first one are shown. A_{300} and A_{500} in the table denote the acceptance of the $\not{E}_T > 300$ GeV and $\not{E}_T > 500$ GeV cut, respectively.
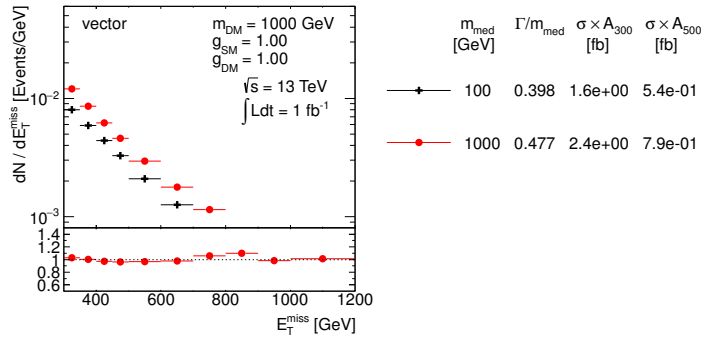
Figure 2.12: Scan over mediator mass. The $\not{E}_T$ distribution is compared for the vector mediator models using the parameters as indicated. Ratios of the normalized distributions with respect to the first one are shown. A_{300} and A_{500} in the table denote the acceptance of the $\not{E}_T > 300$ GeV and $\not{E}_T > 500$ GeV cut, respectively.

Proposed parameter grid   The final step in proposing a parameter grid is to evaluate the sensitivity of Run-2 LHC data with respect to rate and/or kinematics. The parameter scan focuses on two important regions, the light mediator region and the heavy mediator limit to reproduce the EFT limit, and takes into account the projected sensitivities for the mono-jet analysis.

Projected sensitivities for a 14 TeV mono-jet analysis are available from ATLAS [ATL14]. The expected upper limit at 95% con-

fidence level on the product of cross section, acceptance and efficiency, $\sigma \times A \times \epsilon$, in the final Run-1 ATLAS mono-jet analysis [A$^+$15b] is 51 fb and 7.2 fb for $\not{E}_T > 300$ GeV and $\not{E}_T > 500$ GeV, respectively. ATLAS estimates a factor of two increase in sensitivity with the 2015 data. Given that cross section for V+jets processes increases by roughly a factor 2 when going from $\sqrt{s} = 8$ TeV to 13 TeV, similar fiducial cross section limits can be expected with the first Run-2 data as from the final Run-1 analysis. The generator level cross section times the acceptance at $\not{E}_T > 500$ GeV for the model with couplings $g_q = g_{DM} = 1$, a light Dark Matter particle of $m_{DM} = 10$ GeV and a $M_{med} = 1$ TeV vector mediator is at the order of 100 fb, i.e. the early Run-2 mono-jet analysis is going to be sensitive to heavier mediators than this. The value of $\sigma \times A$ at $\not{E}_T > 500$ GeV for 5 TeV vector mediator is at the order of 0.1 fb, therefore this model probably lies beyond the reach of the LHC in the early Run 2 but is still useful to reproduce the EFT result.

Following these arguments, M_{med} grid points are chosen, roughly equidistant in a logarithmic scale: 10 GeV, 20 GeV, 50 GeV, 100 GeV, 200 GeV, 300 GeV, 500 GeV, 1000 GeV and 2000 GeV. In the threshold regime $M_{med} = 2m_{DM}$, the m_{DM} grid points are taken at approximately $M_{med}/2$, namely: 10 GeV, 50 GeV, 150 GeV, 500 GeV and 1000 GeV. Points on the on-shell diagonal are always chosen to be 5 GeV away from the threshold, to avoid numerical instabilities in the event generation. The detailed studies of the impact of the parameter changes on the cross section and kinematic distributions presented earlier in this section support removing some of the grid points and relying on interpolation. The optimized grids proposed for the vector and axial-vector mediators are given in Table. 2.1, containing 36 mass points each. One point at very high mediator mass (5 TeV) is added for each of the DM masses scanned, to aid the reinterpretation of results in terms of contact interaction operators (EFTs) as discussed in Section 4.4.

m_{DM}/ GeV	M_{med}/ GeV									
1	10	20	50	100	200	300	500	1000	2000	5000
10	10	15	50	100						5000
50	10		50	95	200	300				5000
150	10				200	295	500	1000		5000
500	10						500	995	2000	5000
1000	10							1000	1995	5000

Table 2.1: Simplified model benchmarks for s-channel simplified models (spin-1 mediators decaying to Dirac DM fermions in the V and A case, taking the minimum width for $g_q = g_{DM} = 1$)

The presentation of the results in the g_q–g_{DM} plane for fixed masses benefits from cross section scaling and is discussed in Section 2.5.

2.1.3 Additional considerations for V+$\not{E}_T$ signatures

All models detailed in this Section are applicable to signatures where a photon, a W boson, a Z boson or a Higgs boson is radiated from the initial state partons instead of a gluon. The experimental

signature is identified as $V+\not{E}_T$ and it has been studied in Refs. [].

Monojet searches are generally more sensitive with respect to final states including bosons, due to the much larger rates of signal events featuring quark or gluon radiation with respect to radiation of bosons [ZBW13], in combination with the low branching ratios if leptons from boson decays are required in the final state. The rates for the Higgs boson radiation is too low for these models to be considered a viable benchmark [CDM+14]. However, the presence of photons, leptons from W and Z decays, and W or Z bosons decaying hadronically allow backgrounds to be rejected more effectively, making $Z/gamma/W+\not{E}_T$ searches still worth comparing with searches in the jet+$\not{E}_T$ final state.

In the case of a spin-1 mediator, an example Feynman diagram for these processes can be constructed by taking Fig. 2.1 and replacing the gluon with γ, W or Z.

When the initial state radiation is a $W^\pm$ boson, Run 1 searches have considered three benchmark cases adapted from the vector interaction in Ref. [BT13], distinguished by ξ, the strength of the d quark coupling relative the u quark coupling:

$\xi = 0$: Mediator couples to up-type or down-type quarks, but not both;

$\xi = 1$: Mediator couples to up-type and down-type quarks with same strength;

$\xi = -1$: Mediator couples to up-type and down-type quarks with same strength, but opposite sign.

Contemplation of $\xi = -1$ heightened interest in searches for spin-1 mediators with $W^\pm$ bosons in the final state. This choice enhances the cross-section significantly above the other choices and hardens the distribution of missing transverse energy used in the searches. The sensitivity of the $W + \not{E}_T$ search then surpasses that of the jet+$\not{E}_T$ search. However, the situation $\xi = -1$ does not appear in an SU(2)-gauge-invariant simplified model.[2] The simplified model with a vector mediator exchanged in the s-channel model is still viable when $\xi = 1$. Ref. [BCD+15] discusses the viability of departures $\xi < 1$ from both gauge-invariance and experimental points of view. An example of a model that arranges different effective DM couplings to u_L and d_L is detailed in Appendix B.

As in the case of the jet+$\not{E}_T$ models, the width does not have a significant impact on the kinematic distributions relevant for those searches. An example of the particle-level analysis acceptance using the generator-level cuts from Ref. [A+15a] for the photon+$\not{E}_T$ analysis, but raising the photon p_T cut to 150 GeV, is shown in Figure 2.2, comparing a width that is set to $\Gamma = M_{med}/3$ to the minimal width (the ratio between the two widths ranges from 1.05 to 1.5 with increasing mediator masses).

Examples of relevant kinematic distributions for selected benchmark points are shown in Fig. 2.13. Leading-order cross-sections for the chosen benchmark points are shown in Appendix B.

---

[2] It is well-known that the diagrams in which the W couples to u and $\bar{d}$ have opposite sign. This is what gives rise to the "helciity zero" in $u\bar{d} \to Wg$. The relative sign is set by SU(2) and the statement that the mediator is an SU(2) singlet. We can increase the cross section by changing the sign, but to do so we have to give the mediator some SU(2) quantum number, making it, and the associated χ, visible.

Acceptance ratio for $\Gamma = \Gamma_{\min}$ vs $\Gamma = M_{\mathrm{med}}/3$				
	m_{DM}/GeV			
M_{med}/GeV	10	50	200	400
50	0.96	0.99		0.95
100	0.97			
300	1.00	1.02		
600			0.96	
1000	1.01	1.02	1.03	
3000	1.02	1.03		1.01

Table 2.2: Analysis acceptance ratios for the photon+$\not{E}_T$ analysis when varying the mediator width, in the case of a vector mediator exchanged in the s-channel
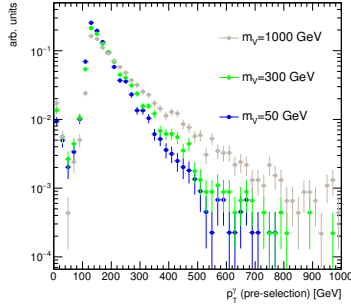
Figure 2.13: Kinematic distributions relevant for searches with W, Z and photons in the final state, for the simplified model with a vector mediator exchanged in the s-channel.

(a) Missing transverse momentum distribution for the photon+$\not{E}_T$ final state, for different mediator mass choices, for $m_{\mathrm{DM}} =$10 GeV.
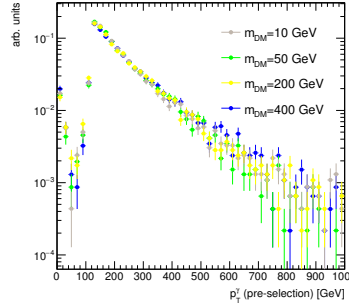
(b) Leading photon transverse momentum distribution for the photon+$\not{E}_T$ final state, for different DM mass choices, with $M_{\mathrm{med}} =$1 TeV.
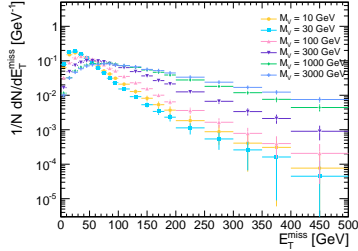
(c) Missing transverse momentum distribution for the leptonic Z+$\not{E}_T$ final state, for different mediator mass choices, for $m_{\mathrm{DM}} =$15 GeV
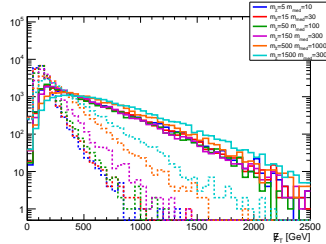
(d) Missing transverse momentum distribution for the hadronic W+$\not{E}_T$ final state.

2.2 Scalar and pseudoscalar mediator, s-channel exchange

In this section, we consider a parallel situation to the vector and axial-vector mediators in the previous sections: a real scalar or a pseudoscalar where the associated scalar is decoupled at higher energies[3]. This section is largely based on Refs. [BFG15, HKSW15] which contain a thorough discussion of these models.

Assuming MFV, spin-0 resonances behave in a similar fashion as the SM Higgs boson. Relative to the vector and axial-vector models discussed above, the scalar models are distinguished by the special consequences of the MFV assumption: the very narrow width of the mediator and its extreme sensitivity to which decays are kinematically available, and the loop-induced coupling to gluons. The interaction Lagrangians are

[3] This assumption does not hold in a UV-complete model where the two components of the complex scalar mediator would be approximately degenerate. The complex scalar case could be studied separately in the case of heavy flavor final states given the sufficiently different kinematics.
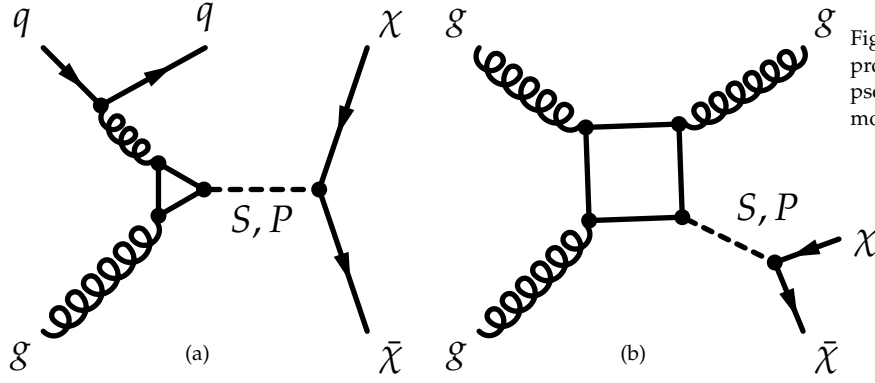
Figure 2.14: One-loop diagrams of processes exchanging a scalar (S) or pseudoscalar (P) mediator, leading to a mono-jet signature.

$$\mathcal{L}_\phi = g_{\text{DM}}\phi\bar{\chi}\chi + \frac{\phi}{\sqrt{2}}\sum_i\left(g_u y_i^u \bar{u}_i u_i + g_d y_i^d \bar{d}_i d_i + g_\ell y_i^\ell \bar{\ell}_i \ell_i\right), \tag{2.6}$$

$$\mathcal{L}_a = ig_{\text{DM}}a\bar{\chi}\gamma_5\chi + \frac{ia}{\sqrt{2}}\sum_i\left(g_u y_i^u \bar{u}_i\gamma_5 u_i + g_d y_i^d \bar{d}_i\gamma_5 d_i +\right.$$

$$\left. g_\ell y_i^\ell \bar{\ell}_i\gamma_5\ell_i\right). \tag{2.7}$$

where ϕ and a are respectively the scalar and pseudoscalar mediators, and the Yukawa couplings y_i^f are normalized to the Higgs vev as $y_i^f = \sqrt{2}m_i^f/v$.

The couplings to fermions are proportional to the SM Higgs couplings, yet one is still allowed to adjust an overall strength of the coupling to charged leptons and the relative couplings of u- and d-type quarks. As in the preceding sections, for the sake of simplicity and straightforward comparison, we reduce the couplings to the SM fermions to a single universal parameter $g_q \equiv g_u = g_d = g_\ell$. Unlike the vector and axial-vector models, the scalar mediators are allowed to couple to leptons.[4]

The relative discovery and exclusion power of each search can be compared in this framework. However, we again emphasize the importance of searching the full set of allowed channels in case violations of these simplifying assumptions lead to significant modifications of the decay rates that unexpectedly favor different channels than the mix obtained under our assumptions. The coupling g_{DM} parameterizes the entire dependence on the structure between the mediator and the dark sector.

Given these simplifications, the minimal set of parameters under consideration is

$$\left\{m_{\text{DM}},\ m_{\phi/a} = M_{\text{med}},\ g_{\text{DM}},\ g_q\right\}. \tag{2.8}$$

Fig. 2.14 shows the one-loop diagrams producing a jet+X signature. The full calculation of the top loop is available at LO for DM pair production in association with one parton.

The minimal mediator width is given by

[4] This contribution plays no role for most of the parameter space considered. The choice to allow lepton couplings follows Refs. [BFG15, HKSW15].

$$\Gamma_{\phi,a} = \sum_f N_c \frac{y_f^2 g_q^2 m_{\phi,a}}{16\pi} \left(1 - \frac{4m_f^2}{m_{\phi,a}^2}\right)^{x/2} + \frac{g_{DM}^2 m_{\phi,a}}{8\pi} \left(1 - \frac{4m_{DM}^2}{m_{\phi,a}^2}\right)^{x/2}$$
$$+ \frac{\alpha_s^2 y_t^2 g_q^2 m_{\phi,a}^3}{32\pi^3 v^2} \left| f_{\phi,a} \left(\frac{4m_t^2}{m_{\phi,a}^2}\right)\right|^2 \tag{2.9}$$

where $x = 3$ for scalars and $x = 1$ for pseudoscalars. The loop
integrals are

$$f_\phi(\tau) = \tau \left[1 + (1 - \tau)\arctan^2\left(\frac{1}{\sqrt{\tau - 1}}\right)\right], \tag{2.10}$$

$$f_a(\tau) = \tau \arctan^2\left(\frac{1}{\sqrt{\tau - 1}}\right) \tag{2.11}$$

for $\tau < 1$, where $\tau = 4m_t^2/m_{\phi,a}^2$, and, for $\tau > 1$,

$$f_\phi(\tau) = \tau \left[1 + (1 - \tau)\left(-\frac{1}{4}\left(\log\frac{1 + \sqrt{1 - \tau}}{1 - \sqrt{1 - \tau}} + i\pi\right)^2\right)\right], \tag{2.12}$$

$$f_a(\tau) = \tau \left(-\frac{1}{4}\left(\log\frac{1 + \sqrt{1 - \tau}}{1 - \sqrt{1 - \tau}} + i\pi\right)^2\right). \tag{2.13}$$

The minimal widths for scalar and pseudo-scalar mediators with
$g_q = g_{DM} = 1$ are shown in Fig. 2.15, illustrating the effect of
choosing the SM Higgs-like Yukawa couplings for the SM fermions.
For the mediator mass above twice the top quark mass m_t, the
minimal width receives the dominant contribution from the top
quark. For lighter mediator masses, Dark Matter dominates as the
couplings to lighter quarks are Yukawa suppressed.
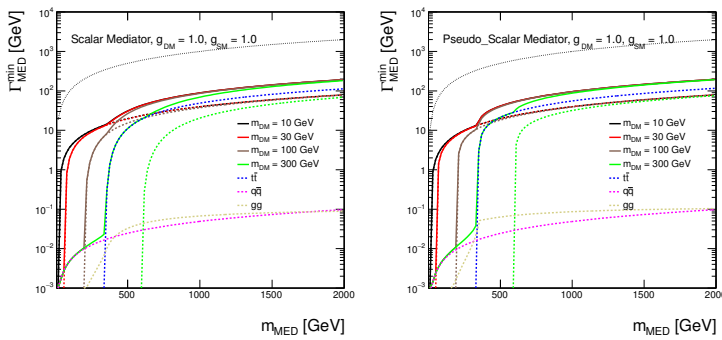
Figure 2.15: Minimal width as a function of mediator mass for scalar and pseudo-scalar mediator assuming couplings of 1. The total width is shown as solid lines for Dark Matter masses of m_{DM} =10 GeV, 30 GeV, 100 GeV and 300 GeV in black, red, brown and green, respectively. The individual contributions from Dark Matter are indicated by dotted lines with the same colors. The contribution from all quarks but top is shown as magenta dotted line and the contribution from top quarks only is illustrated by the dotted blue line. The dotted beige line shows the contribution from the coupling to gluons. The dotted black line shows the extreme case $\Gamma_{min} = M_{med}$.

It can be seen in Fig. 2.16 that the kinematics for the scalar and
pseudoscalar models coincides when considering the diagrams in
Fig. 2.14. For this reason, we recommend to generate only one of
the two models. No preference is given between the two models as
they have the same kinematics, although it is worth noting that the
pseudo-scalar model has been used for a Dark Matter interpretation
of the DAMA signal and of the galactic center excess [ADNP15].
Like in the case of the vector and axial-vector models described

660 in Section 2.1.1, the differences between the cross sections for the
661 scalar and pseudo-scalar samples with the same m_{DM} and M_{med}
662 are increasing with the Dark Matter mass for fixed mediator mass.
663 The pseudo-scalar model gives larger cross sections. Also note the
664 increasing differences between the minimal widths close to the
665 $2m_{DM} = M_{med}$ threshold.
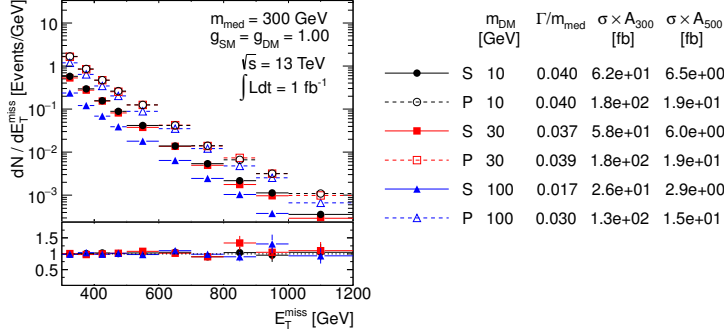
Figure 2.16: Comparison of the $\not{E}_T$ distributions for the scalar and pseudoscalar models for different $M_{med} = 300$ GeV and different Dark Matter masses. Ratios of the normalized distributions with respect to the first one are shown. A_{300} and A_{500} in the table denote the acceptance of the $\not{E}_T > 300$ GeV and $\not{E}_T > 500$ GeV cut, respectively.

2.2.1 *Parameter scan*

667 Similarly as in the case of the vector and axial-vector couplings of
668 spin-1 mediators, scans in the parameter space are performed also
669 for the scalar and pseudo-scalar couplings of the spin-0 mediators
670 in order to decide on the optimized parameter grid for the pre-
671 sentation of Run-2 results. Figures 2.17- 2.21 show the scans over
672 the couplings, Dark Matter mass and mediator mass and the same
673 conclusions apply as in Section 2.1.
674   A scan over the mediator mass is shown in Fig. 2.21 where M_{med}
675 = 300 GeV and 500 GeV are chosen to be below and above $2m_t$. The
676 off-shell Dark Matter production regime is assumed by taking an
677 extreme limit ($m_{DM} = 1$ TeV) in order to study solely the effects of
678 the couplings to quarks. No differences in the kinematic distribu-
679 tions are observed and also the cross sections remain similar in this
680 case. No significant changes appear for mediator masses around
681 the $2m_t$ threshold.

Figure 2.17: Scan over couplings. The $\not{E}_T$ distribution is compared for the scalar mediator models using the parameters as indicated. Ratios of the normalized distributions with respect to the first one are shown. A_{300} and A_{500} in the table denote the acceptance of the $\not{E}_T > 300$ GeV and $\not{E}_T > 500$ GeV cut, respectively.

682   The optimized parameter grid in the M_{med}–m_{DM} plane for scalar
683 and pseudo-scalar mediators is motivated by similar arguments
684 as in the previous section. Therefore, a similar pattern is followed

Figure 2.18: Scan over Dark Matter mass. The $\not{E}_T$ distribution is compared for the scalar mediator models using the parameters as indicated. Ratios of the normalized distributions with respect to the first one are shown. A_{300} and A_{500} in the table denote the acceptance of the $\not{E}_T > 300$ GeV and $\not{E}_T > 500$ GeV cut, respectively.

Figure 2.19: Scan over Dark Matter mass. The $\not{E}_T$ distribution is compared for the scalar mediator models using the parameters as indicated. Ratios of the normalized distributions with respect to the first one are shown. A_{300} and A_{500} in the table denote the acceptance of the $\not{E}_T > 300$ GeV and $\not{E}_T > 500$ GeV cut, respectively.

Figure 2.20: Scan over mediator mass. The $\not{E}_T$ distribution is compared for the scalar mediator models using the parameters as indicated. Ratios of the normalized distributions with respect to the first one are shown. A_{300} and A_{500} in the table denote the acceptance of the $\not{E}_T > 300$ GeV and $\not{E}_T > 500$ GeV cut, respectively.
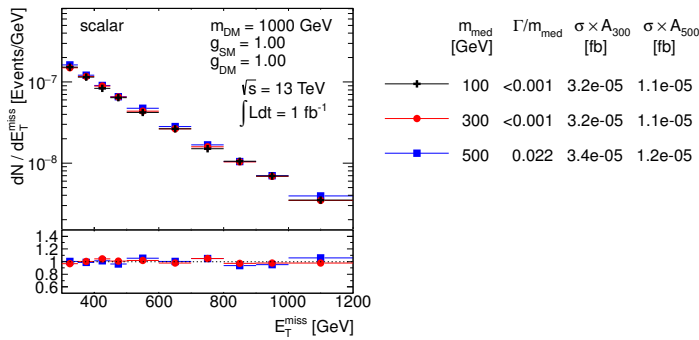
Figure 2.21: Scan over mediator mass. The $\not{E}_T$ distribution is compared for the scalar mediator models using the parameters as indicated. Ratios of the normalized distributions w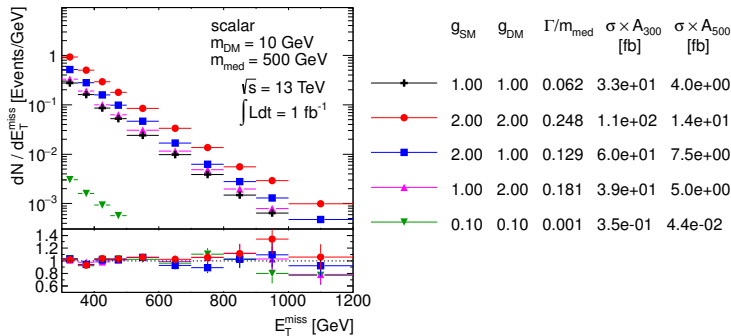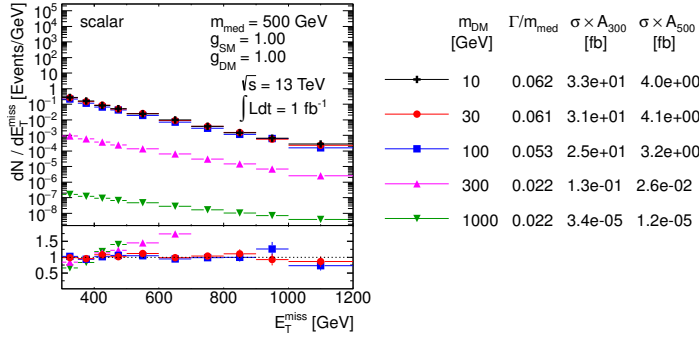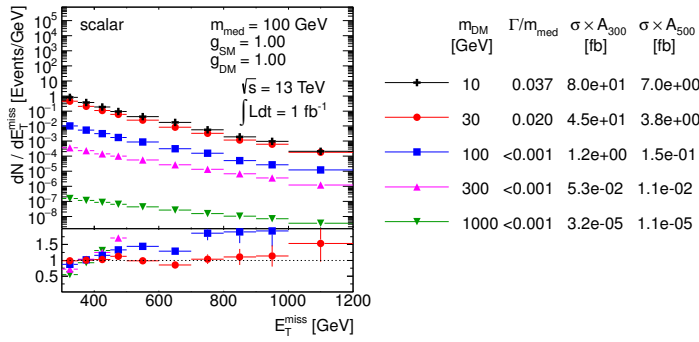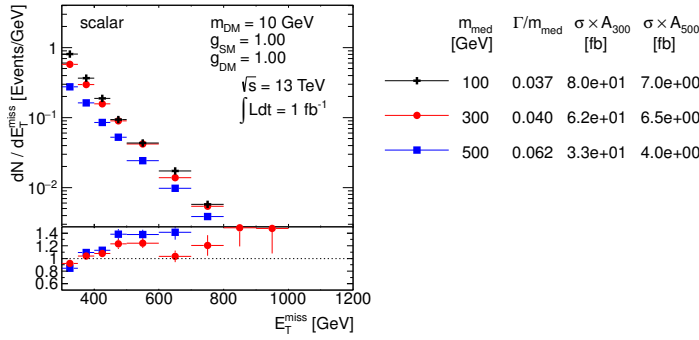ith respect to the first one are shown. A_{300} and A_{500} in the table denote the acceptance of the $\not{E}_T > 300$ GeV and $\not{E}_T > 500$ GeV cut, respectively.

here, taking again $g_q = g_{DM} = 1$. Only the sensitivity to the highest mediator masses has to be re-evaluated. The generator level cross section times the acceptance at $\not{E}_T > 500$ GeV for the model with couplings $g_q = g_{DM} = 1$, light Dark Matter of $m_{DM} = 10$ GeV and a $M_{med} = 500$ GeV scalar mediator is at the order of 10 fb, i.e. just at the edge of the early Run-2 sensitivity. Increasing the mediator mass to 1 TeV pushes the product $\sigma \times A$ down to approximately 0.1 fb, below the LHC sensitivity. Therefore, we choose to remove the 2 TeV mediator mass from the grid and present the final grid with 33 mass points only, as shown in Tab. 2.3. One point at very high mediator mass (5 TeV) is added for each of the DM masses scanned, to aid the reinterpretation of results in terms of contact interaction operators (EFTs).

m_{DM} (GeV)	M_{med} (GeV)								
1	10	20	50	100	200	300	500	1000	5000
10	10	15	50	100					5000
50	10		50	95	200	300			5000
150	10				200	295	500	1000	5000
500	10						500	995	5000
1000	10							1000	5000

Table 2.3: Simplified model benchmarks for s-channel simplified models (spin-0 mediators decaying to Dirac DM fermions in the scalar and pseudoscalar case, taking the minimum width for $g_q = g_{DM} = 1$)

2.2.2 Additional considerations for $V + \not{E}_T$ signatures

The discussion of parameters for the model with a color-singlet, spin-0 mediator parallels that in Section 2.

Even though the sensitivity of mono-boson searches to this model is low and it may not be in reach of early LHC searches, we recommend to generate this model for W, Z and photon searches in order to reproduce the kinematics of contact interaction operators that are further described in Section 3.2.1, for later reinterpretation.

2.2.3 Additional considerations for $t\bar{t}$ and $b\bar{b} + \not{E}_T$ signatures

With the MFV assumption, the top and possibly bottom quark can play a primary role in the phenomenology. The model predicts not only the monojet process described in Section 2.2, but also production of dark matter in association with top (or bottom) pairs, as illustrated in Fig. 2.22. Dedicated searches including jets from heavy flavor quarks in the final state can be designed for this signature. Another class of simplified models, which includes a Dark Matter interpretation among many others, and yields a single top quark in the final state, is detailed in Appendix B.1.

In some theoretically motivated scenario (e.g. for high $tan\beta$ in 2HDM in the pMSSM), spin-0 mediators might couple more strongly to down generation quarks. This assumption motivates the study of final states involving b-quarks as a complementary search to the $t\bar{t}$+DM models, to directly probe the b-quark coupling. In addition to the example illustrated in Fig. 2.22, an example of such
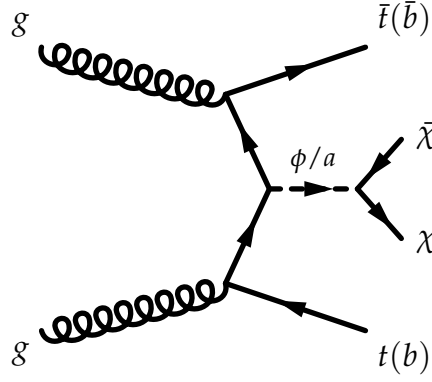
Figure 2.22: Representative Feynman diagram showing the pair production of dark matter particles in association with $t\bar{t}$ (or $b\bar{b}$).

a model can be found in Ref. [BFG15]. Note that, because of the kinematics features of b quark production relative to heavy t quark production, a $b\bar{b}$+DM final state may only yield one experimentally visible b quark, leading to a mono-b signature in a model that conserves b flavor.

The parameter scan for the dedicated $t\bar{t}$+$\not{E}_T$ searches has been studied in detail to target the production mechanism of DM associated with heavy flavor quarks, still sharing many details of the scan for the scalar model with a gluon radiation The benchmark points scanning the model parameters have been selected to ensure that the kinematic features of the parameter space are sufficiently represented. Detailed studies were performed to identify points in the m_{DM}, $m_{\phi,a}$, g_{DM}, g_q (and $\Gamma_{\phi,a}$) parameter space that differ significantly from each other in terms of expected detector acceptance. Because missing transverse momentum is the key observable for searches, the mediator p_T spectra is taken to represent the main kinematics of a model. Another consideration in determining the set of benchmarks is to focus on the parameter space where we expect the searches to be sensitive during the 2015 LHC run. Based on a projected integrated luminosity of $30\,\mathrm{fb}^{-1}$ expected for 2015, we disregard model points with a cross section times branching ratio smaller than 0.1 fb, corresponding to a minimum of one expected event assuming a 0.1% signal efficiency.

The kinematics is most dependent on the masses m_{DM} and $m_{\phi,a}$. Figure 2.23 and 2.24 show typical dependencies for scalar and pseudoscalar couplings respectively. Typically, the mediator p_T spectrum broadens with larger $m_{\phi,a}$. The kinematics are also different between on-shell ($M_{\mathrm{med}} > 2m_{\mathrm{DM}}$) and off-shell ($M_{\mathrm{med}} < 2m_{\mathrm{DM}}$) mediators as discussed in Section 2.2. Furthermore, the kinematic differences in the $\not{E}_T$ spectrum between scalar and pseudoscalar are larger for light mediator masses with respect to heavier mediators. It is therefore important to choose benchmark points covering on-shell and off-shell mediators with sufficient granularity, including the transition region between on-shell and off-shell mediators.

Typically only weak dependencies on couplings are observed (see Fig 2.25) where the variation with width of the integral over parton distributions is unimportant. As shown in Section 2.1.2, for couplings $\sim O(1)$ the width is large enough that the p_T of the mediator is determined mainly by the PDF.

At large mediator masses ($\sim 1.5\,\mathrm{TeV}$) or very small couplings
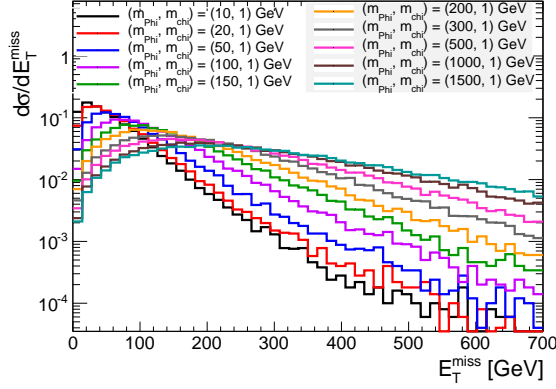
Figure 2.23: Example of the dependence of the kinematics on the scalar mediator mass. The Dark Matter mass is fixed to be m_{DM} =1GeV.
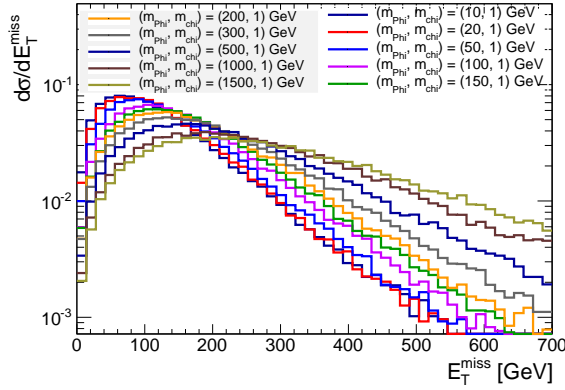
Figure 2.24: Example of the dependence of the kinematics on the pseudoscalar mediator mass. The Dark Matter mass is fixed to be m_{DM} =1GeV.

($\sim 10^{-2}$), width effects are significant, but these regimes have production cross sections that are too small to be relevant for $30\,\mathrm{fb}^{-1}$ and are not studied here. However, with the full Run 2 dataset, such models may be within reach.
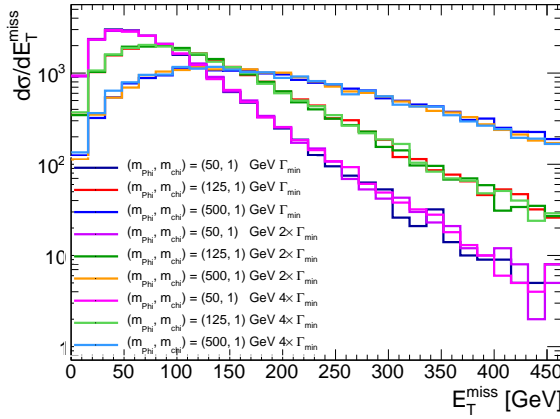
Figure 2.25: Study of the dependence of kinematics on the width of a scalar mediator. The width is increased up to four times the minimal width for each mediator and dark matter mass combination.

Another case where the width can impact the kinematics is when $m_{\phi,a}$ is slightly larger than $2m_\chi$. Here, the width determines the relative contribution between on-shell and off-shell mediators. An example is given in Fig. 2.26. As the minimal width choice pursued in this document is the most conservative one, this effect can be neglected in order to reduce the number of benchmark points to be

772 generated.
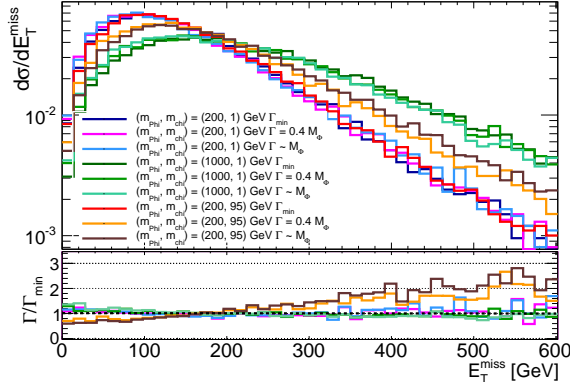
Figure 2.26: Dependence of the kinematics on the width of a scalar mediator. The width is increased up to the mediator mass. Choices of mediator and dark matter masses such that $m_{\phi,a}$ is slightly larger than $2m_\chi$ is the only case that shows a sizeable variation of the kinematics as a function of the width.

773 The points for the parameter scan chosen for this model are
774 listed in Table 2.3, chosen to be harmonized with those for other
775 analyses employing the same scalar model as benchmark. Based on
776 the sensitivity considerations above, DM masses are only simulated
777 up to 500 GeV (but the 5 TeV mediator point is retained) leading to
778 a total of 24 benchmark points. However for these searches we rec-
779 ommend to generate scalar and pseudoscalar models separately, as
780 the kinematics differs due to the different coupling of the mediator
781 to the final state top quarks in the two cases, as shown in Figs. 2.23
782 and 2.24.

783 Similar studies were performed in the $b\bar{b}$ case. It was found that
784 they show the same weak dependence of the kinematics of the
785 event on the mediator width. The same benchmark parameters of
786 the $t\bar{t}$ case could then be chosen.

2.3 Colored scalar mediator, t-channel exchange

788 The preceding sections address models with a Dirac fermion cou-
789 pled to the SM through exchange of a neutral spin-0 or spin-1 par-
790 ticle in an s-channel process. A t-channel process may couple the
791 SM and DM directly, leading to a different phenomenology. For
792 completeness, we examine a model where χ is a Standard Model
793 (SM) singlet, a Dirac fermion; the mediating particle, labeled ϕ, is
794 charged and colored; and the SM particle is a quark. Such mod-
795 els have been studied in Refs. [AWZ14, PVZ14, BB13, DNRT13,
796 CEHL14, BDG+12]. However, this model has not been studied ex-
797 tensively in this forum.

798 Following the example of Ref. [PVZ14], the interaction La-
799 grangian is written as

$$\mathcal{L}_{\text{int}} = g \sum_{i=1,2} (\phi_{(i),L}\bar{Q}_{(i),L} + \phi_{(i),u,R}\bar{u}_{(i),R} + \phi_{(i),d,R}\bar{d}_{(i),R})\chi \qquad (2.14)$$

800 where $Q_{(i),L}$, $u_{(i),R}$ and $d_{(i),R}$ are the SM quarks of the i-th gen-
801 eration and $\phi_{(i),L}$, $\phi_{(i),u,R}$ and $\phi_{(i),d,R}$ are the corresponding me-

802   diators, which (unlike the s-channel mediators) must be heavier
803   than χ. These mediators have SM gauge representations under
804   $(SU(3), SU(2))_Y$ of $(3,2)_{-1/6}$, $(3,1)_{2/3}$ and $(3,1)_{-1/3}$ respectively.
805   Variations of the model previously studied in the literature include
806   coupling to the left-handed quarks only [CEHL14, BDSJ$^+$14], to
807   the $\phi_{(i),u,R}$ [DNRT13] or $\phi_{(i),d,R}$ [PVZ14, A$^+$14a], or some combina-
808   tion [BB13, AWZ14].
809   As for the s-channel models, we assume Minimal Flavor Viola-
810   tion (MFV), setting the mediator masses for each flavor equal; the
811   same logic also applies to the couplings g. The free parameters are
812   then

$$\{m_{\mathrm{DM}}, M_\phi, g\}. \tag{2.15}$$

To do **What about Tait model? (??)**

813   The minimal width of each mediator is expressed, using the
814   example of decay to an up quark, as

$$\Gamma(\phi_{(i)} \to \bar{u}_{(i)}\chi) = \frac{g^2_{(i)}}{16\pi M^3_{\phi_{(i)}}}(M^2_{\phi_{(i)}} - m^2_{u_{(i)}} - m^2_{\mathrm{DM}})$$
$$\times \sqrt{(M^2_{\phi_{(i)}} - (m_{u_{(i)}} + m_{\mathrm{DM}})^2)(M^2_{\phi_{(i)}} - (m_{u_{(i)}} - m_{\mathrm{DM}})^2)}, \tag{2.16}$$

815   which reduces to

$$\frac{g^2_{(i)} M_{\phi_{(i)}}}{16\pi}\left(1 - \frac{m^2_{\mathrm{DM}}}{M^2_{\phi_{(i)}}}\right)^2 \tag{2.17}$$

816   in the limit $M_{\phi_{(i)}}, m_{\mathrm{DM}} \gg m_{u_{(i)}}$.
817   The leading-order processes involved in $\not{E}_T$+jet production are
818   shown in Fig. 2.27. Note that the generation index i for $\phi_{(i)}$ is
819   linked to the incoming fermion(s), and it runs on all three quark
820   generations due to the MFV assumption. However, if the coupling
821   g includes a Yukawa coupling proportional to the quark mass, and
822   g is sufficiently large, LHC searches will still be sensitive to this
823   model, as explained in Section 2.3.3.
824   This model can also give a signal in the $\not{E}_T$ + di-jet channel
825   when, for example, the χ is exchanged in the t-channel and the
826   resulting ϕ pair each decay to a jet + χ. Fig. 2.28 shows the leading
827   order diagrams. Except for the gg induced process, di-jet produc-
828   tion through the third-generation mediator $\phi_{(3),u}$ is not possible,
829   and production through $\phi_{(3),d}$ is again suppressed. The diagram in-
830   volving the t-channel exchange of χ is strongly dependent upon the
831   Dirac fermion assumption. For a Majorana fermion, $q\bar{q}$, $\bar{q}\bar{q}$, and qq
832   production would be possible with the latter having a pronounced
833   enhancement at the LHC.
834   This model is similar to the simplified model considered in SUSY
835   searches, implemented as the MSSM with only light squarks and a
836   neutralino, except for two distinct points: the χ is a Dirac fermion
837   and the coupling g is not limited to be weak scale ($g \ll 1$). In the

MSSM, most of these processes are sub-dominant, even if reso-
nantly enhanced, because the production is proportional to weak
couplings. In the more general theories considered here, g is free
to take on large values of order 1 or more, and thus diagrams ne-
glected in MSSM simulation can occur at a much higher rate here.
While constraints from SUSY jets+$\not{E}_T$ analyses on MSSM mod-
els can be recast to apply to the specific model in this report, DM
searches should also directly test their sensitivity to the MSSM
benchmark models.

Figure 2.27: Leading order mono-jet
t-channel processes, adapted from
[PVZ14].
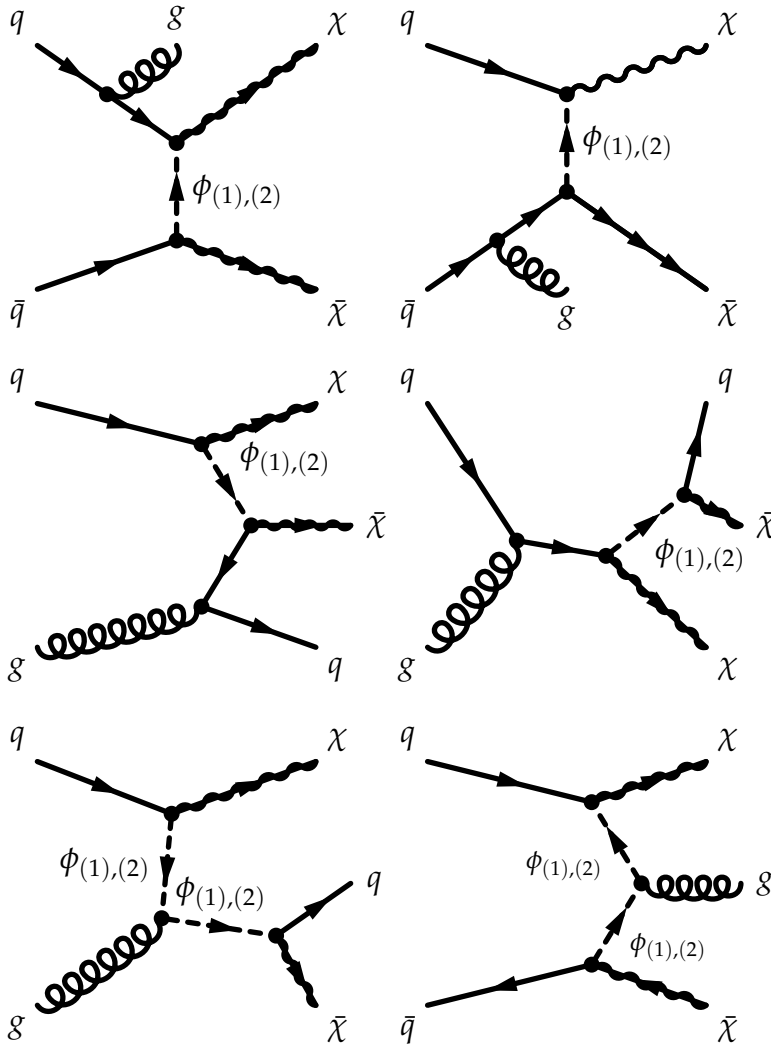
2.3.1   Parameter scan

Ref. [PVZ14] studies the parameter space and obtains bounds on
this model from LHC Run 1 mono-jet and dijets+$\not{E}_T$ data. The
Forum did not exhaustively compare the kinematic distributions
of this model as was done in the s-channel case. While this means
the recommendations below should be taken with more caution, the
model is plausible and distinctive, and it should be included in the
design of LHC searches.
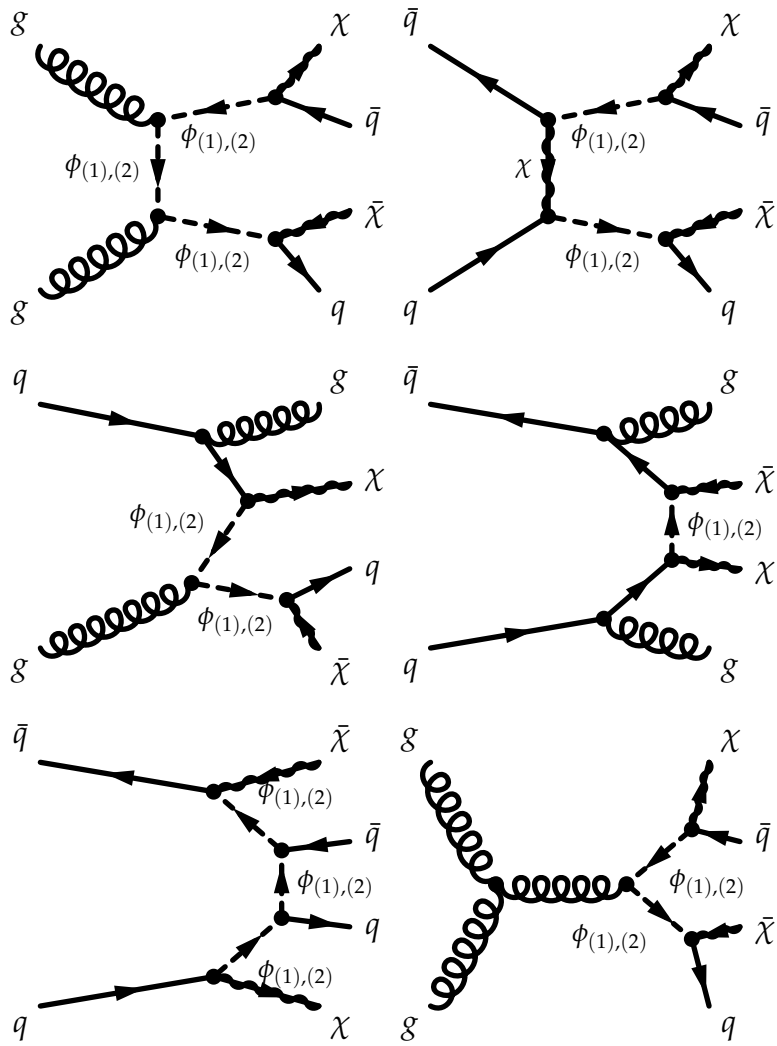
Figure 2.28: Leading order two-jet
t-channel processes, adapted from
[PVZ14].

As in the *s*-channel models, scans should be performed over
m_{DM} and M_ϕ. The viable ranges of both parameters nearly coin-
cide with the scan proposed for the *s*-channel; for simplicity we
recommend adopting the *s*-channel mono-jet grid. In contrast to the
s-channel case, the bounds one obtains from $\slashed{E}_T$+X searches depend
strongly on the width of the mediator, as is visible in Figs. 5 and 6
of Ref. [PVZ14], except in the heavy mediator limit ($M_\phi \approx 2\,\text{TeV}$).
A scan over the width was not available for this report. Thus we
recommend scanning a range of possible widths as discussed in a
more-limited way for the *s*-channel mono-jet, spanning from the
minimal width to a value approaching the particle limit (for exam-
ple, $\Gamma \approx M_\phi/3$ in Ref. [PVZ14]).

2.3.2   Additional considerations for $V + \slashed{E}_T$ signatures

The model parameters with emission of an EW boson generally
follow those in Section 2.3. even though fewer diagrams are in-
volved. A representative Feynman diagram can be constructed by
replacing a final-state gluon in Fig. 2.27 with a γ, W, Z boson. See
Ref. [BDG$^+$12] for a theoretical overview of this model with specific
examples for the $Z+\slashed{E}_T$ final state.

Figure 2.29 shows the $\slashed{E}_T$ distribution for the hadronic $Z+\slashed{E}_T$
final state, with varying dark matter and mediator mass, before any
selection. The acceptance for a series of basic analysis selections ($\slashed{E}_T$
>350 GeV, leading jet $p_T > 40$ GeV, minimum azimuthal angle
between jet and $\slashed{E}_T > 0.4$) applied at the generator level is shown in
Figure 2.30.
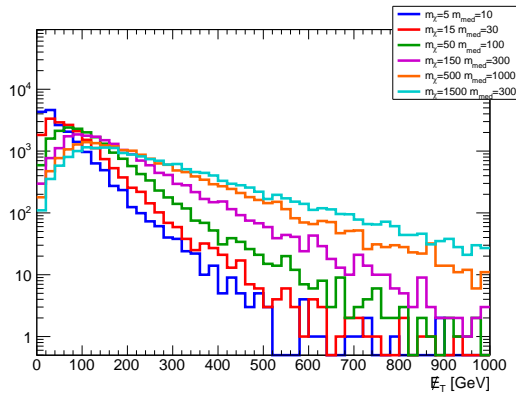
Figure 2.29: Missing transverse momentum distribution for the hadronic $Z+\slashed{E}_T$ final state, for the simplified model with a colored scalar mediator exchanged in the *t*-channel.

The discussion of the parameter scan for the *t*-channel model
in the case of signatures including EW bosons parallels that of the
monojet case.

2.3.3   Additional considerations for signatures with $b-$quarks $+ \slashed{E}_T$

Models of bottom-flavored Dark Matter that are closely related to
the *t*-channel mediated model from this Section have been pro-
posed in Refs. [LKW13, ABHL14]. Here, DM couples preferentially
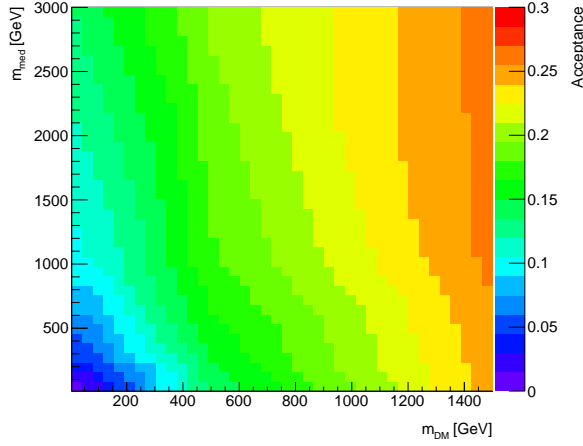
Figure 2.30: Acceptance for the hadronic Z+$\not{E}_T$ final state, for the simplified model with a colored scalar mediator exchanged in the t-channel.

to bottom quarks, with a decoupled third generation. We describe the b-FDM model of Ref. [ABHL14], created to explain the Galactic Center (GC) gamma-ray excess observed in data collected by the Fermi-LAT collaboration [DFH$^+$14, CCW15]. This model favors couplings to third-generation quarks via Yukawa couplings, therefore respecting the MFV assumption.

This model produces an annihilation cross section consistent with the gamma-ray excess that has perturbative values for the couplings and is consistent with LHC constraints on the colored mediator. For parameters capable of explaining the anomalous gamma-ray signal in terms of Dark Matter coupling preferentially to b-quarks, the model predicts a direct detection cross section that is consistent with current constraints, but within the near future reach of Direct Detection experiments and of the upcoming LHC run.

The model contains a Dirac fermion transforming as a flavor triplet, exclusively coupling to right-handed down-type quarks. The third component of the triplet χ_b comprises the cosmological DM. Within the MFV framework, the other fermions in the flavor triplet can be made sufficiently heavy and weakly-coupled that they can be neglected in the analysis. A flavor singlet, color triplet scalar field Φ mediates the interactions between the DM and the Standard Model quarks. The model is similar to the MSSM with a light bottom squark and neutralino, and is thus a flavor-specific example of a t-channel model.

The Lagrangian considered is given by

To do **Spell out implications on MFV assumption, and whether top-flavored could exist too. (??)**

$$-\mathcal{L} \supset g\Phi^*\bar{\chi}_b b_R + \text{h.c.} \qquad (2.18)$$

Parameter scan   The nature of the model is not conducive to a simple scaling behavior that would allow us to reduce the number of points to be simulated. This is because of the interference of diagrams with QCD production of the mediator (which scale as g_s^2) with diagrams that are proportional to the coupling g in the b+$\not{E}_T$ and $b\bar{b}$+$\not{E}_T$ final states. Fixing the couplings also fixes the mediator

918 width, when adopting the minimal width assumption.

919   A full study of the parameter scan for this model was not avail-
920 able for this report; thus we recommend scanning a range of pos-
921 sible widths as discussed in a more-limited way for the *s*-channel
922 mono-jet, spanning from the minimal width to a value approach-
923 ing the particle limit, e.g. $g = 0.5, 1, 2, 3$. A coupling benchmark
924 such as $g = 1$ should be considered for each mass point since this
925 would be a distinctive feature of this benchmark from SUSY mod-
926 els with sbottom squarks (see Section 2.3 for further discussion):
927 Cross-sections for unit couplings can be found in Appendix **??**.
928 The coupling could also be chosen to fulfill constraints from the
929 relic density (see Appendix **??**, with corresponding cross sections in
930 Tables **??** onwards).

931   A scan of Dark Matter and mediator masses should be done in
932 the on-shell region $M_\Phi > m_{\rm DM} + m_b$, since the cross-sections in the
933 off-shell region are too small to be sensitive with early LHC data,
934 spanning from 10 to 500 GeV in $m_{\rm DM}$ and from 10 to 1300 GeV in
935 $M_{\rm med}$.
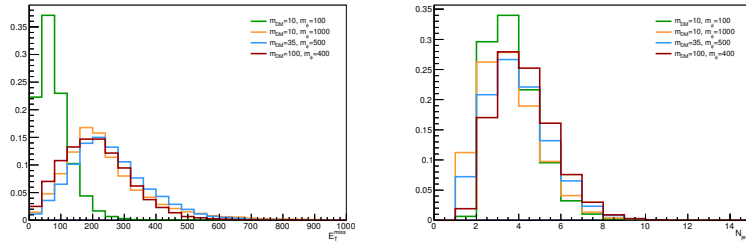
Figure 2.31: MET (left) and jet mul-
tiplicity (right) for various DM and
mediator masses and couplings nor-
malized to the relic density observed
in the early universe.
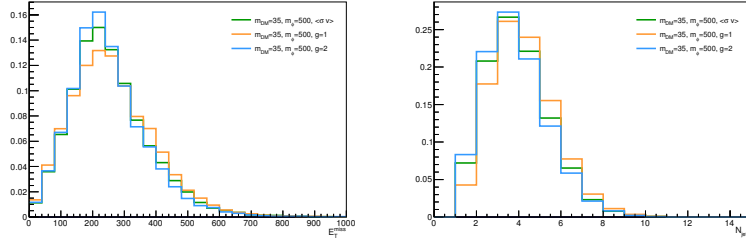
Figure 2.32: MET (left) and jet mul-
tiplicity (right) for $m_{\rm DM} = 35$ GeV
and $M_\Phi = 500$ GeV for couplings
corresponding to relic density weights
and also $g = 1, 2$

936 ## 2.4   *Spin-2 mediator*

937 In models with extra dimensions, the Kaluza-Klein excitations of
938 the graviton could also serve as a mediator between the Standard
939 Model and dark sector physics. This kind of model was not studied
940 in the forum and is not included in the recommendations, but it
941 and models such as Ref. [LPS14] may warrant further study on a
942 longer timescale.

943 ## 2.5   *Presentation of results for reinterpretation of s-channel me-*
944   *diator models*

945 The aim of the parameter grid optimization done for the *s*-channel
946 models in the previous sections is to reduce the parameter space

that must be simulated. We then need a procedure for populating the full parameter space by using the simulated grid points. We recommend doing this as follows:

- When the dependences on parameters are known, the cross sections and efficiencies are general points can be calculated from the grid data.

- In other cases, this information can be obtained by interpolation between the grid points. We have chosen the grid points so that the dependence is sufficiently smooth that this will be possible.

The results of the scan over the couplings presented in the previous sections indicate there are no changes in kinematic distributions for different choices of the coupling strengths. This means that the acceptance remains the same in the whole g_q–g_{DM} plane and it is sufficient to perform the detector simulation only for one single choice of g_q, g_{DM}. The resulting truth-level selection acceptance and the detector reconstruction efficiency can then be applied to all remaining grid points in the g_q–g_{DM} plane where only the generator-level cross section needs to be known. This significantly reduces the computing time as the detector response is by far the most expensive part of the Monte Carlo sample production. However, the number of generated samples can be reduced even further if a parameterization of the cross section dependence from one grid point to another exists. In this section, we describe the details of a cross section scaling procedure that can be used to reinterpret results for a fixed coupling for s-channel mediator models.

The propagator for the s-channel exchange is written in a Breit-Wigner form as $\dfrac{1}{q^2 - M^2_{\mathrm{med}} + i M_{\mathrm{med}} \Gamma}$, where q is the momentum transfer calculated from the two partons entering the hard process after the initial state radiation, which is equivalent to the momentum of the Dark Matter pair. The size of the momentum transfer with respect to the mediator mass allows us to classify the production in the following way:

- off-shell production when $q^2 \gg M_{\mathrm{med}}$ leading to suppressed cross sections,

- on-shell production when $q^2 \sim M_{\mathrm{med}}$ leading to enhanced cross sections,

- effective field theory (EFT) limit when $q^2 \ll M_{\mathrm{med}}$.

All three categories can be distinguished in Fig. 4.1 showing the upper limit on the interaction scale $M^* \equiv M_{\mathrm{med}} / \sqrt{g_q g_{DM}}$ for vector mediator. In the case of the off-shell production and the EFT limit, the first and second term in the propagator dominate, respectively, which reduces the dependence on the mediator width. Therefore, in these cases one can approximate the cross section as

$$\sigma \propto g_q^2 g_{DM}^2. \qquad (2.19)$$

The on-shell production regime is the most interesting one as it gives the best chances for a discovery at the LHC given the cross section enhancement. The propagator term with the width cannot be neglected in this case and, in the narrow width approximation which requires $\Gamma \ll M_{\mathrm{med}}$ (this is not necessarily the case in the benchmarks considered in the scans), one can integrate

$$\int \frac{ds}{(s - M_{\mathrm{med}}^2)^2 + M_{\mathrm{med}}^2 \Gamma^2} = \frac{\pi}{M_{\mathrm{med}} \Gamma} \qquad (2.20)$$

which further implies the cross section scaling

$$\sigma \propto \frac{g_q^2 g_{\mathrm{DM}}^2}{\Gamma}. \qquad (2.21)$$

The narrow with approximation is important here as it ensures an integration over parton distribution functions (PDFs) can be neglected. In other words, it is assumed the integrand in Eq. 2.20 is non-zero only for a small region of s, such that the PDFs can be taken to be constant in this range. By simplifying the dependence of the minimal width on the couplings as $\Gamma \sim g_q^2 + g_{\mathrm{DM}}^2$, one can approximate this scaling rule in the extreme cases as follows

$$\sigma \quad \propto \quad \frac{g_q^2 g_{\mathrm{DM}}^2}{g_q^2 + g_{\mathrm{DM}}^2} \xrightarrow{g_q \ll g_{\mathrm{DM}}} g_q^2 \qquad (2.22)$$

$$\sigma \quad \propto \quad \frac{g_q^2 g_{\mathrm{DM}}^2}{g_q^2 + g_{\mathrm{DM}}^2} \xrightarrow{g_q \gg g_{\mathrm{DM}}} g_{\mathrm{DM}}^2 . \qquad (2.23)$$

However, it is important to keep in mind that this formula omits color and multiplicity factors as well as possible Yukawa suppression, and there is no simple scaling rule for how the cross section changes with the Dark Matter mass and the mediator mass, or for mediators with a large width, because PDFs matter in such cases as well. Therefore, the scaling procedure outlined above is expected to work only for fixed masses and fixed mediator width, assuming the narrow width approximation applies.

Figure 2.33 shows the minimal width over the mediator mass in the g_q–g_{DM} plane for vector and scalar mediators for $M_{\mathrm{med}} = 100$ GeV and 1000 GeV, taking $m_{\mathrm{DM}} = 10$ GeV. The individual colors indicate the lines of constant width, along which the cross section scaling may work for narrow mediators. The limiting case $\Gamma_{\mathrm{min}} = M_{\mathrm{med}}$ defines the upper values of the couplings below which the narrow width approximation can be considered and provides more stringent constraint than the perturbative limit $g_q = g_{\mathrm{DM}} = 4\pi$. For vector and axial-vector mediators, the minimal width is predominantly defined by g_q due to the number of quark flavors and the color factor. On the contrary, both the Standard Model and Dark Matter partial width have comparable contributions in case of scalar and pseudo-scalar mediators if the top quark channel is open ($M_{\mathrm{med}} > 2m_t$). However, mostly g_{DM} defines the minimal width for $M_{\mathrm{med}} < 2m_t$ due to the Yukawa-suppressed light quark couplings.

To do **Reduce plots to mMed<GammaMin region (??)**
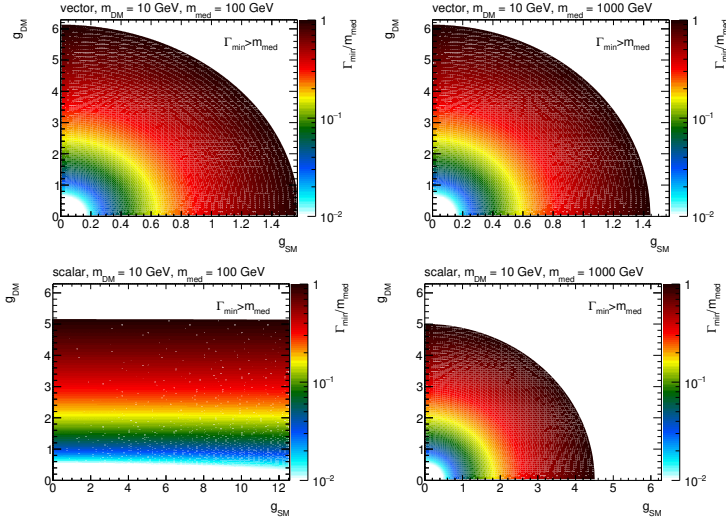
Figure 2.33: Minimal width over the mediator mass for vector (top) and scalar (bottom) mediators as a function of the individual couplings g_q and g_{DM}, assuming $M_{med} = 100$ GeV (left) and $M_{med} = 1$ TeV (right). $m_{DM} = 10$ GeV is considered in all cases. Only the cases with $\Gamma_{min} < M_{med}$ are shown.

The performance of the cross section scaling is demonstrated in Fig. 2.34 where two mass points $M_{med} = 100$ GeV and 1 TeV with $m_{DM} = 10$ GeV are chosen and rescaled from the starting point $g_q = g_{DM} = 1$ according to Eq. 2.21 to populate the whole g_q–g_{DM} plane. This means the width is not kept constant in this test and this is done in purpose in order to point out deviations from the scaling when the width is altered. For each mass point, the rescaled cross section is compared to the generator cross section and the ratio of the two is plotted. For the given choice of the mass points, the scaling seems to work approximately with the precision of $\sim 20\%$ in the region where $\Gamma_{min} < M_{med}$. Constant colors indicate the lines along which the cross section scaling works precisely and there is a remarkable resemblance of the patterns shown in the plots of the mediator width. To prove the scaling along the lines of constant width works, one such line is chosen in Fig. 2.35 for a scalar mediator, defined by $M_{med} = 300$ GeV, $m_{DM} = 100$ GeV, $g_q = g_{DM} = 1$, and the rescaled and generated cross sections are found to agree within 3%.
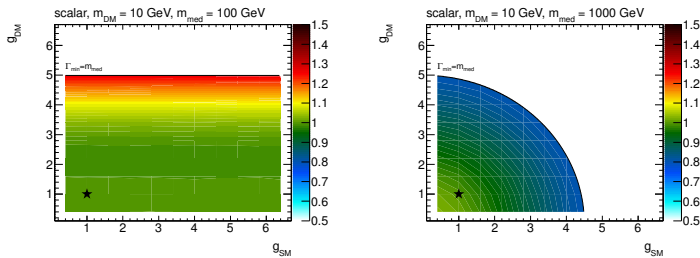
Figure 2.34: Ratio of the rescaled and generated cross sections in the g_q–g_{DM} plane. The point at $g_q = g_{DM} = 1$, taken as a reference for the rescaling, is denoted by a star symbol. Scalar model with $M_{med} = 100$ GeV (left) and 1 TeV (right) is plotted for $m_{DM} = 10$ GeV. The limiting case $\Gamma_{min} = M_{med}$ is indicated by a black line and no results are shown beyond.

Proposed parameter grid for cross-section scaling   We propose to deliver collider results in the g_q–g_{DM} plane using the following prescription, to ease reinterpretation through cross-section scaling:

- Since the shapes of kinematic quantities do not change for different couplings, use the acceptance and efficiency for the available
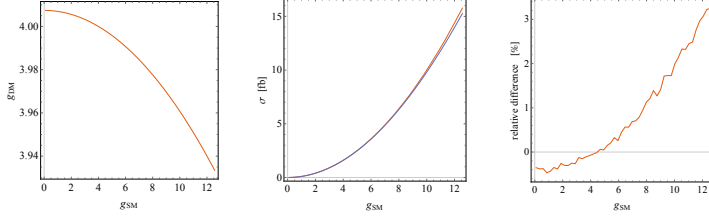
Figure 2.35: Scaling along the lines of constant width. The line of constant width for $M_{\mathrm{med}} = 300$ GeV and $m_{\mathrm{DM}} = 100$ GeV, intercepting $g_{\mathrm{q}} = g_{\mathrm{DM}} = 4$ is shown on left. The generated and rescaled cross sections are compared in the middle, the corresponding ratio is shown on right.

$m_{\mathrm{DM}} = 50$ GeV, $M_{\mathrm{med}} = 300$ GeV, $g_{\mathrm{q}} = g_{\mathrm{DM}} = 1$ grid point from the M_{med}–m_{DM} plane for the scalar and pseudo-scalar mediator. In case of the vector and axial-vector mediator, use the grid point $m_{\mathrm{DM}} = 150$ GeV, $M_{\mathrm{med}} = 1$ TeV, $g_{\mathrm{q}} = 0.25$, $g_{\mathrm{DM}} = 1$.

- Generate additional samples in order to get generator cross sections only. For scalar and pseudo-scalar mediator, choose $m_{\mathrm{DM}} = 50$ GeV, $M_{\mathrm{med}} = 300$ GeV with the following values for $g_{\mathrm{q}} = g_{\mathrm{DM}}$: 0.1, 1, 2, 3. For vector and axial vector mediator, choose $m_{\mathrm{DM}} = 150$ GeV, $M_{\mathrm{med}} = 1$ TeV with the following values for $g_{\mathrm{q}} = g_{\mathrm{DM}}$: 0.1, 0.25, 0.5, 0.75, 1, 1.25, 1.5. The upper values are defined by the minimal width reaching the mediator mass.

To do **Waiting for scalar mediator calculation of perturbativity limit from J. Alcaraz.). (??)**

- Rescale the generator cross sections for on-shell resonance production along the lines of constant width in order to populate the whole g_{q}–g_{DM} plane in the region $\Gamma_{\min} < M_{\mathrm{med}}$. The scaling follows from Eq. 2.21 which for the constant width implies:

$$\sigma' = \sigma \times \frac{g_{\mathrm{q}}'^2 g_{\mathrm{DM}}'^2}{g_{\mathrm{q}}^2 g_{\mathrm{DM}}^2} \ . \tag{2.24}$$

Rescaling to different mediator width   In general it is also important to consider a larger mediator width than $\Gamma_{\min}$ in order to accommodate additional interactions of the mediator with the visible and hidden sector particles [BFG15, HKSW15]. If the narrow width approximation applies, the cross section scaling method described above can be used to reinterpret the results presented for the minimal width, since multiplying the width by factor n is equivalent to changing the coupling strength by factor $\sqrt{n}$, i.e.

$$\sigma(g_{\mathrm{q}}, g_{\mathrm{DM}}, n\Gamma_{\min}(g_{\mathrm{q}}, g_{\mathrm{DM}})) \propto \frac{g_{\mathrm{q}}^2 g_{\mathrm{DM}}^2}{\Gamma_{\min}(\sqrt{n}g_{\mathrm{q}}, \sqrt{n}g_{\mathrm{DM}})} \ . \tag{2.25}$$

The cross section for the sample with couplings g_{q} and g_{DM} and modified mediator width $\Gamma = n\Gamma_{\min}$ can therefore be rescaled from a sample generated with the minimal width corresponding to the couplings scaled by $\sqrt{n}$ as described in the following formula.

$$\sigma(g_{\mathrm{q}}, g_{\mathrm{DM}}, n\Gamma_{\min}(g_{\mathrm{q}}, g_{\mathrm{DM}})) = \frac{1}{n^2}\sigma(\sqrt{n}g_{\mathrm{q}}, \sqrt{n}g_{\mathrm{DM}}, \Gamma_{\min}(\sqrt{n}g_{\mathrm{q}}, \sqrt{n}g_{\mathrm{DM}})) \tag{2.26}$$

The advantage of doing this is in the fact that no event selection and detector response needs to be simulated since the changes in

couplings do not have an effect on the shapes of kinematic distribu-
tions.

It should be noted again that this procedure is only useful when
the narrow width approximation applies. Care must be taken to
ensure that is the case. For example, in the vector and axial-vector
cases, one quickly breaks this approximation even for small n.

2.5.1   Additional considerations for $t\bar{t}$ and $b\bar{b}+\not{E}_T$ signatures

The cross-section scaling considerations shown in 2.5 still apply
for this model. Here we detail the specific studies done for the $t\bar{t}$
model.

Given that the kinematics are similar for all couplings $g =\sim 1$,
we recommend to generate only samples with $g_{DM} = g_q = 1$. It
follows from this that these benchmark points should be a good
approximation for non-unity couplings and for $g_{DM} \neq g_q$, provided
that the sample is rescaled to the appropriate cross section times
branching ratio.

While the simple scaling function

$$\sigma' \times BR' = [\sigma \times BR] \times \left(\frac{g'_q}{g_q}\right)^2 \times \left(\frac{g'_{DM}}{g_{DM}}\right)^2 \times \frac{\Gamma}{\Gamma'} \qquad (2.27)$$

is sufficient for a limited range of coupling values (see Fig. 2.36
for example), this scaling is only approximate (up to 20%) and
relies on the narrow width approximation, ignoring PDFs effects.
We also choose to provide instead a table of cross section times
branching ratio values over a large range of couplings to support
interpretation of search results (see the Appendix **??**). The table lists
couplings from $g = 0.1$ to $g = 3.5$, where the upper limit is chosen
to be close to but lower than the perturbative limit.
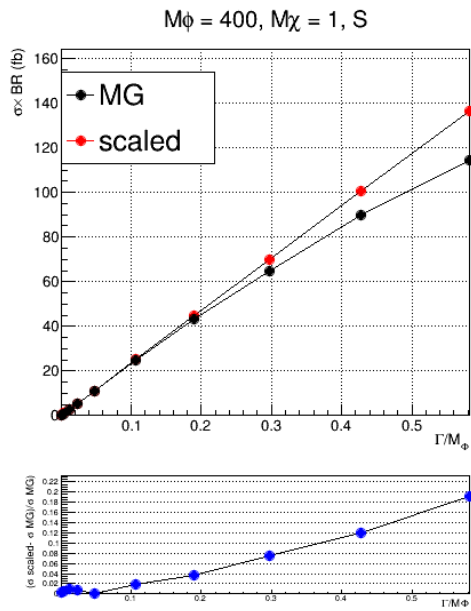
Figure 2.36: An example comparing a simple cross section scaling versus the computation from the generator, for a scalar model with $m_\phi = 400\,\text{GeV}$, $m_{\text{DM}} = 1\,\text{GeV}$ and all couplings set to unity. In this example, the scaling relationship holds for Γ_ϕ / m_ϕ below 0.2, beyond which finite width effects become important and the simple scaling breaks down.

3

Specific models for signatures with EW bosons

In this Section, we consider specific models with a photon, a W boson, a Z boson or a Higgs boson in the final state ($V+\not{E}_T$ signature), accompanied by Dark Matter particles that either couple directly to the boson or are mediated by a new particle. The common feature of those models is that they provide different kinematic distributions with respect to the models described in Section 2.

The models considered in this Section can be divided into two categories:

V-specific simplified models These models postulate direct couplings of new mediators to bosons, e.g. they couple the Higgs boson to a new vector or to a new scalar [CDM$^+$14, BLW14].

Models including a contact operator, where the boson is directly coupled to DM
Shown on the right-hand side of Figure 3.1, these models allow for a contact interaction vertex that directly couples the boson to Dark Matter [CHLR13, CNS$^+$13, CHH15, BLW14]. These models are included in this report devoted to simplified models since UV completions for most of these operators proceed through loops and are not available to date. These models provide a benchmark to motivate signal regions that are unique to searches with EW final states and would otherwise not be studied. However, we recommend to use these models as placeholders and emphasize model-independent results especially in signal regions tailored to these models. Wherever results are interpreted in terms of these operators, a truncation procedure to ensure the validity of the EFT should be employed, as detailed in the next Section (Sec. 4).

The following Sections describe the models within these categories, the parameters for each of the benchmark models chosen, the studies towards the choices of the parameters to be scanned.

3.1   *Specific simplified models including EW bosons, tailored to Higgs+MET searches*

Three benchmark simplified models [CDM$^+$14, BLW14] are recommended for Higgs+$\not{E}_T$ searches:
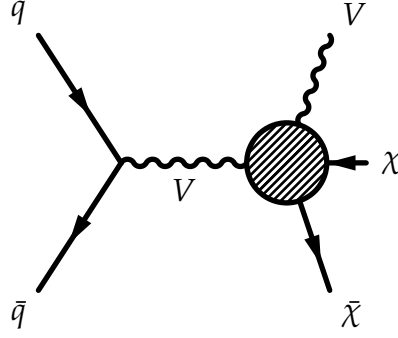
Figure 3.1: Sketch of benchmark models including a contact interaction for V+MET searches, adapted from [NCC$^+$14].

- A model where a leptophobic vector mediator (Z'_B) is exchanged in the s-channel, radiates a Higgs boson and decays into two DM particles (Fig. 3.2 (a));

- A model where a scalar mediator S couples to the SM only through the SM Higgs and decays to two DM particles (Fig. 3.3);

- A model where a vector Z' is produced resonantly and decays into a Higgs boson plus an intermediate heavy pseudoscalar particle A^0, in turn decaying into two DM particles (Fig. 3.2 (b)).
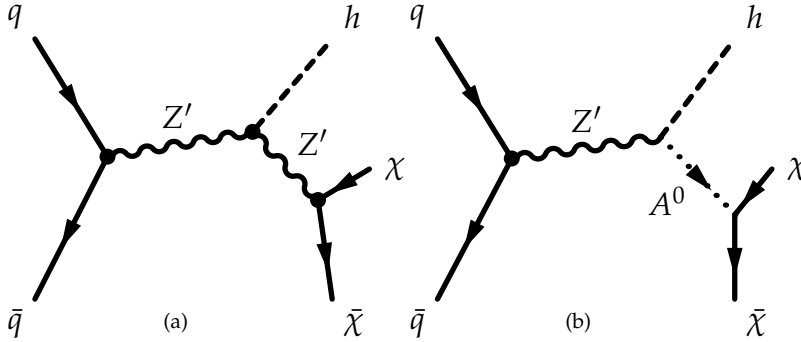
Figure 3.2: Feynman diagrams of leading order processes leading to Higgs+$\not{E}_T$ events: (a) a model with a vector mediator (Z') coupling with DM and with the Higgs boson h, and (b) a 2HDM model with a new invisibly decaying pseudoscalar A^0 from the decay of an on-shell resonance Z' giving rise to a Higgs+$\not{E}_T$ signature .

These models are kinematically distinct from one another, as shown in the comparison of the $\not{E}_T$ spectra in Fig. 3.4 for high and low masses of the pseudoscalar mediator. Figure 3.4 (a) shows the $\not{E}_T$ distribution for models with high mediator masses ($m_S = 1$ TeV, $m_{Z'} = 1$ TeV, $m_{A^0} = 1$ TeV) and DM mass of either 50 (Z'_B and A^0 models) or 65 GeV (scalar mediator model). Figure 3.4 (b) shows the $\not{E}_T$ distribution for models with low pseudoscalar mediator masses ($m_{Z'_B} = 100$ GeV, $m_{Z'} = 1$ TeV, $m_{A^0} = 100$ GeV) and DM mass of 1 TeV for all models.

3.1.1 $\not{E}_T$ +Higgs from a baryonic Z'

The model shown in Fig. 3.2 (a) postulates a new gauge boson Z' corresponding to a new $U(1)_B$ baryon number symmetry. The stable baryonic states included in this model are the DM candidate particles. The mass of the Z' boson is acquired through a baryonic Higgs h_B, which mixes with the SM Higgs boson.
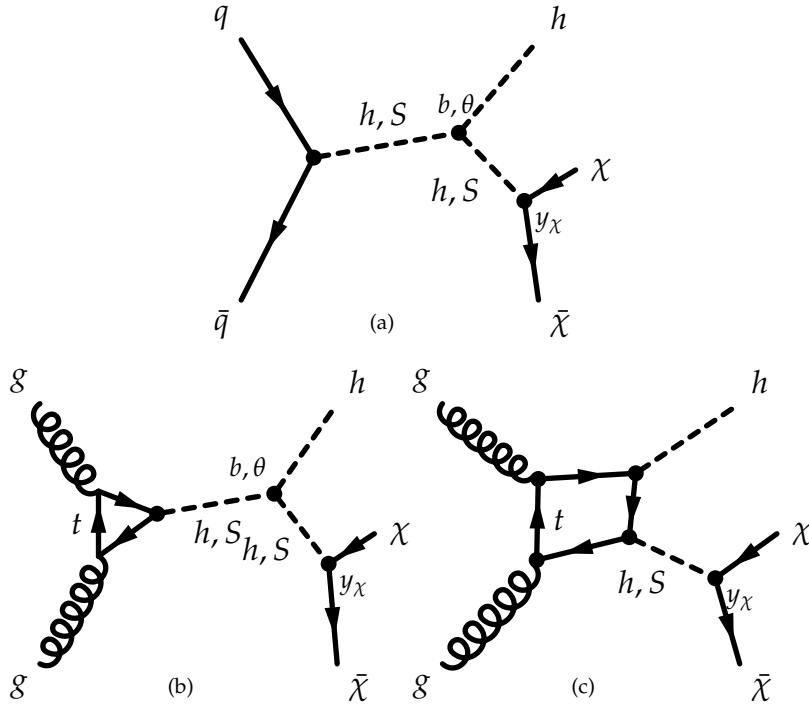
Figure 3.3: Feynman diagrams of leading order processes leading to Higgs+$\not{E}_T$ events for a model with a scalar mediator (S) coupling with DM and with the Higgs boson h.
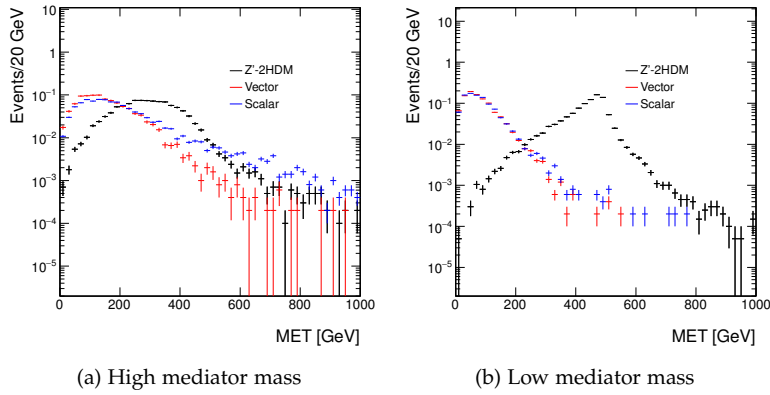
Figure 3.4: Comparison of the missing transverse momentum distributions at generator level in different simplified models leading to a Higgs+$\not{E}_T$ signature. The model parameter settings are detailed in the text.

(a) High mediator mass   (b) Low mediator mass

The interactions between the Z', the quarks and the DM are described by the following Lagrangian:

$$L = g_q \bar{q} \gamma^\mu q Z'_\mu + g_{\text{DM}} \bar{\chi} \gamma^\mu \chi Z'_\mu. \tag{3.1}$$

The quark couplings g_q are fixed to be equal to one third of the gauge coupling g_B, while the DM coupling to the Z' are proportional to the baryon number and to the gauge coupling ($g_\chi = B g_B$). No leptonic couplings of the Z' are allowed, thus evading dilepton constraints. After incorporating the mixing of the baryonic and SM Higgs bosons, this model is is described by the following Lagrangian term at energies below $m_{Z'}$ [1]:

$$L_{\text{eff}} = -\frac{g_q g_{\text{DM}}}{m_{Z'}^2} \bar{q} \gamma^\mu q \bar{\chi} \gamma_\mu \chi \left(1 + \frac{g_{hZ'Z'}}{m_{Z'}^2} h \right), \tag{3.2}$$

The first term of this equation is the standard DMV model in the large $M_{Z'}$ limit. This term can lead to a monojet signature, which can be also used to constrain this model. The second term describes the interaction between the Z' and the SM Higgs boson, via the coupling $g_{hZ'Z'} = \frac{m_{Z'} 2 \sin\theta}{v_B}$, where $\sin\theta$ is the mixing angle between the SM Higgs and the baryonic Higgs h_B, and v_B is the Baryonic Higgs vacuum expectation value. In its most general form, this model can lead to mono-Z signals as well. However, in this case there is no $Z - Z'$ mixing from the $hZ'Z'$ term, since this term arises only after $U(1)_B$ is broken. A mixing angle can come from terms involving the field strengths of Z and Z': this is a free parameter, that is set to be small in the model considered for mono-Higgs signatures.

The predictions of the model depend upon the two additional parameters beyond an s-channel simplified model, namely the mixing angle between baryonic Higgs h_B and the SM-like Higgs boson $\sin\theta$ and the coupling of the mediator to SM-like Higgs boson, $g_{hZ'Z'}$. Thus, a full model is specified by:

$$\{ M_{\text{med}}, m_{\text{DM}}, g_{\text{DM}}, g_q, \sin\theta, g_{hZ'Z'} \}. \tag{3.3}$$

3.1.1.1 Parameter scan

The width of the Z' mediator is calculated using all possible decays to SM particles (quarks) and to pairs of DM particles if kinematically allowed as in the DMV model.

The dependence of the missing transverse momentum ($\not{E}_T$) on the model parameters is studied by varying the parameters one at a time. The variation of parameters other than M_{med} and m_{DM} does not result in significant variations of the $\not{E}_T$ spectrum, as shown in Figures 3.5. Figure 3.6 shows that for an on-shell mediator, varying m_{DM} with the other parameters fixed does not affect the $\not{E}_T$ distribution, while the distribution broadens significantly in the case of an off-shell mediator. For this reason, the same grid in M_{med}, m_{DM} as for the vector mediator of the jet+$\not{E}_T$ search (Table 2.1) is chosen

[1] The operator in Eqn. 3.2 is an effective one, to highlight the two main terms. The full dimension-4 simplified model is used in the model for event generation.

as a starting point. The coupling $g_{hZ'Z'}$, along with g_q and g_{DM}, are subject to perturbativity bounds:

$$g_q, g_{DM} < 4\pi$$

and

$$g_{hZ'Z'} < \sqrt{4\pi} m_{Z'} \sin\theta$$

The value $g_{hZ'Z'}/m_{Z'} = 1$ is chosen as a benchmark value for the generation of Monte Carlo samples since it maximizes the cross section (as shown in the following paragraph) without violating the bounds. The mediator-DM coupling g_{DM} is fixed to 1, and the mediator-quark g_q coupling is fixed to 1/3. The kinematic distributions do not change as a function of these parameters, so results for other values of $g_{hZ'Z'}/m_{Z'}$, g_{DM} and g_q can be obtained through rescaling by the appropriate cross sections.

Figs 3.7 and 3.8 show the kinematic distributions for the two leading jets in the $H \to \bar{b}b$ decay channel, for two values of the mediator mass and varying the DM mass.

Analyses should perform further studies, beyond those studies performed for the forum, to estimate the reach of the analysis with respect to all points in the grid and therefore decide on a smaller set of grid points to be generated.
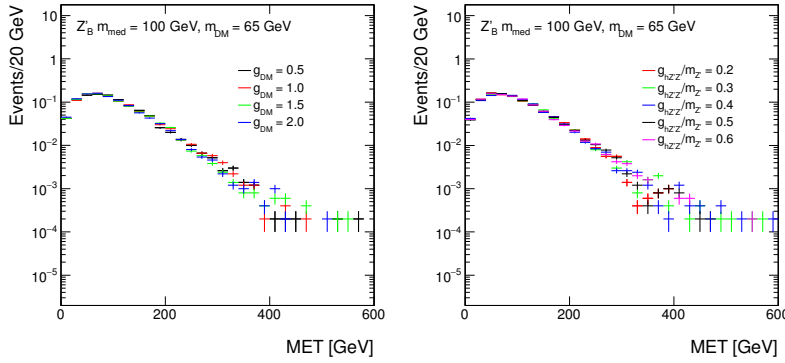
Figure 3.5: Missing transverse momentum distributions at generator level in the vector mediator scenario for different values of: the mediator-dark matter coupling g_{DM} (left), and the coupling between the mediator and the SM-like Higgs boson, scaled by the mediator mass, $g_{hZ'Z'}/m_{Z'}$ (right).
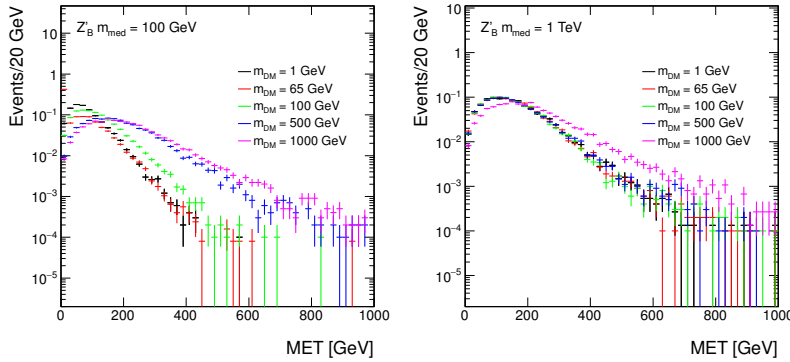
Figure 3.6: Missing transverse momentum distributions at generator level in the vector mediator scenario: for different values of the dark matter mass m_{DM} and a mediator mass of M_{med} = 100 GeV (left) and M_{med} = 1 TeV (right).

(a) Leading $b-$jet transverse momentum

(b) Leading $b-$jet pseudorapidity

Figure 3.7: Comparison of the kinematic distributions for the two leading $b-$jets (from the Higgs decay) in the vector Z' simplified model, when fixing the Z' mass to 100 GeV and varying the DM mass.

(c) Angular distance between the two leading $b-$jets

(a) Leading $b-$jet transverse momentum

(b) Leading $b-$jet pseudorapidity

Figure 3.8: Comparison of the kinematic distributions for the two leading jets from the Higgs decay in the vector Z' simplified model, when fixing the Z' mass to 1000 GeV and varying the DM mass.
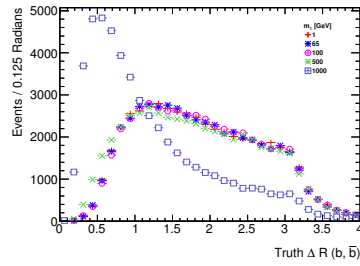
(c) Angular separation of the two leading b-jets

3.1.2 $\not{E}_T$ +*Higgs from a scalar mediator*

A real scalar singlet S coupling to DM can be introduced as a portal between SM and the dark sector through the Higgs field. The most general scalar potential is detailed in Ref. **??**, including terms that break $\mathbb{Z}_2$. This report does not cover the case in which $\mathbb{Z}_2$ holds and therefore the new scalar can be the DM candidate, but follows Ref. **??** introducing an additional coupling to DM that breaks $\mathbb{Z}_2$ and leads to a new invisible decay of S. For this reason, no symmetry is broken and no new interactions arise, so there is no dependence on the vacuum expectation value of S: a shift in the field leads to a redefinition of the model couplings. The new scalar S mixes with the SM Higgs boson, and couples to DM through a Yukawa term y_χ. The relevant terms in the scalar potential are:

$$
V \supset a|H|^2 S + b|H|^2 S^2 + \lambda_h |H|^4
$$
$$
\longrightarrow \tfrac{1}{2}a(h+v)^2 S + \tfrac{1}{2}b(h+v)^2 S^2 + \frac{\lambda_h}{4}(h+v)^4, \qquad (3.4)
$$

where a, b are new physics couplings and λ_h is the Higgs quartic coupling.

The additional Lagrangian terms for this model are:

$$
L \supset -y_\chi \bar{\chi}\chi(\cos\theta\, S - \sin\theta\, h) - \frac{m_q}{v}\bar{q}q(\cos\theta\, h + \sin\theta\, S) \qquad (3.5)
$$

where θ is the mixing angle between the Higgs boson and the new scalar.

Mono-Higgs signals in this second model arise through processes shown in Fig. 3.3 (a,b), or through the radiation of a Higgs boson from the t quark in the production loop, in Fig. 3.3 (c). The first two processes depend on the $h^2 S$ and hS^2 cubic terms in Eq. (3.4). At leading order in $\sin\theta$, these terms are:

$$
V_{\text{cubic}} \approx \frac{\sin\theta}{v}(2m_h^2 + m_S^2)h^2 S + b\,v\,h\,S^2 + ... \qquad (3.6)
$$

with a and λ_h expressed in terms of $\sin\theta$ and m_h^2, respectively. At leading order of $\sin\theta$, the $h^2 S$ term is fixed once the mass eigenvalues m_h, m_S and mixing angle are specified. The $h\,S^2$ term is not fixed and remains a free parameter of the model, depending on the new physics coupling b.

3.1.2.1 *Parameter scan*

The model is described by five parameters:

1. the Yukawa coupling of heavy scalar to dark matter, g_{DM} (also referred to as y_χ)

2. the mixing angle between heavy scalar and SM-like Higgs boson, $\sin\theta$;

3. the new physics coupling, b;

1252   4. mass of heavy scalar, m_S, also termed M_{med};

1253   5. mass of dark matter. m_{DM};

1254   The mixing angle is constrained from current Higgs data to sat-
1255   isfy $\cos\theta = 1$ within 10% and therefore $\sin\theta \lesssim 0.4$. This provides a
1256   starting point for the parameter scan in this model: we recommend
1257   to set $\sin\theta = 0.3$. Figure 3.10 shows that there is no dependence
1258   of the kinematics from the value of this angle, and different values
1259   can be obtained via rescaling the results for this mixing angle ac-
1260   cording to the relevant cross-section. It can also be observed from
1261   Figures 3.11 and 3.9 that the kinematics of this model follows that
1262   of the equivalent jet+$\not{E}_T$ model: only small changes are observed in
1263   the on-shell region, while the relevant distributions diverge when
1264   the mediator is off-shell. For this reason, the same grid in M_{med},
1265 m_{DM} as for the scalar mediator of the jet+$\not{E}_T$ search (Table 2.3) is
1266   chosen as a starting point. The Yukawa coupling to DM y_{DM} is
1267   set to 1, the new physics coupling between scalar and SM Higgs b
1268   = 3. Results for other values can be obtained via a rescaling of the
1269   results for these parameters.

To do **Estimate the sensitivity and possibly prune parameter scan. (??)**
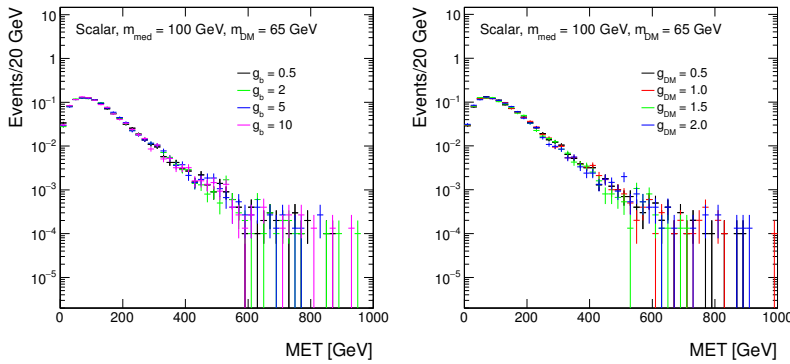
Figure 3.9: Missing transverse momentum distributions at generator level in the scalar mediator scenario, for different values of: the new physics coupling g_b (left), and the mediator-dark matter coupling g_{DM} (right).
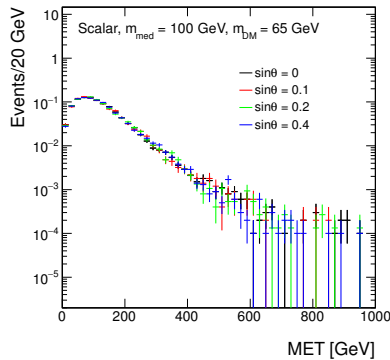
Figure 3.10: Missing transverse momentum distributions at generator level in the scalar mediator scenario: for different values of the mixing angle $\sin\theta$.

1270   Figs. 3.12 and 3.13 show the kinematic distributions for the two
1271   leading jets in the $H \to \bar{b}b$ decay channel, for two values of the
1272   mediator mass and varying the DM mass.

Figure 3.11: Missing transverse momentum distributions at generator level in the scalar mediator scenario: for different values of the dark matter mass m_{DM} and a mediator mass of $M_{med} = 100$ GeV (left) and $M_{med} = 1$ TeV (right).
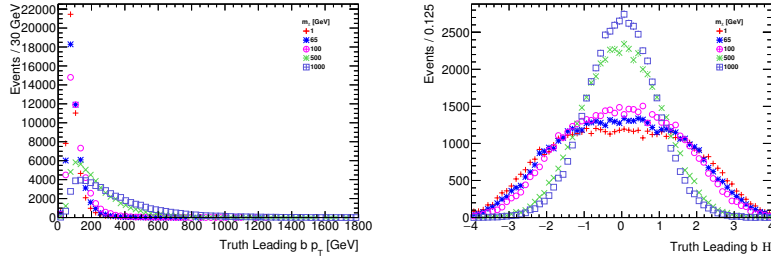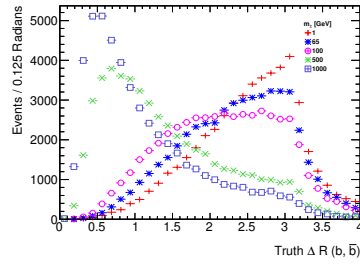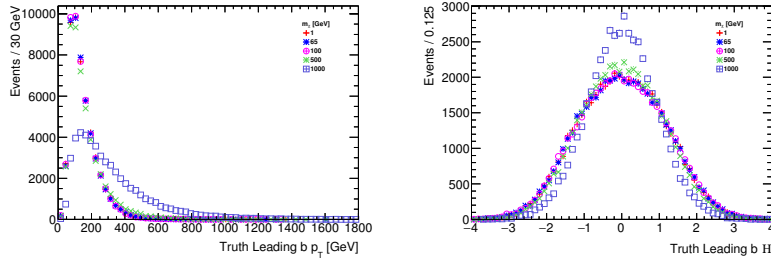

(a) Leading $b-$jet transverse momentum

(b) Leading $b-$jet pseudorapidity

(c) Angular distance between the two leading $b-$jets
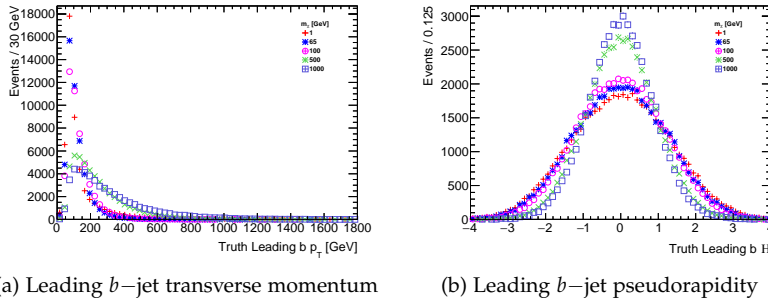
Figure 3.12: Comparison of the kinematic distributions for the two leading jets from the Higgs decay in the scalar simplified model, when fixing the new scalar mass to 100 GeV and varying the DM mass.
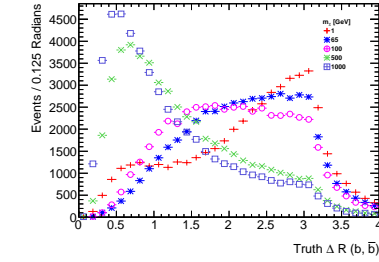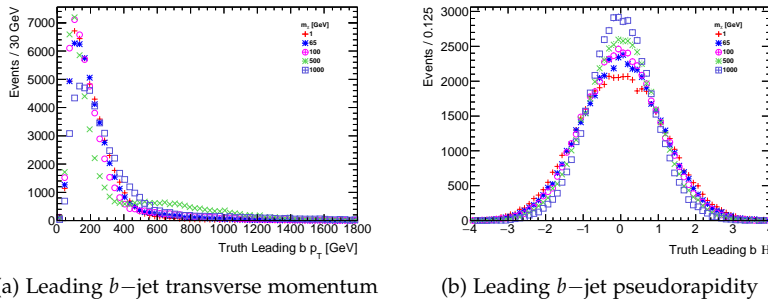
(a) Leading $b-$jet transverse momentum

(b) Leading $b-$jet pseudorapidity
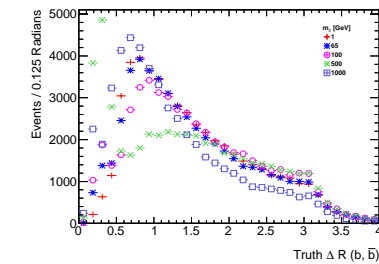
(c) Angular distance between the two leading $b-$jets

Figure 3.13: Comparison of the kinematic distributions for the two leading jets from the Higgs decay in the scalar simplified model, when fixing the new scalar mass to 1000 GeV and varying the DM mass.

3.1.3   Higgs+$\slashed{E}_T$ signal from 2HDM model with a Z' and a new pseu
doscalar

In this simplified model [BLW14], a new Z' resonance decays to a
Higgs boson h plus a heavy pseudoscalar state A^0 in the 2HDM
framework, which in turn decays to a DM pair. This model is represented in the diagram in Fig. 3.2 (b).

   The motivation for coupling the dark matter to the pseudoscalar
is that dark matter coupling to a Higgs or Z' boson is generically
constrained by other signal channels and direct detection. A reason
to consider this model is that it has different kinematics due to
the on-shell Z' production, where for heavy Z' masses the $\slashed{E}_T$ and
p_T spectra are much harder. This model can satisfy electroweak
precision tests and constraints from dijet resonance searches, and
still give a potentially observable Higgs+$\slashed{E}_T$ signal.

   This model comprises two doublets, where Φ_u couples to up-
type quarks and Φ_d couples to down-type quarks and leptons:

$$-\mathcal{L} \supset y_u Q \tilde{\Phi}_u \bar{u} + y_d Q \Phi_d \bar{d} + y_e L \Phi_d \bar{e} + \text{h.c.} \tag{3.7}$$

   After electroweak symmetry breaking, the Higgs doublets attain
vacuum expectation values v_u and v_d, and in unitary gauge the
doublets are parametrized as

$$\Phi_d = \frac{1}{\sqrt{2}} \begin{pmatrix} -\sin\beta\, H^+ \\ v_d - \sin\alpha\, h + \cos\alpha\, H - i\sin\beta\, A^0 \end{pmatrix},$$

$$\Phi_u = \frac{1}{\sqrt{2}} \begin{pmatrix} \cos\beta\, H^+ \\ v_u + \cos\alpha\, h + \sin\alpha\, H + i\cos\beta\, A^0 \end{pmatrix} \tag{3.8}$$

where h, H are neutral CP-even scalars, $H^\pm$ is a charged scalar, and
A^0 is a neutral CP-odd scalar. In this framework, $\tan\beta \equiv v_u/v_d$,
and α is the mixing angle that diagonalizes the $h - H$ mass squared
matrix. We take $\alpha = \beta - \pi/2$, in the limit where h has SM-like
couplings to fermions and gauge bosons as per Ref. [CGT13], and
$\tan\beta \geq 0.3$ as implied from the perturbativity of the top Yukawa
coupling. The Higgs vacuum expectation values lead to $Z - Z'$
mass mixing, with a small mixing parameter given by

$$\epsilon \equiv \frac{1}{M_{Z'}^2 - M_Z^2} \frac{g g_z}{2\cos\theta_w} (z_d v_d^2 + z_u v_u^2)$$

$$= \frac{(M_Z^0)^2}{M_{Z'}^2 - M_Z^2} \frac{2 g_z \cos\theta_w}{g} z_u \sin^2\beta, \tag{3.9}$$

where z_i are the Z' charges of the two Higgs doublets, and g and g_z
related to the mass-squared values in absence of mixing $(M_Z^0)^2 = g^2(v_d^2 + v_u^2)/(4\cos^2\theta_w)$ and $(M_{Z'}^0)^2 = g_z^2(z_d^2 v_d^2 + z_u^2 v_u^2 + z_\phi^2 v_\phi^2)$.

   The production cross section for this model scales as $(g_z)^2$, as the
decay width for this process to leading order in ϵ (Eq. 3.9) is

$$\Gamma_{Z' \to hA^0} = (g_z \cos\alpha \cos\beta)^2 \frac{|p|}{24\pi} \frac{|p|^2}{M_{Z'}^2}. \tag{3.10}$$

1295 where the center of mass momentum for the decay products $|p| =$

1296 $\frac{1}{2M_{Z'}} \sqrt{(M_{Z'}^2 - (m_h + m_{A^0})^2)(M_{Z'}^2 - (m_h - m_{A^0})^2)}$.

1297 *3.1.3.1   Parameter scan*

1298 The model is described by five parameters:

1299 • the pseudoscalar mass M_{A^0},

1300 • the DM mass m_{DM},

1301 • the Z' mass, $M_{Z'}$,

1302 • $\tan\beta (\equiv v_u/v_d)$,

1303 • the Z' coupling strength g_z.

1304 To study the signal production and kinematic dependencies on
1305 these parameters, we produced signal samples varying each of the
1306 five parameters through MADGRAPH5_AMC@NLO for the matrix
1307 element, PYTHIA for the parton shower, and DELPHES[dF⁺14] for
1308 a parameterized detector-level simulation.

1309 As seen in Fig. 3.14, variations of $\tan\beta$ does not lead to any
1310 kinematic difference and the production cross section simply scales
1311 as a function of $\tan\beta$. Hence we recommend to fix $\tan\beta$ to unity in
1312 the signal generation.
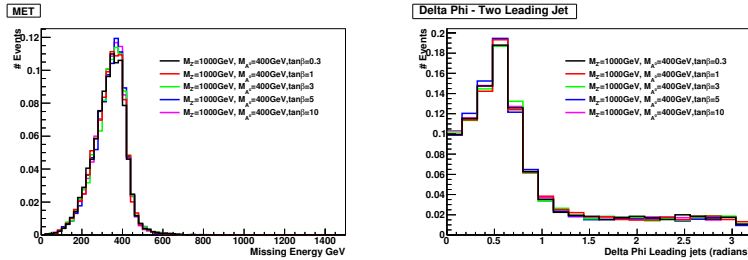
(a) $\not{E}_T$ distribution (b) $\Delta\phi$ distance between the two $b-$ jets

Figure 3.14: Kinematic distributions of the signal process varying $\tan\beta$, in the case of a Higgs boson decaying into two b quarks, after parameterized detector simulation: no kinematic dependency is observed

1313 Similarly, variations of g_z do not lead to any kinematic changes.
1314 The value of g_z for a given $M_{Z'}$ and $\tan\beta$ can be set according to
1315 the maximum value allowed by electroweak global fits and dijet
1316 constraints, as described in [BLW14]. Since this parameter does not
1317 influence the kinematics, we leave it up to individual analyses on
1318 whether they generate benchmark points only according to these
1319 external constraints.

1320 Since the DM pair are produced as a result of the decay of A^0,
1321 there are minimal kinematic changes when varying m_{DM} as long
1322 as $m_{\mathrm{DM}} < M_{A^0}/2$ so that A^0 production is on-shell, as shown in
1323 Fig. 3.15 and 3.16 (before detector simulation).

1324 We recommend to produce signal events for a fixed $g_z = 0.8$,
1325 $\tan\beta = 1$ and $m_{\mathrm{DM}} = 100$ GeV. For these values, we scan the 2-D
1326 parameter space of $M_{Z'}, M_{A^0}$ with $M_{Z'} = 600, 800, 1000, 1200, 1400$ GeV,
1327 and $M_{A^0} = 300, 400, 500, 600, 700, 800$ GeV with $M_{A^0} < M_{Z'} - m_h$,
1328 for a total of 24 points. The choice of scan is justified by the sen-
1329 sitivity study in [BLW14]: the expected LHC sensitivity for Run-2

(a) $\not{E}_T$ distribution

(b) $\Delta\phi$ distance between the two $b-$ jets
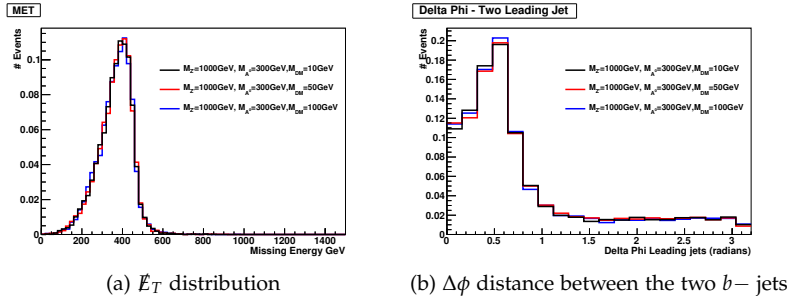
Figure 3.15: Kinematic distributions of the signal process varying m_{DM}: minimal kinematic dependency on m_{DM} as expected when A^0 is produced on-shell. Plots shown for $M_{Z'} = 1000$ GeV, $M_{A^0} = 300$ GeV.
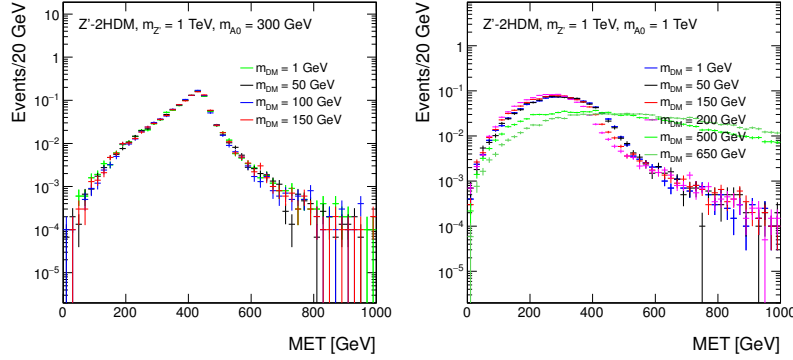
Figure 3.16: Missing transverse momentum distributions at generator level in the Z' +2HDM scenario for different values of the dark matter mass m_{DM}, with $m_{Z'} = 1$ TeV and $m_{A^0} = 300$ GeV (left) and $m_{A^0} = 1$ TeV (right).

is up to $M_{Z'} \sim 1.5$ TeV. For the parameter scan, the DM mass is fixed to 100 GeV. For two $M_{Z'}$, M_{A^0} value sets, we vary the DM mass to obtain sample cross section for rescaling results. All LO cross sections for the various parameter scan points are reported in Appendix B. The parameter scan excludes the off-shell region, as the cross-sections are suppressed and the LHC would not have any sensitivity to these benchmark points in early data.

The kinematic distributions with varying $M_{Z'}$ for fixed M_{A^0} are shown in Fig. 3.17, while the dependency on M_{A^0} is shown in Fig. 3.18.

(a) $\not{E}_T$ distribution

(b) Leading $b-$jet p_T distribution
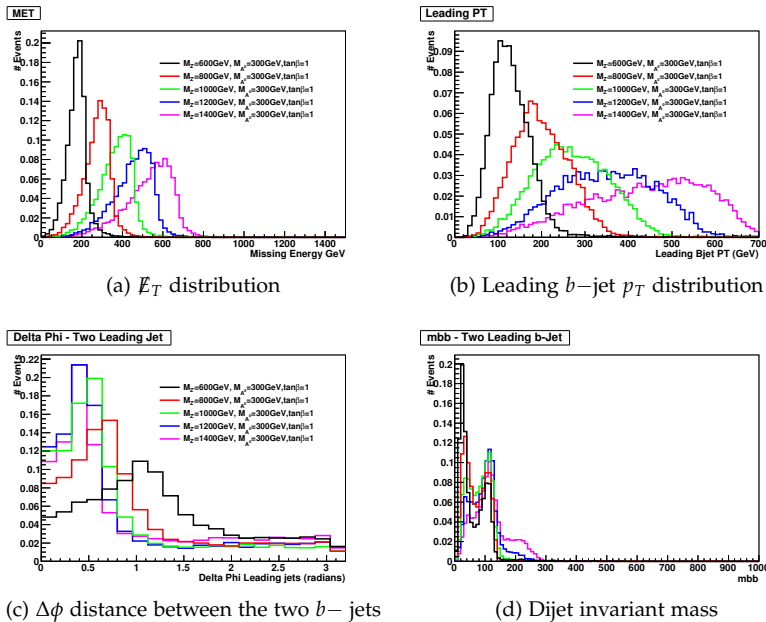
Figure 3.17: Kinematic distributions of the signal process varying $M_{Z'}$, for $m_{\mathrm{DM}} = 100$ GeV, $M_{A^0} = 300$ GeV.

(c) $\Delta\phi$ distance between the two $b-$ jets

(d) Dijet invariant mass

(a) $\not{E}_T$ distribution

(b) Leading $b-$jet p_T distribution

(c) $\Delta\phi$ distance between the two $b-$ jets

(d) Dijet invariant mass
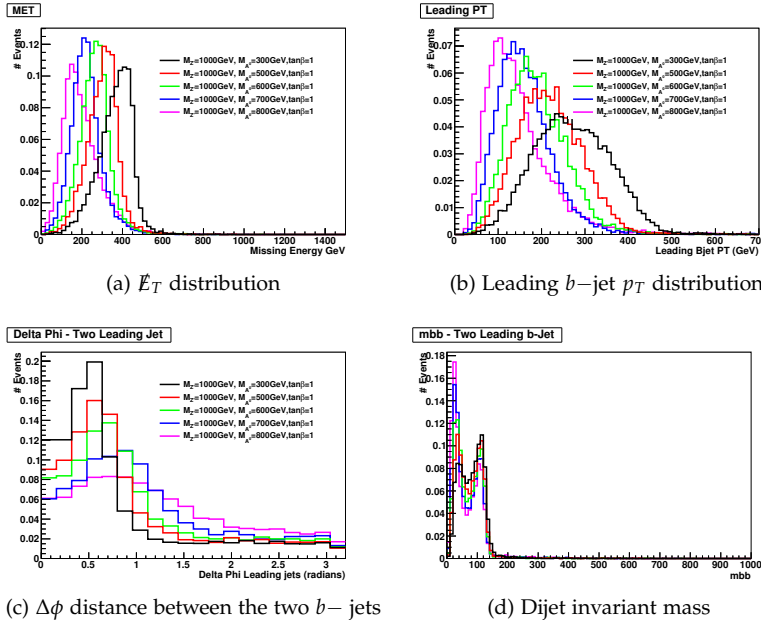
Figure 3.18: Kinematic distributions of the signal process varying M_{A^0}, for $m_{\mathrm{DM}} = 100$ GeV, $M_{Z'} = 1000$ GeV.

This model also allows for an additional source of Higgs plus $\not{E}_T$ signal with a similar kinematics (Fig. 3.19, shown with detector simulation samples) to the signal process from the decay of $Z' \rightarrow hZ$, where the Z decays invisibly. The partial decay width for the Z' is:

$$\Gamma_{Z' \rightarrow hZ} = (g_z \cos\alpha \sin\beta)^2 \frac{|p|}{24\pi} \left(\frac{|p|^2}{M_{Z'}^2} + 3\frac{M_Z^2}{M_{Z'}^2} \right), \qquad (3.11)$$

The values for the Z' masses scanned for those samples should follow those of the previous samples, namely values of $M_{Z'} = 600, 800, 1000, 1200, 1400$ GeV. This signal process has no M_A dependence.
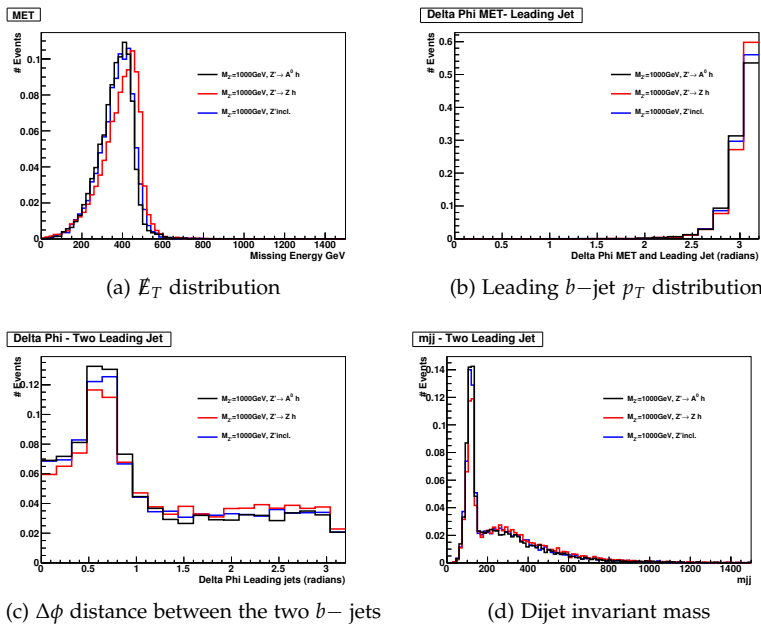
To do **What about visible decays of Z? And isn't monojet still more sensitive? (??)**

Figure 3.19: Kinematic distributions of $Z' \rightarrow A^0 h$ exclusive production, $Z' \rightarrow Zh$ exclusive production and Z' inclusive production for $M_{Z'} = 1000$ GeV and $M_{A^0} = 300$ GeV

(a) $\not{E}_T$ distribution

(b) Leading $b-$jet p_T distribution

(c) $\Delta\phi$ distance between the two $b-$ jets

(d) Dijet invariant mass

1349 THE IMPLEMENTATION OF THESE MODELS IS DISCUSSED IN AP-
1350 PENDIX A.2.1.

3.2   EFT models with direct DM-boson couplings

1352 The EFT operators considered in this section do not have a sim-
1353 plified model completion for Dirac fermion Dark Matter available
1354 to date. They provide kinematic distributions that are unique to
1355 mono-boson signatures, and that in most cases are not reproduced
1356 by an equivalent simplified model.[2]

1357   A complete list of effective operators with direct DM/boson cou-
1358 plings for Dirac DM, up to dimension 7, can be found in [CHLR13,
1359 CNS$^+$13, CHH15]. Higher dimensional operators, up to dimen-
1360 sion 8, leading to Higgs+$\not{E}_T$ signatures, are mentioned in [CNS$^+$13,
1361 BLW14]. The first part of this Section outlines the main characteris-
1362 tics for a limited number of these models that could be considered
1363 in Run-2 searches. However, the EFT approximation made for these
1364 operators can be problematic, see Ref. **??** for discussion. For this
1365 reason, model-independent results as in Appendix C should be
1366 privileged over considering these operators as realistic benchmarks.

1367   However, another consideration that emerged from the Fo-
1368 rum discussion was that the EFT approach allows more model-
1369 independence when reinterpreting results, making it worth still
1370 having results available in terms of these operators. Furthermore,
1371 once simplified models are available for those operators, EFT re-
1372 sults can be used as a limiting case for consistency checks. We
1373 devote the end of this Section to a discussion on the presentation of
1374 results from this model, including an assessment of their reliabil-
1375 ity using a conservative procedure that is only dependent on EFT
1376 parameters.

3.2.1   Dimension 5 operators

1378 The lowest dimension benchmark operators we consider are effec-
1379 tive dimension 5, such as the one depicted in Figure 3.20.
1380   Following the notation of [CNS$^+$13], models from this category
1381 have a Lagrangian that includes terms such as:

$$\frac{m_W^2}{\Lambda_5^3}\, \bar{\chi}\chi \; W^{+\mu}W^-_\mu + \frac{m_Z^2}{2\Lambda_5^3}\, \bar{\chi}\chi \; Z^\mu Z_\mu \,, \qquad (3.12)$$

1382 where m_Z and m_W are the masses of the Z and W boson, W^μ and
1383 Z^μ are the fields of the gauge bosons, χ denotes the Dark Matter
1384 fields and Λ_5 is the effective field theory scale . Note that these
1385 operators are of true dimension 7, but reduce to effective dimension
1386 5 once the Higgs vacuum expectation values, contained in the W
1387 and Z mass terms, are inserted. As such, one expects these that
1388 operators would naturally arise in UV complete models where
1389 Dark Matter interacts via a Higgs portal where heavy mediators
1390 couple to the Higgs or other fields in an extended Higgs sector. In

[2] Wherever this is the case, we recommend only the generation of simplified model result as the results can be rescaled and reinterpreted.

To do **The nomenclature in different models differs from literature:** Λ_5 vs λ **(??)**

Figure 3.20: Diagram for EFT operators giving rise to a Higgs+$\not{E}_T$ signature.
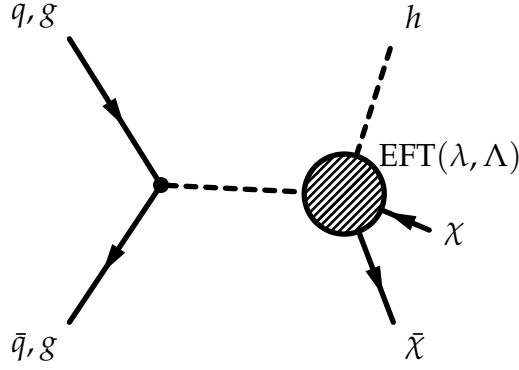
such models the full theory may be expected to contain additional operators with Higgs-Dark Matter couplings [DFMQ13].

Concentrating on mono-gauge boson signals, the above operator induces signatures with $\not{E}_T$ in conjunction with Z and W bosons at tree level, while at loop level it induces couplings to photon pairs and $Z\gamma$ through W loops. In these models, a clear relation exists between final states with photons, EW bosons and Higgs boson.

As shown in Fig. 3.21 kinematics of this model can be approximated by that of a simplified model including a high-mass scalar mediator exchanged in the s-channel described in Section 2.2.2. For this reason, the list of benchmark models with direct boson-DM couplings for photon, Z and W only includes dimension 7 operators: the scalar model with initial state radiation of an EW boson is already recommended and its results can be rescaled.

The Higgs+$\not{E}_T$ analysis, however, will not consider the scalar simplified model as benchmark, due to the very low sensitivity in early LHC analyses, and will instead use this dimension 5 operator.
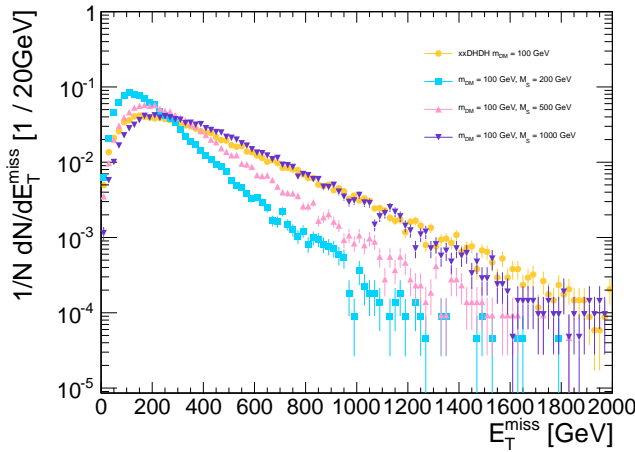
Figure 3.21: Comparison of the missing transverse momentum for the simplified model where a scalar mediator is exchanged in the s-channel and the model including a dimension-5 scalar contact operator, in the leptonic Z+$\not{E}_T$ final state

₁₄₀₈ *3.2.1.1   Parameter scan*

₁₄₀₉ The two parameters of this model are the scale of new physics λ
₁₄₁₀ and the DM particle mass. SM-DM coupling and new physics scale
₁₄₁₁ are related by $g_{DM} = (246 \text{ GeV})/\lambda$. .

₁₄₁₂   The initial value of the new physics scale λ chosen for the sam-
₁₄₁₃ ple generation is 3 TeV; this is a convention and does not affect the
₁₄₁₄ signal kinematics; the cross-section of the samples can be rescaled
₁₄₁₅ according to the λ^3 dependence when deriving the constraints on
₁₄₁₆ this scale. However, more care should be given when rescaling
₁₄₁₇ Higgs+$\not{E}_T$ operators of higher dimensions, as different diagrams
₁₄₁₈ have a different λ dependence.

   The DM mass values for the benchmark points to be simulated
are chosen to span a sufficient Dark Matter range leading to differ-
ent kinematics, that is within the LHC sensitivity for early searches
and that is consistent across the various signatures and EFT op-
erators. We therefore start the mass scan at $m_{DM} = 1$ GeV, where
collider experiments are complementary to direct and indirect de-
tection and choose the last point corresponding to a DM mass of
1 TeV. We recommend a scan in seven mass points, namely:

$$m_{DM} = 1, 10, 50, 100, 200, 400, 800, 1300 \text{ GeV}.$$

₁₄₁₉   A set of kinematic distributions from the Higgs+$\not{E}_T$ signature
₁₄₂₀ where the Higgs decays into two $b-$quarks is shown in Fig. 3.22,
₁₄₂₁ for points similar to those of the grid scan proposed.
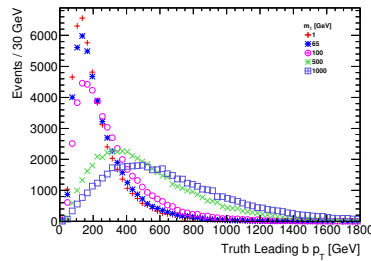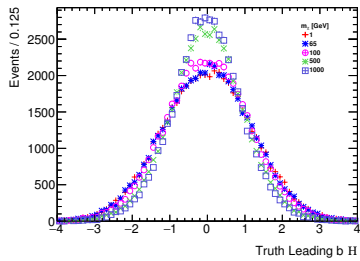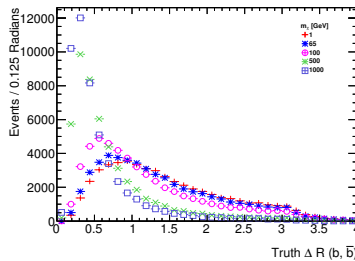
To do **Clarify the reason why this happens in MadGraph5_aMC@NLO through explicit Lagrangian terms? (??)**

To do **Waiting for plot by Bhawna Gomber showing this (??)**

To do **Include unpublished study of rescaling for dimension-8 operators by N. Whallon in dimension-8 section. (??)**

(a) Leading $b-$jet transverse momentum

(b) Leading $b-$jet pseudorapidity

(c) Angular distance between the two leading $b-$jets

Figure 3.22: Comparison of the kine-matic distributions for the two leading $b-$ jets (from the Higgs decay) in the model with direct interactions between the Higgs boson and the DM particle, when varying the DM mass.

₁₄₂₂ *3.2.2   Dimension 7 operators*

The dimension-7 benchmark models contain the $SU(2)_L \times U(1)_Y$
gauge-invariant couplings between DM fields and the kinetic terms

of the EW bosons. The CP-conserving scalar couplings of this type
can be written as

$$\frac{c_1}{\Lambda_S^3} \, \bar{\chi}\chi \, B_{\mu\nu} B^{\mu\nu} + \frac{c_2}{\Lambda_S^3} \, \bar{\chi}\chi \, W_{\mu\nu}^i W^{i,\mu\nu} \,. \tag{3.13}$$

Here $B_{\mu\nu} = \partial_\mu B_\nu - \partial_\nu B_\mu$ and $W_{\mu\nu}^i = \partial_\mu W_\nu^i - \partial_\nu W_\mu^i + g_2 \epsilon^{ijk} W_\mu^j W_\mu^k$
are the $U(1)_Y$ and $SU(2)_L$ field strength tensor, respectively, and g_2
denotes the weak coupling constant. In the case of the pseudoscalar
couplings, one has instead

$$\frac{c_1}{\Lambda_P^3} \, \bar{\chi}\gamma_5\chi \, B_{\mu\nu} \tilde{B}^{\mu\nu} + \frac{c_2}{\Lambda_P^3} \, \bar{\chi}\gamma_5\chi \, W_{\mu\nu}^i \tilde{W}^{i,\mu\nu} \,, \tag{3.14}$$

where $\tilde{B}_{\mu\nu} = 1/2\,\epsilon_{\mu\nu\lambda\rho} B^{\lambda\rho}$ and $\tilde{W}_{\mu\nu}^i = 1/2\,\epsilon_{\mu\nu\lambda\rho} W^{i,\lambda\rho}$ are the dual
field strength tensors. In addition to the CP-conserving interactions
(3.13) and (3.14), there are also four CP-violating couplings that are
obtained from the above operators by the replacement $\bar{\chi}\chi \leftrightarrow \bar{\chi}\gamma_5\chi$.

The effective interactions introduced in (3.13) and (3.14) appear in models of Rayleigh DM [WY12]. Ultraviolet completions
where the operators are generated through loops of states charged
under $U(1)_Y$ and/or $SU(2)_L$ have been proposed in [WY13] and
their LHC signatures have been studied in [LSWY13]. If these new
charged particles are light, the high-p_T gauge bosons that participate in the $\not{E}_T$ processes considered here are able to resolve the
substructure of the loops. This generically suppresses the cross
sections compared to the EFT predictions [HKU13], and thus will
weaken the bounds on the interaction strengths of DM and the EW
gauge bosons to some extent. Furthermore, the light charged mediators may be produced on-shell in pp collisions, rendering direct
LHC searches potentially more restrictive than $\not{E}_T$ searches. Making
the above statements precise would require further studies beyond
the timescale of this forum.

Since for $\Lambda_S = \Lambda_P$ the effective interactions (3.13) and (3.14)
predict essentially the same value of the mono-photon, mono-Z and
mono-W cross section [CNS$^+$13, CHH15], we consider below only
the former couplings. We emphasize however that measurements
of the jet-jet azimuthal angle difference in $\not{E}_T + 2j$ events may be
used to disentangle whether DM couples more strongly to the
combination $B_{\mu\nu} B^{\mu\nu}$ ($W_{\mu\nu}^i W^{i,\mu\nu}$) or the product $B_{\mu\nu} \tilde{B}^{\mu\nu}$ ($W_{\mu\nu}^i \tilde{W}^{i,\mu\nu}$) of
field strength tensors [CHLR13, CHH15].

After EW symmetry breaking the interactions (3.13) induce direct
couplings between pairs of DM particles and gauge bosons. The
corresponding Feynman rule reads:

$$\frac{4i}{\Lambda_S^3} \, g_{V_1 V_2} \left(p_1^{\mu_2} p_2^{\mu_1} - g^{\mu_1\mu_2} \, p_1 \cdot p_2 \right), \tag{3.15}$$

where p_i (μ_i) denotes the momentum (Lorentz index) of the vector
field V_i and for simplicity the spinors associated with the DM fields

have been dropped. The couplings $g_{V_i V_j}$ take the form:

$$
\begin{aligned}
g_{\gamma\gamma} &= c_w^2 c_1 + s_w^2 c_2\,, \\
g_{\gamma Z} &= -s_w c_w \left(c_1 - c_2\right)\,, \\
g_{ZZ} &= s_w^2 c_1 + c_w^2 c_2\,, \\
g_{WW} &= c_2\,,
\end{aligned}
\tag{3.16}
$$

with s_w (c_w) the sine (cosine) of the weak mixing angle. Note that our coefficients c_1 and c_2 are identical to the coefficients C_B and C_W used in [CHH15], while they are related via $k_1 = c_w{}^2 c_1$ and $k_2 = s_w{}^2 c_2$ to the coefficients k_1 and k_2 introduced in [CNS$^+$13].

The coefficients c_1 and c_2 appearing in (3.16) determine the relative importance of each of the $\not{E}_T$ channels and their correlations. For example, one observes that:

- Only c_2 enters the coupling between DM and W bosons, meaning that only models with $c_2 \neq 0$ predict a mono-W signal;

- If $c_1 = c_2$ the mono-photon (mono-Z) signal does not receive contributions from diagrams involving Z (photon) exchange;

- Since numerically $c_w^2/s_w^2 \simeq 3.3$ the mono-photon channel is particularly sensitive to c_1.

3.2.2.1 Parameter scan

As stated above and shown in Ref. [NCC$^+$14], the kinematic distributions for dimension-7 scalar and pseudoscalar operators only shows small differences. This has been verified from a generator-level study: the signal acceptance after a simplified analysis selection ($\not{E}_T >$ 350 GeV, leading jet $p_T > 40$ GeV, minimum azimuthal difference between either of the two jets and the $\not{E}_T$ direction > 0.4) is roughly 70% for both. We therefore only suggest to generate one of the two models.

The differences in kinematics for the various signatures are negligible when changing the coefficients c_1 and c_2, since these coefficient factorize in the matrix element. Only the case $c_1 = c_2 = 1$ is generated as benchmark; other cases are left for reinterpretation as they will only need a rescaling of the cross-sections.

3.2.3 Higher dimensional operators

Many higher dimensional operators can induce signals of photons or $W/Z/H$ bosons in the final state. A complete list can be found in Refs. [CDM$^+$14, BLW14, PS14] and references therein.

Although with lower priority with respect to the operators above, a representative dimension-8 operators can be chosen as benchmark, with the form:

$$
\frac{1}{\Lambda^4} \bar{\chi}\gamma^\mu \chi B_{\mu\nu} H^\dagger D^\nu H
$$
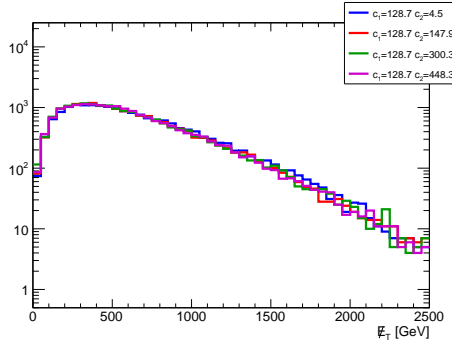
(a) Missing transverse momentum distribution.
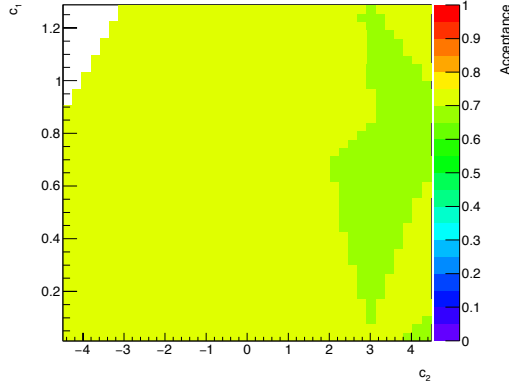
(b) Acceptance.

Figure 3.23: $\not{E}_T$ distribution and acceptance for the dimension-7 model with a hadronically decaying Z in the final state, for the scalar and pseudoscalar operators representing direct interactions between DM and bosons. The y axis units are multiplied by 100.

In this case, the new physics scale is Λ is connected with the coupling of the DM as $y_\chi = \dfrac{1}{\Lambda^4}$. An advantage of this operator is that it includes all signatures with EW bosons, allowing to assess the relative sensitivity of the various channels with the same model. The kinematics for this operator is different with respect to other operators, leading to a harder $\not{E}_T$ spectrum, as illustrated by comparing the leading $b-$jet distribution for the dimension 5 operator to the dimension 8 operator.

To do **Is more detail needed here? (??)**
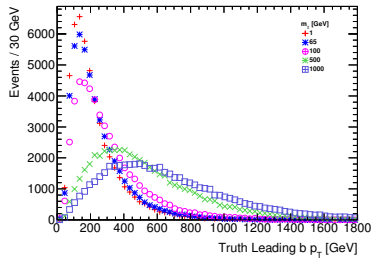
(a) Dimension 5 operator
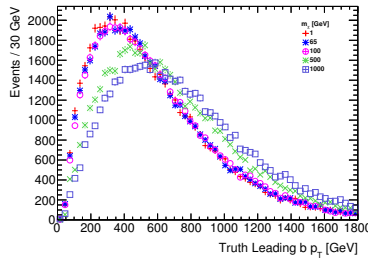
(b) Dimension 7 operator

Figure 3.24: Comparison of the transverse momentum for the leading $b-$ jet from the Higgs decay for a dimension 5 and dimension 7 operator with direct boson-DM couplings.

3.2.4 *Validity of EW contact operators and possible completions*

It is important to remember that the operators described in this section may present problems in terms of the validity of the contact interaction approach for the energy scales reached at the LHC.

As outlined in [BLW14], designing very high $\not{E}_T$ search signal regions that are exclusively motivated by the hard $\not{E}_T$ spectra of the dimension 7 and 8 operators will mean that the momentum transfer in the selected events is larger. This in turn means that processes at that energy scale (mediators, particles exchanged in loops) are accessible, and a simple contact interaction will not be able to correctly describe the kinematics of these signals.

Contact interaction operators like the ones in this section remain useful tools for comparison of the sensitivity of different search channels, and for reinterpretation of other models under the correct assumptions. To date, there are no UV-complete models available for most of those operators: dimension-7 operators are particularly challenging since their completion involves loops [3].

However, this may be the focus of future theoretical exploration, as discussed in Ref. [CHH15]. An example of a complete model for scalar DM corresponding to the dimension-5 operator is provided in the Appendix B. Providing results for the pure EFT limit of these models will prove useful to cross-check the implementation of future.

Given these considerations, the recommendations on the presentation of the results for these models are:

- Deliver fiducial limits on the cross section of any new physics events, without any model assumption, according to the guidelines in Appendix C.

- Assess the percentage of events that pass a condition of validity for the EFT approximation that only depends, and present results removing of the invalid events using the procedure in Section 4 alongside the raw EFT results;

THE IMPLEMENTATION FOR THESE MODELS IS DISCUSSED IN APPENDIX A.2.2.

[3] An example case for the need of loop completions is a simplified model with an additional scalar exchanged at tree level. The scalar couples to WW and ZZ in a gauge-invariant way, Integrating out the mediator does not lead to the Lorentz structure of a dimension-7 operator, so it is not possible to generate dimension-7 operators that satisfy gauge and Lorentz invariance at the same time. A model with a spin-1 mediator cannot be considered as an candidate for completion either, since dimension-7 operators only have scalar or pseudoscalar couplings.

4
Presentation of EFT results

Most of this report has focused on simplified models. Here, we wish to emphasize the utility and applicability of Effective Field Theories (EFTs) in the interpretation of DM searches at the LHC. Given our current lack of knowledge about the nature of a DM particle and its interactions, a model independent interpretation of the collider bounds appears mandatory. This approach should be complemented with an interpretation within a choice of simplified models, which however cannot exhaust the set of possible completions of an effective Lagrangian. Even though the EFT requires an assessment of the conditions that define its applicability, results provided using of a single simplified model at a time do not characterize the full breadth of an EFT that can represent results for many completions at once. In some cases, such as composite WIMPs [], the contact interaction framework is the correct one to constrain new confinement scales.

One problem that has arisen is the attempt to derive a limit on nucleon-dark matter scattering cross sections based on collider data. Experiments that directly probe the nucleon-dark matter scattering cross section are testing the regime of small momentum transfers, where the EFT approximation always holds. Collider experiments are sensitive to large momentum transfers: This is a regime where careful treatment is necessary since the condition of applicability of the EFT may not hold [1].

Ideally, experimental constraints should be shown as bounds of allowed signal events in the kinematic regions considered for the search, as detailed in Appendix C. Constraints comparing different experiments should be expressed as a function of the model parameters rather than on related observables, where the complementarity still be manifest, although this is a point that should be developed further after the conclusion of the work of this Forum. Analyses should do this systematically; until that is done, results can be presented using one of the several prescriptions in the literature [BDSMR14, BDSG$^+$14, BDSJ$^+$14, A$^+$15b, RWZ15]. that can be used to quote bounds on EFT operators.

We first illustrate the problem that can arise with EFTs at colliders by considering an effective interaction

$$(\bar{\psi}\psi)(\bar{\chi}\chi)\frac{g}{\Lambda^2}$$

To do **CD: Asked Tim for reference (??)**

[1] Furthermore, mapping EFT results from high to low momentum requires particular care for some of the operators, see Ref. **??** for a thorough discussion.

that couples SM and DM fields. The strength of this interaction can be parametrized by $f = \frac{g}{\Lambda^2}$. A monojet signature can be generated by applying perturbation theory in the QCD coupling (assuming ψ is a quark, for example). An experimental search will place a limit on f. For a fixed f, a small value of g will correspond to a small value of Λ. The EFT approximation breaks down if $Q > \Lambda$, where Q is a typical hard scale of the process. Thus the limit on small g can only be reliable if the kinematic region $Q > \Lambda$ is removed from the prediction. On the other hand, if, for the same value of f, a large Λ is assumed so that the full kinematic region can be used, a large value of g is required, raising the question if perturbation theory is even applicable.

In the first part of this Section, we summarize some methods that can be used to improve the reliability of the EFT approximation. These methods are described in detail in Refs. [BDSMR14, BDSG$^+$14, BDSJ$^+$14, A$^+$15b, RWZ15, BLW14]. We then propose a recommendation for the presentation of EFT results for early Run-2 LHC searches.

4.1   Outline of the procedure described in Refs. [BDSG$^+$14, A$^+$15b]

A standard approach has been to consider a simplified model and use the connection that the model provides between mediator mass and scale of the interaction to determine the reliability of the EFT approximation. For a tree-level interaction between DM and the Standard Model (SM) via some mediator with mass M_{med}, the EFT approximation corresponds to expanding the propagator for the mediator in powers of $Q_{\mathrm{tr}}^2/M_{\mathrm{med}}^2$, truncating at lowest order, and combining the remaining parameters into a single parameter M_* (also called Λ in the literature). For an example scenario with a Z'-type mediator (leading to some combination of operators D5 to D8 in the EFT limit) this corresponds to setting

$$\frac{g_{\mathrm{DM}}g_{\mathrm{q}}}{Q_{\mathrm{tr}}^2 - M^2} = -\frac{g_{\mathrm{DM}}g_{\mathrm{q}}}{M^2}\left(1 + \frac{Q_{\mathrm{tr}}^2}{M^2} + \mathcal{O}\left(\frac{Q_{\mathrm{tr}}^4}{M^4}\right)\right) \simeq -\frac{1}{M_*^2}, \qquad (4.1)$$

where Q_{tr} is the momentum carried by the mediator, and g_{DM}, g_{q} are the DM-mediator and quark-mediator couplings respectively. Similar expressions exist for other operators. Clearly the condition that must be satisfied for this approximation to be valid is that $Q_{\mathrm{tr}}^2 < M^2 = g_{\mathrm{DM}}g_{\mathrm{q}}M_*^2$. In this framework, there are three regions to consider:

- $Q_{\mathrm{tr}}^2 \sim M^2$, in which case the EFT misses a resonant enhancement, and it is conservative to ignore this enhancement;

- $Q_{\mathrm{tr}}^2 \ll M^2$, in which case the EFT is a good approximation; and

- $Q_{\mathrm{tr}}^2 \gg M^2$, in which case the signal cross section should fall according to a power of Q_{tr}^{-1} instead of M^{-1}. This is the problematic kinematic region.

We can use the condition $Q_{tr}^2 < M^2 = g_{DM}g_q M_*^2$ to restrict the kinematics of the signal and remove events for which the high-mediator-mass approximation made in the EFT would not be reliable. This leads to a smaller effective cross-section, after imposing the event selection of the analysis. This truncated signal can then be used to derive a new, more conservative limit on M_* as a function of $(m_{DM}, g_{DM}g_q)$.

For the example D5-like operator, $\sigma \propto M_*^{-4}$, and so there is a simple rule for converting a rescaled cross section into a rescaled constraint on M_* if the original limit is based on a simple cut-and-count procedure. Defining σ_{EFT}^{cut} as the cross section truncated such that all events pass the condition $\sqrt{g_{DM}g_q}M_*^{rescaled} > Q_{tr}$, we have

$$M_*^{rescaled} = \left(\frac{\sigma_{EFT}}{\sigma_{EFT}^{cut}}\right)^{1/4} M_*^{original}, \qquad (4.2)$$

which can be solved for $M_*^{rescaled}$ via either iteration or a scan. Similar relations exist for a given UV completion of each operator. The details and application of this procedure to ATLAS results can be found in Ref. [A$^+$15b] for a range of operators. Knowledge of the UV completion for a given is necessary for this procedure; this introduces a model-dependence that was not present in the not-truncated EFT results.

If a search is not simply a counting experiment and exploits the shapes of kinematic distributions, the condition on the momentum transfer should be applied on the benchmarks using generator level information, by discarding events that are invalid. This provides the necessary rescaling of the cross section while keeping the information on the change in the kinematic distributions due to the removal of the invalid events.

4.2 *Outline of the procedure described in Ref. [RWZ15]*

In [RWZ15] a procedure to extract model independent and consistent bounds within the EFT is described. This procedure can be applied to any effective Lagrangian describing the interactions between the DM and the SM, and provides limits that can be directly reinterpreted in any completion of the EFT.

The range of applicability of the EFT is defined by a mass scale M_{cut}, a parameter which marks the upper limit of the range of energy scales at which the EFT can be used reliably, independently of the particular completion of the model. Regardless of the details of the full theory, the energy scale for which the EFT is a good approximation is less than the center-of-mass energy E_{cm}, the total invariant mass of the hard final states of the reaction.

The condition ensuring that the EFT approximation is appropriate is, by definition of M_{cut},

$$E_{cm} < M_{cut}. \tag{4.3}$$

For example, in the specific case of a tree level mediation with a single mediator, M_{cut} can be interpreted as the mass of that mediator.

There are then at least three free parameters describing an EFT: the DM mass m_{DM}, the scale M_* of the interaction, and the cutoff scale M_{cut}.

We can use the same technique as above to restrict the signal to the events for which $E_{cm} < M_{cut}$, using only these events to derive the exclusion limits on M_* as a function of (m_{DM}, M_{cut}). We can also define an *effective coupling strength* $M_{cut} = g_* M_*$, where g_* is a free parameter that substitutes the parameter M_{cut}, and therefore derive exclusions on M_* as a function of (m_{DM}, g_*). This allows us to see how much of the theoretically allowed parameter space has been actually tested and how much is still unexplored; For example, in the Z'-type model considered above, g_* is equal to $\sqrt{g_{DM}g_q}$. The resulting plots are shown in [RWZ15] for a particular effective operator.

The advantage of this procedure is that the obtained bounds can be directly and easily recast in any completion of the EFT, by computing the parameters M_*, M_{cut} in the full model as functions of the parameters of the complete theory. On the other hand, the resulting limits will be weaker than those obtained using Q_{tr} and a specific UV completion.

4.3 Comments on Unitarity Considerations

4.4 Presentation of EFT results

A full discussion of the presentation of collider results is left to work beyond this Forum, where ATLAS, CMS, the theory community and the Direct and Indirect Detection communities are involved. In this report we recommend two strategies for the presentation of results in terms of Effective Field Theories. We divide the EFT operators in two categories: those which can be mapped to one or more UV-complete simplified models, such as those commonly used in LHC searches so far and detailed in [GIR+10], and those for which no UV completion is available, such as those outlined in Section 3.2. The For the first case, the EFT is supposed to cover the cases where the mediating particles are heavy, thus overlapping with the simplified models outlined in this report. Results for this first class of operators can be recast starting from simplified models with high mediator masses, therefore removing the need to explicitly simulate EFT events but still effectively providing experimental limits for those operators. For the second class of models, a truncation procedure should be applied for various hypotheses on the goodness of the EFT approximation, and the truncated results presented alongside the full EFT results.

Three proposals for the treatment of EFT have been stated so far, to complement raw EFT results: (1) truncate using Q_{tr}, (2) truncate and iterate using Q_{tr}, and (3) truncate using E_{cm}. The reliability of the EFT approximation can also be quantified by presenting the sensitivity of the results to R, the fraction of events that satisfy $\hat{s} > M_{cut}^2$, for example.

4.5 Recommendation for contact interaction theories with simplified models available

If a simplified model can be mapped to a given EFT, then the model's high-mediator-mass limit will converge to the EFT. This can be seen in Fig. 4.1, where the limits on the scale of the interaction of a Z'-like simplified model are presented in terms of the mediator mass [2]. The limits at high mediator mass for this model are equivalent to those of the corresponding EFT benchmark. For this reason, experimental collaboration should deliver results for high-mass mediators instead of pure EFT results, and leave further reinterpretation to theorists.

We therefore recommend the addition of one point at very high mediator mass (5 TeV) to the scan, for each of the DM masses for the simplified models described in Section 2. The truncation procedure in Section 4.2 can be used to fine-tune the mediator mass to be simulated for this purpose.

[2] This plot only serves as exemplification of the convergence of the simplified model to a contact interaction operator: before this report, ATLAS and CMS searches presented search results up to very high couplings and therefore high widths, potentially probing unphysical corners of phase space
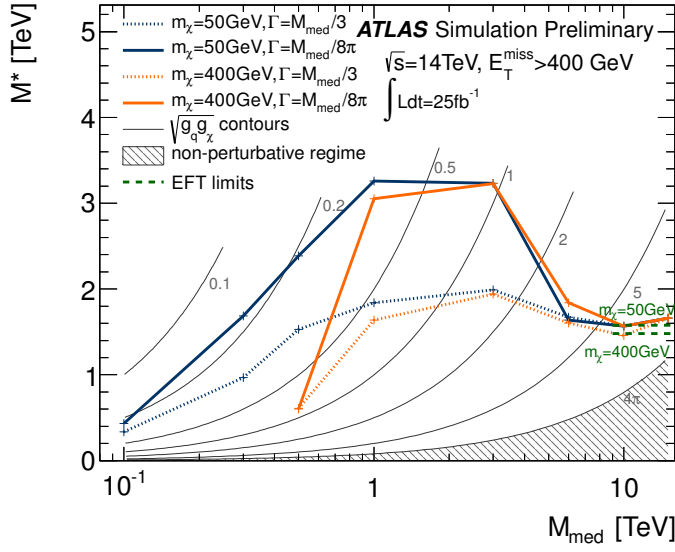
Figure 4.1: Comparison of the 95% CL lower limits on the scale of the interaction of a Z'-like simplified model at 14 TeV, in terms of the mediator mass. Corresponding limits from EFT models are shown on the same plot as green dashed lines to show equivalence between the two models for high mediator masses. Taken from Ref. [ATL14].

4.6   Recommendation for truncation of EFT benchmarks with no simplified models available

Whenever a UV completion is not available, EFT results can still be a source of useful information as described in Section 3.2.4. However, we can only naively control how well the EFT approximation holds. Despite the fact that a propagator was introduced to motivate the truncation procedure for s-channel models, the prescription depends upon the simplified model to derive the energy scaling that is used for the comparison with the momentum transfer. The simple fact remains that the effective coupling of the operator – g/Λ^n – should not allow momentum flow $Q > \Lambda$ or $g > 4\pi$. Given our ignorance of the actual kinematics, the truncation procedure suggested for this purpose is the one described in Section 4.2, as it is independent from any UV completion details.

Because there is no UV completion, the parameter M_{cut} can be treated more freely than an explicit function of g and Λ. It makes sense to choose M_{cut} such that we identify the transition region where the EFT stops being a good description of UV complete theories. This can be done using the ratio R, which is defined as the fraction of events for which $s_{hat} > M_{cut}^2$. For large values of M_{cut}, no events are thrown away in the truncation procedure, and R=1. As M_{cut} becomes smaller, eventually all events are thrown away in the truncation procedure, i.e. $R = 0$, and the EFT gives no exclusion limits for the chosen acceptance.

We propose a rough scan over M_{cut}, such that we find the values of M_{cut} for which R ranges from 0.1 to 1. The analysis can then perform a scan over several values of M_{cut}, and show the truncated limit for each one of them alongside the naive limit corresponding to $R = 1$.

5
Recommendations for evaluation of signal theoretical uncertainties

[Comment on proper PDF sets to use, concerns about sea quark PDF in b-initiated diagrams (perhaps the latter belongs in the b-flavored DM section]

5.1 POWHEG

A comprehensive and careful assessment of theoretical uncertainties plays a much more important role for the background estimations (especially when their evaluation is non-entirely data-driven) than it does for signal simulations. Nevertheless, when using POWHEG it is possible to study scale and PDF errors for the dark matter signals. A fast reweighting machinery is available in POWHEG-BOX that allows one to add, after each event, new weights according to different scale or PDF choices, without the need to regenerate all the events from scratch.

To enable this possibility, the variable `storeinfo_rwgt` should be set to 1 in the POWHEG input file when the events are generated for the first time[1]. After each event, a line starting with

`#rwgt`

is appended, containing the necessary information to generate extra weights. In order to obtain new weights, corresponding to different PDFs or scale choice, after an event file has been generated, a line

`compute_rwgt 1`

should be added in the input file along with the change in parameters that is desired. For instance, `renscfact` and `facscfact` allow one to study scale variations on the renormalization and factorization scales around a central value. By running the program again, a new event file will be generated, named `<OriginalName>-rwgt.lhe`, with one more line at the end of each event of the form

`#new weight,renfact,facfact,pdf1,pdf2`

---

[1] Notice that even if the variable is not present, by default it is set to 1.

followed by five numbers and a character string. The first of these numbers is the weight of that event with the new parameters chosen. By running in sequence the program in the reweighting mode, several weights can be added on the same file. Two remarks are in order.

- The file with new weights is always named

  ```
  <OriginalName>-rwgt.lhe
  ```

  hence care has to be taken to save it as

  ```
  <OriginalName>.lhe
  ```

  before each iteration of the reweighting procedure.

- Due to the complexity of the environment where the program is likely to be run, it is strongly suggested as a self-consistency check that the first reweighting is done keeping the initial parameters. If the new weights are not exactly the same as the original ones, then some inconsistency must have happened, or some file was probably corrupted.

It is possible to also have weights written in the version 3 Les Houches format. To do so, in the original run, at least the token

```
lhrwgt_id 'ID'
```

must be present. The reweighting procedure is the same as described above, but now each new run can be tagged by using a different value for the lhrwgt_id keyword. After each event, the following lines will appear:

```
<rwgt>
<wgt id='ID'>
<wgt id='ID1'>
</rwgt>
```

A more detailed explanation of what went into the computation of every single weight can be included in the <header> section of the event file by adding/changing the line

```
lhrwgt_descr 'some info'
```

in the input card, before each "reweighting" run is performed. Other useful keywords to group together different weights are lhrwgt_group_name and lhrwgt_group_combine.

More detailed information can be obtained by inspecting the document in /Docs/V2-paper.pdf under the common POWHEG-BOX-V2 directory.

5.2 MadGraph5_aMC@NLO *and* SysCalc

SysCalc is a package for use with MadGraph5_aMC@NLO that can calculate dedicated event weights for certain theoretical systematic uncertainties. The output is an XML-based file with all relative weights embedded. These weights can then be used to account for the different systematic uncertainties, namely variations on the α_s emission scale factors, factorization (μ_F) and normalization (μ_R) scales, matching scales, and different parton distribution function (PDF) sets.

The requirements of the package as inputs are :

- A systematics file (which can be generated by MadGraph 5 v. 1.6.0 or later) [A⁺14b, AHM⁺11].

- The Pythia-PGS package (v. 2.2.0 or later) [SMS06]. This is needed only in the case of matching scales variations.

- The availability of LHAPDF5 [WBG05].

- A configuration file (i.e. a text file) specifying the parameters to be varied.

SysCalc supports all leading order computations generated in MadGraph5_aMC@NLO including fixed-order computation and matched-merged computation performed in the MLM scheme [MMPT07]. MadGraph5_aMC@NLO stores additional information inside the event in order to have access to all the information required to compute the convolution of the PDFs with the matrix element for the various supported systematics.

Below follows an example configuration file which could serve as an example:

```
# Central scale factors
scalefact:
0.5 1 2
# Scale correlation
# Special value -1:  all combination (N**2)
# Special value -2:  only correlated variation
# Otherwise list of index N*fac_index + ren_index
#    index starts at 0
scalecorrelation:
-1
# α_s emission scale factors
alpsfact:
0.5 1 2
# matching scales
matchscale:
30 40 80
# PDF sets and number of members (optional)
PDF:
CT10.LHgrid 53
MSTW2008nlo68cl.LHgrid
```

Without matching/merging, SysCalc is able to compute the variation of renormalisation and factorisation scale (parameter `scalefact`) and the change of PDFs. The variation of the scales can be done in a correlated and/or uncorrelated way, basically

following the value of the `scalecorrelation` parameter which can take the following values:

- -1 : to account for all N^2 combinations.

- -2 : to account only for the correlated variations.

- A set of positive values corresponding to the following entries (assuming *0.5, 1, 2* for the `scalefact` entry):

  0: $\mu_F = \mu_F^{\text{orig}}/2, \mu_R = \mu_R^{\text{orig}}/2$

  1: $\mu_F = \mu_F^{\text{orig}}/2, \mu_R = \mu_R^{\text{orig}}$

  2: $\mu_F = \mu_F^{\text{orig}}/2, \mu_R = \mu_R^{\text{orig}}*2$

  3: $\mu_F = \mu_F^{\text{orig}}, \quad \mu_R = \mu_R^{\text{orig}}/2$

  4: $\mu_F = \mu_F^{\text{orig}}, \quad \mu_R = \mu_R^{\text{orig}}$

  5: $\mu_F = \mu_F^{\text{orig}}, \quad \mu_R = \mu_R^{\text{orig}}*2$

  6: $\mu_F = \mu_F^{\text{orig}}*2, \mu_R = \mu_R^{\text{orig}}/2$

  7: $\mu_F = \mu_F^{\text{orig}}*2, \mu_R = \mu_R^{\text{orig}}$

  8: $\mu_F = \mu_F^{\text{orig}}*2, \mu_R = \mu_R^{\text{orig}}*2$

Without correlation, the weight associated to the renormalisation scale is the following:

$$\mathcal{W}_{\text{new}}^{\mu_R} = \frac{\alpha_S^N(\Delta * \mu_R)}{\alpha_S^N(\mu_R)} * \mathcal{W}_{\text{orig}}, \tag{5.1}$$

where Δ is the scale variation considered, $\mathcal{W}_{\text{orig}}$ and $\mathcal{W}_{\text{new}}$ are respectively the original/new weights associated to the event. N is the power in the strong coupling for the associated event (interference is not taken account on an event by event basis). The weight associated to the scaling of the factorisation scale is:

$$\mathcal{W}_{\text{new}}^{\mu_F} = \frac{f_{1,\text{orig}}(x_1, \Delta * \mu_F) * f_{2,\text{orig}}(x_2, \Delta * \mu_F)}{f_{1,\text{orig}}(x_1, \mu_F) * f_{2,\text{orig}}(x_2, \mu_F)} * \mathcal{W}_{\text{orig}}, \tag{5.2}$$

where $f_{i,\text{orig}}$ are the probabilities from the original PDF set associated to the incoming partons, which hold a proton momentum fraction x_1 and x_2 for the first and second beam respectively.

The variations for the PDF are given by the corresponding weights associated to the new PDF sets:

$$\mathcal{W}_{\text{new}}^{\text{PDF}} = \frac{f_{1,\text{new}}(x_1, \mu_F) * f_{2,\text{new}}(x_2, \mu_F)}{f_{1,\text{orig}}(x_1, \mu_F) * f_{2,\text{orig}}(x_2, \mu_F)} * \mathcal{W}_{\text{orig}}, \tag{5.3}$$

where $f_{i,\text{new}}$ is the new PDF probability associated to parton i.

In presence of matching, MADGRAPH5_AMC@NLO performs already a scale and PDF rescaling, such that the scale of the strong interaction is set according to a parton shower history (selected via a k_T clustering). SYSCALC can perform the associated re-weighting (parameter `alpsfact`) by dividing and multiplying by the associated factor.

For each vertex of the clustering (associated to a scale μ_i), this corresponds to the following factor for a Final State Radiation :

$$\mathcal{W}_{\text{new}}^{\text{FSR}} = \frac{\alpha_s(\Delta * \mu_i)}{\alpha_s(\mu_i)} * \mathcal{W}_{\text{orig}}, \qquad (5.4)$$

and the following expression for Initial State Radiation (associated to a scale μ_i and fraction of energy x_i):

$$\mathcal{W}_{\text{new}}^{\text{ISR}} = \frac{\alpha_s(\Delta * \mu_i)}{\alpha_s(\mu_i)} \frac{\frac{f_a(x_i, \Delta * \mu_i)}{f_b(x_i, \Delta * \mu_{i+1})}}{\frac{f_a(x_i, \mu_i)}{f_b(x_i, \mu_{i+1})}} * \mathcal{W}_{\text{orig}}, \qquad (5.5)$$

where μ_{i+1} is the scale of the next vertex in the initial state clustering history.

SysCalc can include the weight associated to different merging scales in the MLM matching/merging mechanism (for output of the `pythia6` package or `pythia-pgs` package). In that case, the parton-shower keeps track of the scale of the first emission and applies then a veto to account for the minimal allowed value for the matching scale according to the cut performed at parton-level. SysCalc will then test for each of the values specified in the parameter `matchscale` if the event passes the MLM criteria or not. If it does not, then a zero weight is associated to the event, while if it does, then a weight 1 is kept. As a reminder, those weights are the equivalent of having a (approximate) Sudakov form-factor and removing at the same time the double counting between the events belonging to different multiplicities.

Finally, we give an example of the SysCalc output which follows the LHEF v3 format. The following block appears in the header of the output file:

```
<header>
  <initrwgt>
    <weightgroup type="Central scale variation" combine="envelope">
      <weight id="1"> mur=0.5 muf=0.5 </weight>
      <weight id="2"> mur=1 muf=0.5 </weight>
      <weight id="3"> mur=2 muf=0.5 </weight>
      <weight id="4"> mur=0.5 muf=1 </weight>
      <weight id="5"> mur=1 muf=1 </weight>
      <weight id="6"> mur=2 muf=1 </weight>
      <weight id="7"> mur=0.5 muf=2 </weight>
      <weight id="8"> mur=1 muf=2 </weight>
      <weight id="9"> mur=2 muf=2 </weight>
    </weightgroup>
    <weightgroup type="Emission scale variation" combine="envelope">
      <weight id="10"> alpsfact=0.5</weight>
      <weight id="11"> alpsfact=1</weight>
      <weight id="12"> alpsfact=2</weight>
    </weightgroup>
    <weightgroup type="CT10nlo.LHgrid" combine="hessian">
      <weight id="13">Member 0</weight>
      <weight id="14">Member 1</weight>
      <weight id="15">Member 2</weight>
      <weight id="16">Member 3</weight>
      ...
      <weight id="65">Member 52</weight>
    </weightgroup>
  </initrwgt>
</header>
```

For each event, the weights are then written as follows:

```
<rwgt>
  <wgt id="1">83214.7</wgt>
  <wgt id="2">61460</wgt>
  <wgt id="3">47241.9</wgt>
  <wgt id="4">101374</wgt>
  ...
  <wgt id="64">34893.5</wgt>
  <wgt id="65">41277</wgt>
</rwgt>
```

6
Conclusions

Points to be made in a conclusion:

To do **write the conclusion (??)**

- In the case of s-channel simplified models, in particular, there is complementarity between searches for dark matter and visible particles. Thus, limits on invisible decays must be consistent with dijet and dilepton searches. In the case of the mono-top simplified model, limits on visible single-top final states must be considered.

- There are many implicit assumptions that have not been laid out entirely in our presentation. As stated earlier, the term *dark matter* in this report refers to a putative dark matter candidate. The details of a particular mono-X analysis rely on the fact that a WIMP exists, and that it is collider-stable. The observation of a signal consistent with WIMP production does can only provide indirect or confirming evidence of a dark matter particle.

- The presentation of results comparing different experimental frontiers has to be done carefully and clearly. We see the need for broader discussions on this topic.

- The experiments should aim to present limits on production cross sections corrected for acceptance when this is viable.

- The Appendix contains a presentation of some models that came out in our discussions that were not deemed a priority for early Run2 analyses. However, these should be considered in the future.

This is a placeholder table

First name	Last Name	Grade
John	Doe	7.5
Richard	Miles	2

A

Appendix: Implementation of Models

A.1 Implementation of s-channel and t-channel models for $\not{E}_T$ +X analyses

There are several matrix element implementations of the DM production through spin-0 and spin-1 mediators. This Appendix collects the generator recommendations and available implementations of these models for different final states, together with studies of the matching between the matrix element and the parton shower.

A.1.1 Implementation of models for mono-jet signature

For a spin-1 mediator, the implementation in POWHEG generates DM pair production with 1 parton at next-to-leading order (NLO), whilst MadGraph5_aMC@NLO and MCFM are at leading order (LO) [1]. As shown in POWHEG Ref. [HKR13], including NLO corrections result in an enhancement in the cross section as compared to LO and though this is not significant, it does lead to a substantial reduction in the dependence on the choice of the renormalization and factorization scale and hence the theoretical uncertainty on the signal prediction. Since NLO calculations are available for the process in POWHEG, we recommend to proceed with POWHEG as the generator of choice.

For a spin-0 mediator in the mono-jet final state, the top-quark loop is the most important consideration. The matrix element implementation of the s-channel spin-0 mediated DM production is available in MCFM [FW13, HKSW15] and POWHEG [HR15] with the full top-loop calculation at LO. The POWHEG and MCFM implementations include the full calculation of the top loop for DM pair production with 1 parton at LO. For consistency with the spin-1 generation, we recommend using POWHEG for this case as well.

Here, we document some specific settings needed to run the POWHEG generation for the Dark Matter models. POWHEG parameter cards for all models can be found on the Forum SVN repository [For15h, For15j, For15k, For15i].

- POWHEG can handle the generation of events (be it at LO or NLO) in two different modes explained in the following. The second one is the recommended one. The relevant keywords in the input card are `bornsuppfact` and `bornktmin`.

  1. unweighted events:
     `bornsuppfact`: negative or absent
     `bornktmin <PT>`
     This runs the program in the most straightforward way, but most likely it is not the more convenient choice, as will be explained below. POWHEG will generate unweighted events using a sharp lower cut (with value PT) on the leading-jet p_T. Since this is a generation cut, the user should make sure that the value used for `bornktmin` is lower than the actual analysis cut to be eventually used. It is good practice to use as a value in the input card a transverse momentum 10-20% smaller than the final analysis cut, and check that the final result is independent, by exploring an even smaller value of `bornktmin`. The drawback of this running mode is that it's difficult to populate well and in a single run both the low-p_T region as well as the high-pT tail.

  2. weighted events:
     `bornsuppfact <PTS>`
     `bornktmin <PT>`

[1] spin-0 and spin-1 mediator models will also be provided in the near future to the same precision in MadGraph5_aMC@NLO [A+14b].

POWHEG will now produce weighted events, thereby allowing to generate a single sample that provides sufficient statistics in all signal regions. Events are still generated with a sharp lower cut set by bornktmin, but the bornsuppfact parameter is used to set the event suppression factor according to

$$F(k_T) = \frac{k_T^2}{k_T^2 + \texttt{bornsuppfact}^2} \ .$$ (A.1)

In this way, the events at, for instance, low $\not{E}_T$, are suppressed but receive an higher weight, which ensures at the same time higher statistics at high $\not{E}_T$. We recommend to set bornsuppfact to 1000.

The bornktmin parameter allows to suppress the low $\not{E}_T$ region even further by starting the generation at a certain value of k_T also in this running mode. It is recommended to set this parameter to half the lower analysis $\not{E}_T$ cut. For instance for the event selection used in the CMS/ATLAS monojet analyses, assuming the lowest $\not{E}_T$ region being defined above 300 GeV, the proposed value for bornktmin is 150. However, this parameter should be set keeping in mind the event selection of all the analyses that will use these signal samples and hence a threshold lower than 150 may be required.

• Remove the runningwidth keyword, or set it to 0, which is the default value. Running with fixed widths is the recommended option. Although there are limitations, this is the more straightforward, simple and transparent option, and it was used for Forum studies.

While not recommended, the alternative, a running width for the propagator of the *s*-channel mediator, can be selected by setting runningwidth to 1. In this case the denominator of the mediator's propagator

$$Q^2 - M^2 + iM\Gamma$$

is replaced by

$$Q^2 - M^2 + iQ^2\frac{\Gamma}{M}$$

where Q is the virtuality of the mediator, and M and Γ are its mass and width respectively. See Ref. [BBB$^+$89] for a discussion.

• Set the parameters defining the bounds on the invariant mass of the Dark Matter pair, mass_low and mass_high, to -1. In this way, POWHEG will assign values internally.

• The minimal values for ncall1, itmx1, ncall2, itmx2 are 250000, 5, 1000000, 5 for the vector model, respectively.

• The minimal values for ncall1, itmx1, ncall2, itmx2 are 100000, 5, 100000, 5 for the scalar top-loop model, respectively.

• When NLO corrections are included (as for instance in the vector model), negative-weighted events could happen and should be kept in the event sample, hence withnegweights should be set to 1. If needed, their fraction can be decreased by setting foldsci and foldy to bigger value (2 for instance). foldphi can be kept to 1.

• Since the scalar model with top-loop is computed as a leading order process, set L0events and bornonly are set to 1 internally.

• One can benefit from the automatic calculation of systematic uncertainties associated with the choice of hard scale and PDFs as described in Section 5.

SAMPLING CONSIDERATIONS FOR HEAVY NARROW MEDIATORS Figure 2.7 suggests a change in the shape of the $\not{E}_T$ distribution for a $M_{\text{med}} = 5$ TeV mediator once $\Gamma_{\text{min}}/M_{\text{med}}$ is of the order of a percent or lower. Such heavy mediators, although inacessible by the LHC data, are interesting since they provide a good approximation for benchmark EFT models. The observed difference among the simplified models in the plot arises from the fact that the region of low invariant masses of the Dark Matter pair, $m_{\bar{\chi}\chi}$, is suppressed due to narrow Breit-Wigner peak that only probes a narrow window of parton distribution functions. For wider mediators, the low mass region is significantly enhanced by parton distribution functions at low Bjorken x, as illustrated in Fig. 2.8. This explains why the sample with the narrowest mediator in Fig. 2.7 is heavily suppressed in terms of production cross section and also gives different $\not{E}_T$ shape. Furthermore, Fig. 2.7 compares the vector model with 5 TeV mediator to the D5 EFT sample and reveals that the simplified models with larger mediator widths (e.g. for couplings of 1) are the ones resembling the kinematics

To do **Emanuele:"On the usage of fixed or running width. It is my opinion that one should use fixed widths. Although clearly there are limitations, I think this goes into the direction of making all as simple and transparent as possible. Moreover, all the discussions in the last months as well as the large majority of runs were done with fixed widths. Since there was some interest over the last couple of weeks, here is my suggestion for the POWHEG section." (??)**

To do **Steve: The reason I originally asked the question was because we saw about 20 years ago that there were cases when using this prescription was important. Now, this is mainly for SM particles, but we apply it throughout for non-SM ones. If we find no significant difference, then we can say it. But, if we are starting from scratch, why shouldn't we include as much correct physics as we can? (??)**

of contact interactions. This is because the production in the EFT model is always off-shell, i.e. no peak in the $m_{\bar{\chi}\chi}$ distribution is present.

However, the complete story of generating heavy narrow mediators is a cautionary tale about understanding the details of the generator tools. Observations of kinematic changes or cross section suppression in the generated samples do not always come from physics, but may be a consequence of under-sampling phase space in the generator implementation, where a cutoff for the regions far away from the mediator mass is generally used. One must take care to correctly set the width of the Breit-Wigner used for the sampling. This is illustrated in Fig. A.1 showing the invariant mass of the Dark Matter pair in the samples generated in MadGraph5_aMC@NLO for a $M_{\text{med}} = 7$ TeV scalar mediator with different coupling strengths, using the default settings `bwcutoff` equal to 15. In all cases, it is expected to observe a peak around the mediator mass with a tail extending to $m_{\bar{\chi}\chi} \to 0$, significantly enhanced by parton distribution functions at low Bjorken x. For coupling strength 1 and 3, the massive enhancement at $m_{\bar{\chi}\chi} \to 0$ implies that resonant production at $m_{\bar{\chi}\chi} = 7$ TeV is statistically suppressed such that barely any events are generated there. However, for narrower mediators with couplings below 1, the peak around 7 TeV is clearly visible in the generated sample and the dominant tail at $m_{\bar{\chi}\chi} \to 0$ is artificially cut off, leading to unphysical cross section predictions and kinematic shapes.
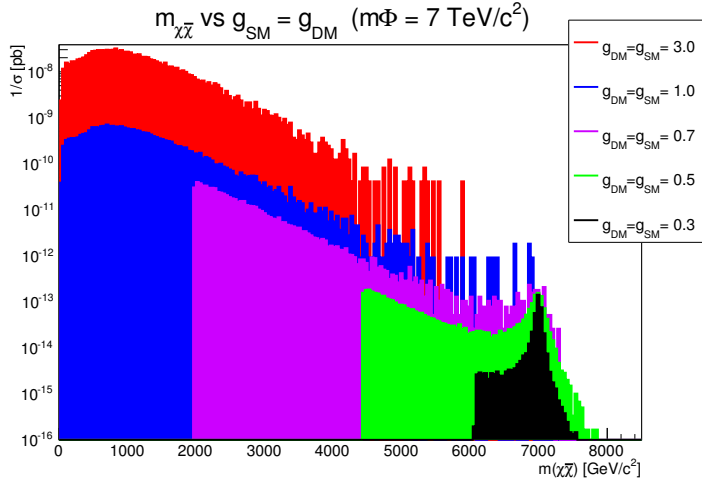
Figure A.1: Invariant mass of the Dark Matter pair in the scalar mediator samples with $m_{\text{DM}} = 1$ GeV, $M_{\text{med}} = 7$ TeV and different coupling strengths.

A.1.2   Parton matching studies

Whenever models for mono-jet final states are generated in MadGraph5_aMC@NLO, it is necessary to avoid double counting the partons from matrix elements and parton showering in PYTHIA 8 using a parton matching technique. Based on the comparative study in Ref. [A+08], there is some advantage to using the CKKW-L matching scheme. However, the current CKKW-L matching scheme is not amenable to the event generation model of the experimental collaborations. Most large scale event generation is performed using LHE files that have a mix (or "soup") of different parton level processes in each file. This is easy to handle using the MLM matching scheme provided as a PYTHIA 8 plugin.

A.1.2.1   Implementation of MLM matching

Here, add the process generation steps, and the matching parameters for LHE file production. Also, provide the PYTHIA 8 configuration to produce hadronic events.

The validation of matching has been performed extensively by the collaborations for a large number of SM and BSM models, and need not be reproduced here.

In order to describe the signal kinematics correctly and save time during MC production, the parton emissions will only be generated up to a certain multiplicity. The higher multiplicity samples usually have small enough cross sections and the corresponding parts of the phase space can be sufficiently approximated by parton showering in PYTHIA 8. A dedicated study comparing samples generated with up to 1-, 2-, or 3-parton multiplicities was performed, using again the settings for the CKKW-L k_t-merging with the 80 GeV matching scale and the `Merging:nJetMax` parameter adjusted accordingly. Figure A.2 shows the $\not{E}_T$ distribution of the samples at $\not{E}_T > 250$ GeV.

To do **This is probably a TODO for Steve M. (??)**

With an event selection requiring $\not{E}_T$ and the leading jet p_T being larger than 250 GeV and allowing for up to 3 jets with $p_T > 30$ GeV, the sample generated with up to 1 parton has 17.4% smaller yield compared to the sample with up to 3 partons, while the yield of the sample with up to 2 partons is only 2.2% smaller. Note the jet multiplicity cut is importnat here as the agreement between the two samples improves at higher $\not{E}_T$ when the cut is not applied. A similar comparison is shown in Fig. A.3 for the jet multiplicity in the events with the leadning jet $p_T > 250$ GeV, where an agreement at the level of $\sim 3\%$ between the samples with up to 2 and 3 parton emissions is observed for number of jets up to 7. This justifies it is sufficient to produce samples with up to 2 parton emissions only at the generator level and ignore generating higher parton emissions.

(a) No jet multiplicity cut   (b) $N_{\text{jet}} \leqslant 3$
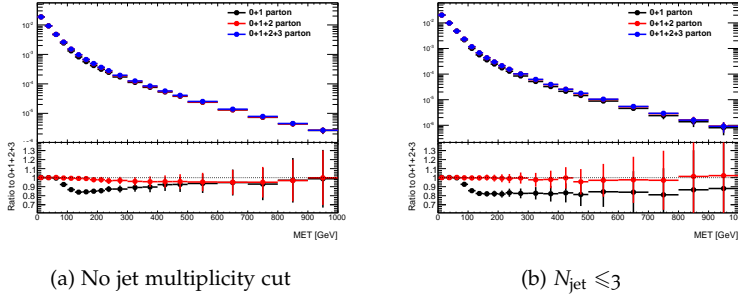
Figure A.2: Missing transverse momentum distributions for EFT D5 sample with CKKW-L matching scale at 80 GeV produced with maximum 1 (black), 2 (red) and 3 (blue) partons emitted at the generator level. The ratios are shown with respect to the latter sample.
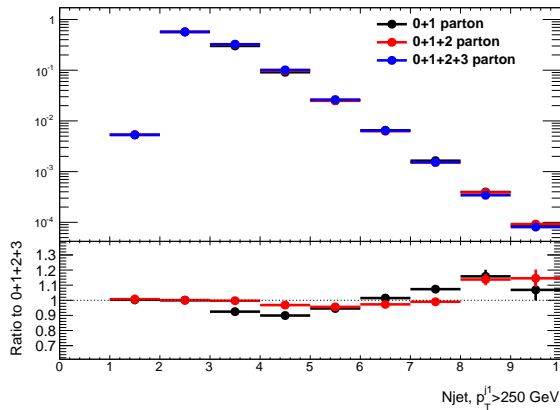
Figure A.3: Multiplicity of jets with $p_T > 30$ GeV and $|\eta| < 2.8$ for EFT D5 sample with CKKW-L matching scale at 80 GeV produced with maximum 1 (black), 2 (red) and 3 (blue) partons emitted at the generator level. The ratios are shown with respect to the latter sample. The leading jet p_T is required to be larger than 250 GeV.

A.1.3   *Implementation of models for EW final states*

These models are generated at leading order with MADGRAPH5_AMC@NLO 2.2.2, using Pythia8 for the parton shower. Parameter cards can be found on the Forum SVN repository [For15a]. No parton matching is required.

A.1.4   *Implementation of models with heavy flavor quark signatures*

The models for the $t\bar{t}$ and $b\bar{b}$ signatures are generated at leading order with MADGRAPH5_AMC@NLO 2.2.2, using Pythia8 for the parton shower. No matching is needed. Parameter cards can be found on the Forum SVN repository [For15d]. No parton matching is required.

We simulate the bFDM model using the MG5_aMC v2.2.3, using Pythia8 for the parton shower. No matching is needed. The corresponding card files can be found on the Forum SVN repository [For15f].

A.1.4.1   *Quark flavor scheme and masses*

In this particular model we recommend an additional care when choosing the flavor scheme generation and whether quarks should be treated as massive or massless.

The production of DM+$b\bar{b}$, Dark Matter in association with b jets via a decay of a (pseudo) scalar boson, is dominated in simplified mediator models by the gluon-gluon initiated production, similar to the production of Z+$b\bar{b}$ at the LHC. The Z+$b\bar{b}$

2141 process has been studied in detail in the Z(ll)+b-jets final state, which can be used
2142 to validate both the modeling of DM+bb and, its main background, Z(vv)+$b\bar{b}$. In
2143 this context, the p_T of the Z boson is related to the observed MET, whereas the b-jet
2144 kinematics determines the ratio of mono-b/di-b signatures in the detector.
2145 For basic kinematic criteria applied to Z+$b\bar{b}$ production, this process leads in
2146 $\sim$ 90% of the events to a signature with only 1 b-jet in the acceptance ('Z+1b-jet
2147 production') and only in $\sim$ 10% of the events to a signature with 2 b-jets in the
2148 detector ('Z+2b-jets production'). The production cross section of the Z+$b\bar{b}$ pro-
2149 cess are calculated in the 'five-flavor scheme', where b quarks are assumed mass-
2150 less, and the 'four-flavor scheme', where massive b quarks are used [CEMW04,
2151 MMW05, CEMW06], and data favor the cross-section predictions in the five-flavor
2152 scheme [C$^+$14]. We therefore recommend to calculate the cross sections of these
2153 models in the 5-flavor scheme, as in the repository. The PDF used to calculate these
2154 cross section is NNPDF3.0 (lhaid 263000).
2155 It is found that the best modeling of two b-quarks final states is achieved using a
2156 4-flavor scheme and a massive treatment of the b-quarks [C$^+$14, C$^+$13, Col15]. We
2157 recommend to use in the generation NNPDF3.0 set (lhaid 263400). Since figure A.4
2158 shows that there is no significant difference in the kinematics between either flavor
2159 scheme used for DM+$b\bar{b}$ production, we recommend the 4-flavor scheme to follow
2160 the observation in the Z+$b\bar{b}$ measurements.
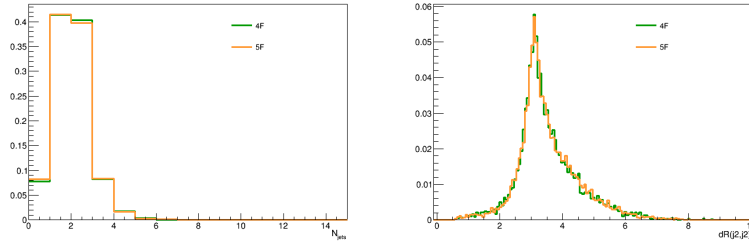
Figure A.4: Comparison of the jet multiplicity (left) and angular correction $\Delta R(j_1, j_2)$ (right) for the DM+$b\bar{b}$ scalar model generated in the 4-flavor and 5-scheme. The samples are generated for $m_\chi = 1$ GeV and $m_\phi = 10$ GeV.

A.2   Implementation of specific models for $V + \not{E}_T$ analyses

A.2.1   Model implementation for mono-Higgs models

2163 All three Higgs+$\not{E}_T$ models are generated at leading order with MadGraph5_aMC@NLO
2164 2.2.2, using pythia 8 for the parton shower. No matching is needed. The Mad-
2165 Graph5_aMC@NLO implementations of the scalar and vector models can be
2166 found on the Forum SVN repository [For15g], while the 2HDM model can be found
2167 at this link [For15b].
2168 In all cases, it is recommended not to handle the h decay through MadGraph5_aMC@NLO
2169 as it does not include the proper h branching ratios, or, if using MadGraph5_aMC@NLO,
2170 then the resulting cross section should be rescaled to match onto the correct branch-
2171 ing ratio.

2172 MadGraph5_aMC@NLO details for scalar mediator Higgs+MET model
2173 In this model, the contribution from the $gghS$ box is included through an effec-
2174 tive Lagrangian evaluated in the large m_t limit. This may overestimate the rates of
2175 the $h + \not{E}_T$ signal [HKU13], but a full evaluation is left to future studies.

2176 MadGraph5_aMC@NLO details for 2HDM Higgs+MET model
2177 The two couplings that can be changed in the implemented model follow the
2178 nomenclature below:

2179 • Tb - $\tan\beta$

2180 • gz - g_z, gauge coupling of Z' to quarks

2181 The other couplings are not changed, including gx (the $A\bar{\chi}\chi$ coupling) which has lit-
2182 tle impact on the signal. $\sin\alpha$ is fixed internally such that $\cos(\beta - \alpha) = 0$. The width
2183 of the Z' and A can be computed automatically within MadGraph5_aMC@NLO.
2184 The couplings here don't affect the signal kinematics, so they can be fixed to default
2185 values and then the signal rates can be scaled appropriately.
2186 The nomenclature for the masses in the implemented model is:

2187 • MZp - PDG ID 32 - Z'

2188 • MA0 - PDG ID 28 - A

2189   • MX - PDG ID 1000022 - dark matter particle

2190   The other masses are unchanged and do not affect the result. Both $Z' \rightarrow hZ(\bar{\nu}\nu)$
2191   and $Z' \rightarrow hA(\bar{\chi}\chi)$ contribute to the final state, scaling different with model pa-
2192   rameters. We recommend to generate them separately, and then add the two signal
2193   processes together weighted by cross sections.

A.2.2   *Implementation of EFT models*

2195   These models are generated at leading order with MADGRAPH5_AMC@NLO 2.2.2,
2196   using PYTHIA 8 for the parton shower. No matching is performed. Parameter cards
2197   can be found on the Forum SVN repository: [For15g] for operators with Higgs+MET
2198   final states and [For15c] for $W/Z/\gamma$ final states.

B

Appendix: Additional models for Dark Matter searches

B.1 Models with a single top−quark + $\not{E}_T$

Many different theories predict final states with a single top and associated missing transverse momentum (monotop), some of them including dark matter candidates. A simplified model encompassing the processes leading to this phenomenology is described in Refs. [AFM11, AAB$^+$14, BCDF15], and is adopted as one of the benchmarks for Run 2 LHC searches.

The simplified model is constructed by imposing that the model Lagrangian respects the electroweak $SU(2)_L \times U(1)_Y$ gauge symmetry and by requiring minimality in terms of new states to supplement to the Standard Model fields. As a result, two monotop production mechanisms are possible. In the first case, the monotop system is constituted by an invisible (or long-lived with respect to detector distances) fermion χ and a top quark. It is produced, as shown in the diagram of B.1 (a) where a colored resonance φ lying in the triplet representation of $SU(3)_C$ decays into a top quark and a χ particle. In the second production mode, the monotop state is made of a top quark and a vector state V connected to a hidden sector so that it could decay invisibly into, e.g., a pair of dark matter particles as studied in [BCDF15]. The production proceeds via flavor-changing neutral interactions of the top quark with a quark of the first or second generation and the invisible V boson (see the diagrams of B.1 (b) and (c)).
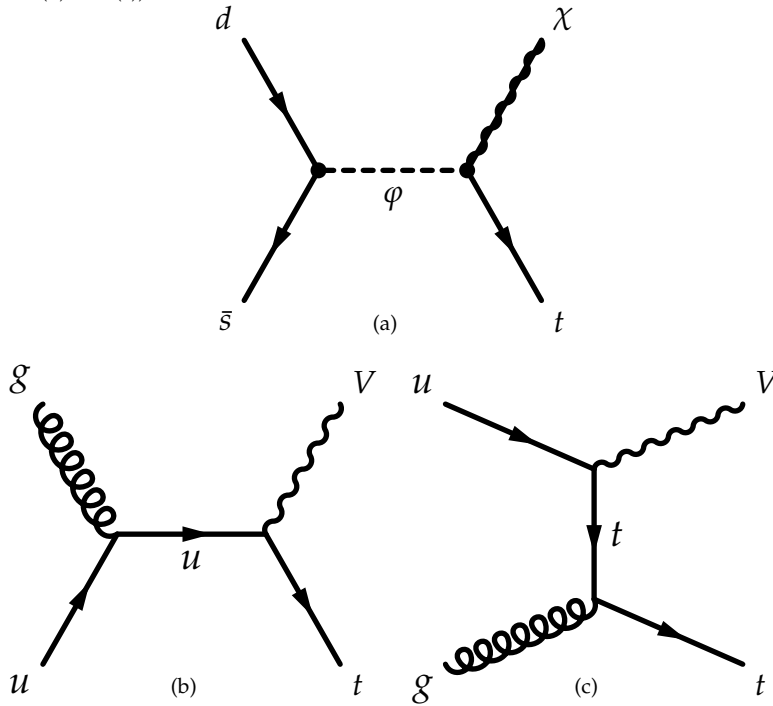
Figure B.1: Feynman diagrams of leading order processes leading to monotop events: production of a coloured scalar resonance φ decaying into a top quark and a spin-1/2 fermion χ (a), $s-$ (b) and t-channel (c) non resonant production of a top quark in association with a spin-1 boson V decaying invisibly.

RESONANT PRODUCTION

In this case, a colored 2/3-charged scalar (φ) is produced and decays into a top quark and a spin-1/2 invisible particle, χ. The dynamics of the new sector is

described by the following Lagrangian:

$$\mathcal{L} = \left[\varphi \bar{d}^c \left[a_{SR}^q + b_{SR}^q \gamma_5 \right] d + \varphi \bar{u} \left[a_{SR}^{1/2} + b_{SR}^{1/2} \gamma_5 \right] \chi + \text{h.c.} \right], \tag{B.1}$$

where u (d) stands for any up-type (down-type) quark, the notation SR refers to the monotop production mechanism via a scalar resonance and all flavor and color indices are understood for clarity.

In the notation of [AAB$^+$14], the couplings of the new colored fields to down-type quarks are embedded into the 3×3 antisymmetric matrices a_{SR}^q (scalar couplings) and b_{SR}^q (pseudoscalar couplings) while those to the new fermion χ and one single up-type quark are given by the three-component vectors $a_{SR}^{1/2}$ and $b_{SR}^{1/2}$ in flavor space.

Under the form of Eq. (B.1), the Lagrangian is the one introduced in the original monotop search proposal [AFM11]. It has been used by the CMS collaboration for Run I analyses after neglecting all pseudoscalar components of the couplings and adding the vector resonance case for which minimality requirements are difficult to accommodate [K$^+$15]. In contrast, the study of Ref. [BCDF15] has imposed electroweak gauge invariance and required minimality. This enforces all new couplings to be right-handed so that

$$a_{SR}^{1/2} = b_{SR}^{1/2} = \frac{1}{2} y_s^* \qquad \text{and} \qquad a_{SR}^q = b_{SR}^q = \frac{1}{2} \lambda_s \, , \tag{B.2}$$

where the objects y_s and λ_s are a tridimensional vector and a 3×3 matrix in flavor space respectively. This class of scenarios is the one that has been adopted by the ATLAS collaboration for its Run I monotop searches [ATL15] and will be considered by both collaborations for Run II analyses.

The resulting model can be likened to the MSSM with an R-parity violating of a top squark to the Standard Model down-type quarks and an R-parity conserving interaction of a top quark and a top-squark to a neutralino.

Non-Resonant production

For non-resonant monotop production, the monotop state is produced via flavor-changing neutral interactions of the top quark, a lighter up-type quark and a new invisible vector particle V. This is the only case considered, as having a new scalar would involve in particular a mixing with the SM Higgs boson and therefore a larger number of free parameters. The Lagrangian describing the dynamics of this non-resonant monotop production case is:

$$\mathcal{L} = \left[V_\mu \bar{u} \gamma^\mu \left[a_{FC}^1 + b_{FC}^1 \gamma_5 \right] u + \text{h.c.} \right] \tag{B.3}$$

where the flavor and color indices are again understood for clarity.

The strength of the interactions among these two states and a pair of up-type quarks is modeled via two 3×3 matrices in flavor space a_{FC}^1 for the vector couplings and b_{FC}^1 for the axial vector couplings.

As for the resonant case, the Lagrangian of Eq. (B.3) is the one that has been used by CMS after reintroducing the scalar option for the invisible state and neglecting all pseudoscalar interactions [CMS14]. As already mentioned, a simplified setup motivated by gauge invariance and minimality has been preferred so that, as shown in Ref. [BCDF15], we impose all interactions to involve right-handed quarks only in order to simplify the model phenomenology,

$$a_{FC}^1 = b_{FC}^1 = \frac{1}{2} a_R \tag{B.4}$$

where a_R denotes a 3×3 matrix in flavor space. This implies the vector field to be an $SU(2)_L$ singlet.

Model parameters and assumptions

The models considered as benchmarks for the first LHC searches contain further assumptions in terms of the flavor structure of the model with respect to the Lagrangians of the previous subsection.

In order to have an observable monotop signature at the LHC, the Lagrangians introduced above must include not too small couplings of the new particles to first and second generation quarks. For simplicity, we assumed that only channels enhanced by parton density effects will be considered, so that we fix

$$(a_R)_{13} = (a_R)_{31} = a \, ,$$
$$(\lambda_s)_{12} = -(\lambda_s)_{21} = \lambda \qquad \text{and} \qquad (y_s)_3 = y \, , \tag{B.5}$$

all other elements of the matrices and vectors above being set to zero.

To do **There is still an on-going study that should be finished very soon (by the end of the week). The point is that CMS is fixing the y parameters in the way that the branching ratio of the scalar resonance into a monotop system is close to 100%, while ATLAS is fixing y = lambda. We are investigating both cases so to conclude**

IMPLEMENTATION

The Monte Carlo simulation relevant for this case is discussed in Appendix A.

B.1.1   Parameter scan

Under all the assumptions of the previous sections, the parameter space of the resonant model is defined by four quantities, namely the mass of the new scalar field φ, the mass of the invisible fermion χ and the strengths of the interactions of the scalar resonance with the monotop system y and with down-type quarks λ. One of both coupling parameters could however be traded with the width of the resonance.

The parameter space of the non-resonant model is defined by two parameters, namely the mass of the invisible state V and its flavour-changing neutral coupling to the up-type quarks a_R.

In the case of the non-resonant model, the invisible vector is connected to a hidden sector that could be, in its simplest form, parameterized by a new fermion [BCDF15]. This has effects on the width of the invisible V state.

A consensus between the ATLAS and CMS collaborations has been reached in the case of non-resonant monotop production. The results have been described above. In contrast, discussions in the context of resonant monotop production are still on-going. The related parameter space contains four parameters and must thus be further simplified for practical purposes. Several options are possible and a choice necessitates additional studies that will be achieved in a near future.

It has been verified that the kinematics do not depend on the width of the invisible state in the case where this width is at most 10% of the V-mass. This is illustrated in Figures B.2 and B.3, where we respectively show the invariant-mass and transverse-momentum spectra of the V-boson when it decays into a top-up final state and for different V-boson masses. The results are however independent of the visible or invisible decay modes as we are only concerned with the kinematical properties of the invisible state.
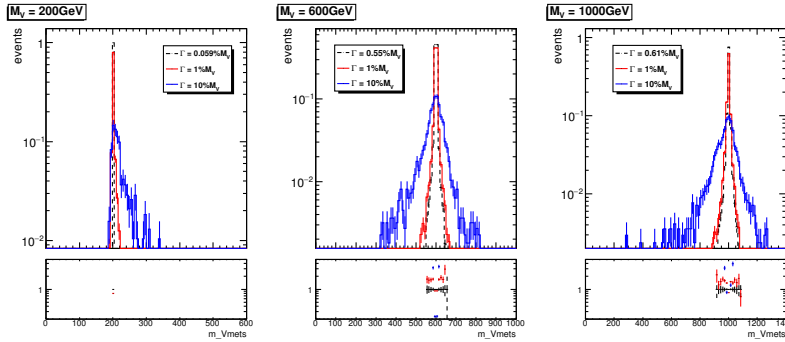
To do **Pictures will be improved in the next drafts. (??)**

Figure B.2: Distributions of the invariant mass of the V boson in the case of the process $pp \to tV \to t(t\bar{u} + \text{c.c.})$. We have imposed that the V-boson is produced on-shell and have chosen its mass to be $m_V = 200$, 600 and 1000 GeV (left, central and right panels). Moreover, we have considered three possible cases for the total width of the V-boson, which has been fixed to 0.61%, 0.1% and 10% of the mass.
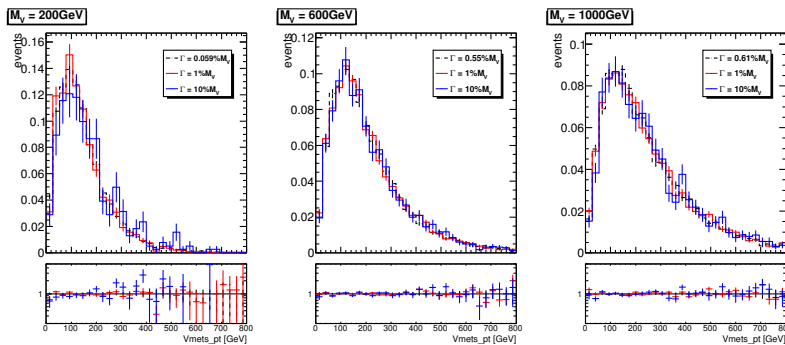

Figure B.3: Same as Figure B.2 in the case of the transverse-momentum distribution of the V-boson.

B.1.2   Single Top Models

Card files for MADGRAPH5_AMC@NLO are provided on the Forum SVN repository [For15e], corresponding to the Lagrangian from [AFM11]. Each coupling

To do **This section is being reworked by B. Fuks (??)**

constant of this model can be set via the parameter card and the blocks which are relevant for the two models used for the experimental searches are described below. The relevant parameters in the MADGRAPH5_AMC@NLO parameter cards, also expressed in the notation introduced in the previous Section, are as follows for the two models considered.

1. Resonant scalar model described by the Lagrangian (B.1)

   - AQS and BQS: 3×3 matrices (flavour space) fixing the coupling of the scalar ϕ (S stands for scalar) and *down*-type quarks (Q stands for quarks), previously called a^q/b^q_{SR}.

   - A12S and B12S: 3×1 matrices (flavor space) fixing the coupling of the new fermion χ (where 12 stands for spin-1/2 fermion) and *up*-type quarks, previously called $a^{1/2}_{VR}$.

2. Non-resonant vectorial model described by the Lagrangian (B.3)

   - A1FC and B1FC: 3×3 matrices (flavor space) fixing the coupling of the vector V (1 stands for vector) and *up*-type quarks, previously called a^1_{FC}.

   - particle name: the dark matter candidate χ is not implemented

The width of the scalar resonance and of the new vector are set to all allowed decays in the ATLAS implementation, while the only allowed decay in the CMS implementation to the new fermion and a top quark for the resonant model.

> To do **Continue discussion between ATLAS and CMS to reach an agreement, or include instructions to compare results. (??)**

B.2   Further W+$\not{E}_T$ models with possible cross-section enhancements

As pointed out in Ref. [BCD$^+$15], the mono-W signature can probe the iso-spin violating interactions of dark matter with quarks. The relevant operators after the electroweak symmetry breaking is

$$\frac{1}{\Lambda^2}\overline{\chi}\gamma_\mu\chi\left(\overline{u}_L\gamma^\mu u_L + \xi\overline{d}_L\gamma^\mu d_L\right). \tag{B.6}$$

Here, we only keep the left-handed quarks because the right-handed quarks do not radiate a W-gauge boson from the weak interaction. As the LHC constraints the cutoff to higher values, it is also important to know the corresponding operators before the electroweak symmetry. At the dimension-six level, the following operator

$$\frac{c_6}{\Lambda^2}\overline{\chi}\gamma_\mu\chi\,\overline{Q}_L\gamma^\mu Q_L \tag{B.7}$$

conserves iso-spin and provides us $\xi = 1$ [BCD$^+$15]. At the dimension-eight level, new operators appear to induce iso-spin violation and can be

$$\frac{c_8^d}{\Lambda^4}\overline{\chi}\gamma_\mu\chi\,(H\overline{Q}_L)\gamma^\mu(Q_L H^\dagger) + \frac{c_8^u}{\Lambda^4}\overline{\chi}\gamma_\mu\chi\,(\tilde{H}\overline{Q}_L)\gamma^\mu(Q_L \tilde{H}^\dagger). \tag{B.8}$$

After inputting the vacuum expectation value of the Higgs field, we have

$$\xi = \frac{c_6 + c_8^d\,v_{\text{EW}}^2/2\Lambda^2}{c_6 + c_8^u\,v_{\text{EW}}^2/2\Lambda^2}. \tag{B.9}$$

For a nonzero c_6 and $v_{\text{EW}} \ll \Lambda$, the iso-spin violation effects are suppressed. On the other hand, the values of c_6, c_8^d and c_8^u depend on the UV-models.

There is one possible UV-model to obtain a zero value for c_6 and non-zero values for c_8^d and c_8^u. One can have the dark matter and the SM Higgs field charged under a new $U(1)'$ symmetry. There is a small mass mixing between SM Z-boson and the new Z' with a mixing angle of $\mathcal{O}(v_{\text{EW}}^2/M_{Z'}^2)$. After integrating out Z', one has different effective dark matter couplings to u_L and d_L fields, which are proportional to their couplings to the Z boson. For this model, we have $c_6 = 0$ and

$$\xi = \frac{-\frac{1}{2} + \frac{1}{3}\sin^2\theta_W}{\frac{1}{2} - \frac{2}{3}\sin^2\theta_W} \approx -2.7 \tag{B.10}$$

and order of unity.

B.3 Simplified model corresponding to dimension-5 EFT operator

As an example of a simplified model corresponding to the dimension-5 EFT operator described in Section 3.2, we consider a Higgs portal with a scalar mediator. Models of this kind are among the most concise versions of simplified models that produce couplings of Dark Matter to pairs of gauge-bosons. Scalar fields may couple directly to pairs of electroweak gauge bosons, but must carry part of the electroweak vacuum expectation value. One may thus consider a simple model where Dark Matter couples to a a scalar singlet mediator, which mixes with the fields in the Higgs sector.

$$L \subset m_s S^2 + \lambda S^2 H^2 + \lambda' S H^2 + y S \chi \overline{\chi} \tag{B.11}$$

Where H is a field in the Higgs sector that contains part of the electroweak vacuum expectation value, S is a heavy scalar singlet and χ is a Dark Matter field. There is then an s-channel diagram where DM pairs couple to the singlet field S, which then mixes with a Higgs-sector field, and couples to W and Z bosons. This diagram contains 2 insertions of EW symmetry breaking fields, corresponding in form to the effective dimension-5 operator in Section 3.2.1.

B.4 Inert 2HDM Model

For most of the simplified models included in this report, the mass of the mediator and couplings/width are non-trivial parameters of the model. In these scenarios, we remain agnostic about the theory behind the dark matter sector and try to parameterize it in simple terms.

We have not addressed how to extend the simplified models to realistic and viable models which are consistent with the symmetries of the Standard Model. Simplified models often violate gauge invariance which is a crucial principle for building a consistent BSM model which incorporates SM together with new physics. For example, with a new heavy gauge vector boson mediating DM interactions, one needs not just the dark matter and its mediator, but also a mechanism which provides mass to this mediator in a gauge invariant way.

Considering both the simplified model and other elements necessary for a consistent theory is a next logical step. The authors of [BCI$^+$] term these Minimal Consistent Dark Matter (MCDM) models. MCDM models are at the same time still toy models that can be easily incorporated into a bigger BSM model and explored via complementary constraints from collider and direct/indirect DM search experiments as well as relic density constraints. We discuss this model here both on its own merits and as an example of the flexibility of the simplified model approach.

The idea of an inert Two-Higgs Doublet Model (i2HDM) was introduced more than 30 years ago in [DM78, LHNOT07, DS09, GHS13, BCI$^+$]. It is an extension of the SM with a second scalar doublet ϕ_2 with no direct coupling to fermions. This doublet has a discrete Z_2 symmetry, under which ϕ_2 is odd and all the other fields are even. The Lagrangian of the odd sector is,

$$\mathcal{L} = \frac{1}{2}(D_\mu \phi_2)^2 - V(\phi_1, \phi_2) \tag{B.12}$$

with the potential V containing mass terms and $\phi_1 - \phi_2$ interactions:

$$\begin{aligned} V = & -m_1^2(\phi_1^\dagger \phi_1) - m_2^2(\phi_2^\dagger \phi_2) + \lambda_1(\phi_1^\dagger \phi_1)^2 + \lambda_2(\phi_2^\dagger \phi_2)^2 \\ & + \lambda_3(\phi_2^\dagger \phi_2)(\phi_1^\dagger \phi_1) + \lambda_4(\phi_2^\dagger \phi_1)(\phi_1^\dagger \phi_2) + \frac{\lambda_5}{2}\left[(\phi_1^\dagger \phi_2)^2 + (\phi_2^\dagger \phi_1)^2\right], \end{aligned} \tag{B.13}$$

where ϕ_1 and ϕ_2 are SM and inert Higgs doublets respectively carrying the same hypercharge. These doublets can be parameterized as

$$\phi_1 = \frac{1}{\sqrt{2}}\begin{pmatrix} 0 \\ v+H \end{pmatrix} \qquad \phi_2 = \frac{1}{\sqrt{2}}\begin{pmatrix} \sqrt{2}h^+ \\ h_1 + ih_2 \end{pmatrix} \tag{B.14}$$

In addition to the SM, i2HDM brings four more degrees of freedom coming from the inert doublet in the form of Z_2-odd charged scalar h$^\pm$ and two neutral Z_2-odd scalars h$_1$ and h$_2$. The lightest neutral scalar, h_1 is identified as the dark matter candidate. The i2HDM model has been explored at the phenomenological level from the perspective of collider DM searches [BPtV01, AHT08, ATYY14, BCI$^+$]. This model could produce $\not{E}_T$ +jet, Z, and Higgs as well as $\not{E}_T$ +VBF signatures at the LHC (see Figs. B.4–B.9).

An experimental analysis of the parameter space has recently been performed in Ref. [BCI$^+$]. The authors of that study have implemented the model in CalcHEP

Figure B.4: Feynman diagrams for $gg \to h_1 h_1 + g$ process contributing to mono-jet signature, adapted from [BCI+].
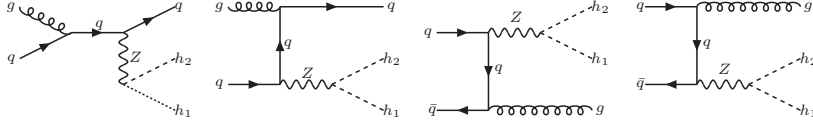
Figure B.5: Feynman diagrams for $q\bar{q} \to h_1 h_2 + g$ ($gq \to h_1 h_2 + q$) process contributing to mono-jet signature, adapted from [BCI+].

and micrOMEGAs and propose a set of benchmark points (Table. B.1). Though the overall parameter space of i2HDM is 5-dimensional, the parameter space relevant to a specific LHC signature is only 1-2 dimensional. In the mono-jet case, one can use two separate simplified models, a $gg \to h_1 h_1 + g$ process (via Higgs mediator) and a $q\bar{q} \to h_1 h_2 + g$ ($gq \to h_1 h_2 + q$) process (using Z-boson mediator) to capture the physics relevant to the search.
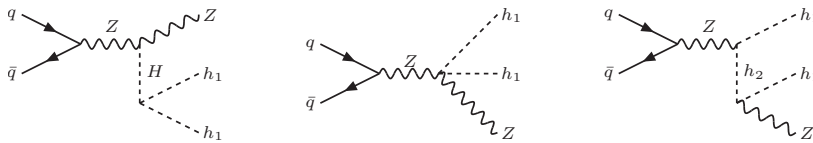
Figure B.6: Feynman diagrams for $q\bar{q} \to h_1 h_1 + Z$ process contributing to mono-Z signature, adapted from [BCI+].
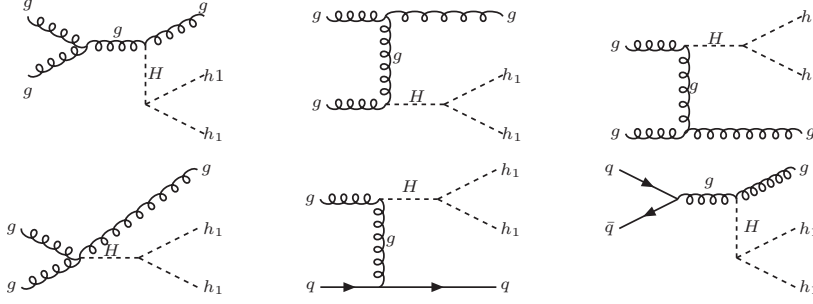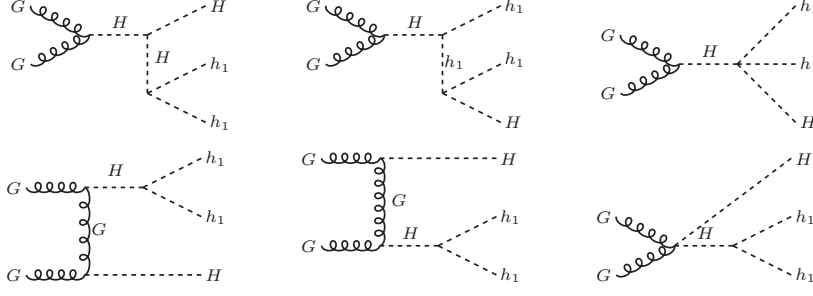
Figure B.7: Feynman diagrams for $gg \to h_1 h_1 + H$ process contributing to mono-Higgs signature, adapted from [BCI$^+$].
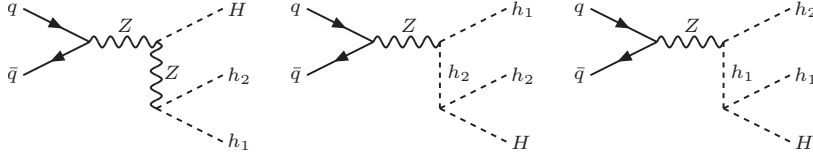
Figure B.8: Feynman diagrams for $q\bar{q} \to h_1 h_2 + H$ process contributing to mono-Higgs signature, adapted from [BCI$^+$].
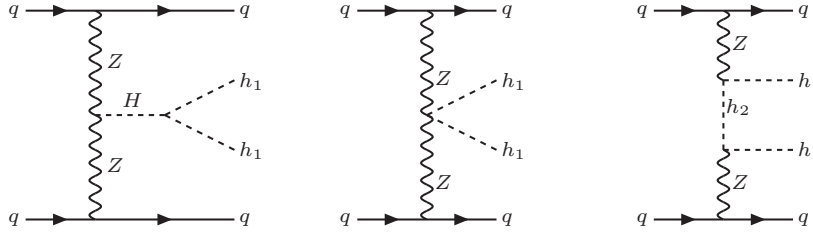
Figure B.9: Diagrams for $qq \to qqh_1 h_1$ DM production in vector boson fusion process, adapted from [BCI$^+$].

Benchmark	1	2	3	4	5
M_{h_1} (GeV)	45	53	66	82	120
M_{h_2} (GeV)	55	189	77	89	140
$M_{h_\pm}$ (GeV)	130	182	122	150	200
λ_2	0.8	1.0	1.1	0.9	1.0
λ_{345}	-0.010	-0.024	$+0.022$	-0.090	-0.100
Ω_h^2	1.1×10^{-1}	8.1×10^{-2}	9.9×10^{-2}	1.5×10^{-2}	2.1×10^{-3}
σ_{SI} (fb)	1.9×10^{-7}	7.9×10^{-7}	4.2×10^{-7}	4.5×10^{-7}	2.6×10^{-6}
σ_{LHC} (fb)	1.7×10^2	7.7×10^2	4.3×10^{-2}	1.2×10^{-1}	2.3×10^{-2}

Table B.1: Five benchmarks for i2HDM in $(M_{h_1}, M_{h_2}, M_{h_\pm}, \lambda_2, \lambda_{345})$ parameter space. We also present the corresponding relic density (Ω_{h^2}), the spin-independent cross section for DM scattering on the proton, and the LHC cross section at 13 TeV for mono-jet process $pp \to h_1, h_1 + jet$ for $p_T^{jet} > 100$ GeV cut.

C
Appendix: Presentation of experimental results for reinterpretation

We suggest the following to collider searches, when presenting results from the recommended benchmarks:

- Provide limits in collider language, on fundamental parameters of interaction: couplings and masses of particles in simplified model.

- Translate limits to non-collider language, for a range of assumptions in order to convey a rough idea of the range of possibilities. The details of this point are left for work beyond the scope of this Forum.

- Provide all necessary material for theorists to reinterpret simplified model results as building blocks for more complete models (e.g. signal cutflows, acceptances, etc). This point is detailed further in this appendix.

- As detailed in [KAM$^+$12], model-independent results in terms of limits on cross-section times acceptance of new phenomena should be provided for all cases, but especially when EFTs are employed as benchmarks.

Along with the design of new searches to hunt for new physics at the LHC, it is important to consider information needed in order to reinterpret the searches outside of the collaborations. The following is a non-exhaustive list of recommendations in order to make reinterpretation easier and faster. This appendix details considerations for reimplementation of the analysis as well as for using the simplified model results directly given by the collaborations.

One of the important developments in recent years is an active development of the analyses recasting codes [DFK$^+$15, CDFW14, KSTR15, CY11, KPSW]. The aim of these codes is to provide a public library of reimplemented and validated LHC analyses. Such libraries can then be used to analyze validity of a BSM scenario in a systematic and effective manner. The availability of public libraries further facilitates a unified framework and can lead to an organized and central structure to preserve LHC information in a long run.

In order to be able to develop such codes, it is important to get complete and systematic information from the collaborations.

- **Data digitization**: Availability of digitized data is one of the primary requirement. All information given by collaborations in the form of plots should be made available in a digitized format. Platforms such as HepData can be used in oder to maintain a centralized manner. In case when HepData can not be used, digitized data can be provided via analyses twiki pages. This information primarily includes expected and observed exclusion lines along with their $\pm 1\sigma$ uncertainty, expected and observed upper limits in case of simplified models, efficiency maps and all kinematic distributions as reported in the analysis. Units should be clearly specified. If the digitized figures are made available as a C macro or a ROOT file, the names of the objects should be clearly identifiable e.g. expected upper limits of a particular topology/model given as a ROOT file can be labeled as `KEY: TH2D ExpectedUpperLimit;1`. Furthermore, these digitized files can potentially contain more information (larger axes ranges) than displayed on the plot. This will help facilitate understand what happens beyond the limits displayed in the plot, e.g. a distribution for number of jets can be artificially limited to a point in the plot (for the purpose of clarity of figure) , however, this artificial limit leads to a sharp cutoff in the plot. While validating the analysis it is often necessary to compare the distributions beyond such artificial limits, having this information digitized will be of a great help in such cases.

C.1   Reimplementing analyses

This section lists information necessary in order to reimplement an analysis. Analysis reimplementation usually consists of several stages. Usually, one starts with reading the analysis note carefully, following which the preselection and event selection cuts are identified. These are then mimicked using a code typically written in C++. The detector simulation is carried out by using public detector simulation software e.g. Delphes [dF⁺14]. The resulting ROOT file is then analyzed using the C++ code written in the previous step.

- **Analysis documentation**: The collaborations should provide a cutflow table with every analysis, such a cutflow table will naturally define the order of cuts implemented in an analysis. There are several preselection criteria which can not be easily simulated in phenomenology, e.g. MET cleaning. Numbers should be provided after such cuts so that theorists can rescale their number of events in order to account for such cuts. Efficiencies of several reconstructed objects are given as an input to detector simulation software like Delphes. It is thus very useful to get parametrized efficiencies for reconstructed objects (as a function of the rapidity η and/or transverse momentum p_T), along with the working points at which they were evaluated (e.g. loose, tight selection). Object definitions should be clearly identifiable.

- **Validation**: Validation corresponds to re-deriving the results as given by collaborations in order to verify that the implementation of the analysis is correct. Usually most of the bug catching takes place in the phase of validation. The following items are necessary in order to recreate the results.

    - Monte Carlo generators: Monte Carlo generators along with the exact versions used to produce the event files should be listed.

    - Production cross sections: The order of production cross sections (e.g. LO,NLO,NLL) as well as the codes which were used to compute them should be provided. A table of reference cross sections for several values of particle masses such as ones provided by SUSY cross section working group will be highly appreciated.

    - Process Generation: Details of the generated process, detailing number of additional partons generated.

    - Availability of the LHE files: selected LHE files (detailing at least a few events if not the entire file) corresponding to the benchmarks listed in the analysis should be made available in order to cross check process generation. Experimental collaborations may generate events on-the-fly without saving the intermediate LHE file; we advocate that the cross-check of process generation is straight-forward if this information is present, so we encourage the generation of a few selected benchmark points allowing for a LHE file to be saved. For models concerning SUSY, corresponding SLHA files of benchmark files should also be details. Special attention should be paid to list the parameters which change the production cross section or kinematics of the process e.g. mixing angles.

    - Process cards: Process cards includes PDF choices, details of matching algorithms and scales and details of process generation. If process cards are not available, above items should be clearly identified.

    - model files: For models which are not already implemented in MAD-GRAPH5_aMC@NLO, availability of the corresponding model files in UFO format [DDF⁺12] is highly desired. It details the exact notation used in the model and hence sets up a complete framework. In case MAD-GRAPH5_aMC@NLO is not used, enough information should be provided in order to clearly identify the underlying model used for interpretations.

- **Limit setting**: Detailed description of the likelihood used in order to derive the limits should be given, this can contain statistical procedure within the analysis text itself, however direct availability of the limit setting code as a workspace in RooStats or HistFitter [BBC⁺15] is highly desirable.

- **Binned backgrounds**: For analyses using techniques such as sliding windows or an unbinned technique, the Standard Model backgrounds should be given in the form of bins. These backgrounds can then be interpolated.

- **Recast code**: Finally, the collaborations can provide an analysis code directly implemented in one of the public recasting codes detailed above. Such codes can be published via INSPIRE in order to track the versioning and citations.

C.2 *Simplified model interpretations*

The analyses almost always provide at least one simplified model interpreta-
tion along with the search results. These interpretations are simple and can be
used in order to take a quick survey of viability of parameter space. Codes such
as [KKL$^+$14b, KKL$^+$14a, PSWZ14] can make use of the simplified model results
given in the form of 95% Confidence Level (CLs) upper limit or efficiency maps in
order to test Beyond the Standard Model parameter space. It will thus be extremely
useful if the results are given in a form as easily usable by the theory community.

- **Direct usability of the results**: The results given should be as useful as possible.
  For example, for a simplified model containing dark matter mass m_{DM}, medi-
  ator mass M_{med} and couplings g_{DM}, g_{q} it will be extremely useful to have 95%
  CLs upper limits on the product of couplings $\sqrt{g_{\mathrm{DM}} g_{\mathrm{q}}}$ or cross section times
  branching ratio as a function of m_{DM}, M_{med}. Limits on visible cross sections of
  the simplified models considered for interpretations should be made available.

- **Smooth grids**: The usage of simplified model results relies on interpolating
  between upper limit values. In order to facilitate the interpolation, regions
  where large variation of upper limits is observed should contain denser grid, if a
  uniform grid over the entire plane is not possible. For simplified model involving
  more than three parameters (two masses and product of couplings), slices of
  upper limits in the additional dimensions will be very useful e.g. for a simplified
  model involving one step cascade decay, upper limits can be provided for several
  values of intermediate mass in the plane of mother - daughter masses. Results
  with only one slice often render invalid to be used in a general model testing.

- **Availability of acceptance and efficiency maps**: Finally, acceptance and effi-
  ciency maps for all the signal regions involved in the analysis should be made
  available. These results are not only useful for model testing using simplified
  models but also to validate implementation of the analysis. Information about the
  most sensitive signal region as a function of masses is also very useful in order
  to determine the validity of approximate limit setting procedures being used by
  theorists (in the absence of any other sophisticated limit setting technique).

D

Appendix: Additional details and studies within the Forum

D.1 Further information for baryonic Zprime Model

D.1.1 Cross-section scaling

The dependence of the cross section of the $pp \rightarrow H\chi\bar{\chi} + X$ process on $g_{hZ'Z'}$ is shown in Figure D.1. The curves have been fit to second-order polynomials, where y is the cross-section and x is the coupling $g_{hZ'Z'}$.

For $m_{med} = 100$ GeV, the fit function is

$$y = -0.12 - 3.4 \times 10^{-3}x + 2.7 \times 10^{-4}x^2$$

. For $m_{med} = 1$ TeV, the fit function is is

$$y = 0.0012 - 2.4 \times 10^{-7}x + 1.5 \times 10^{-7}x^2$$

,

$$y = -0.12 - 3.4 \times 10^{-3}x + 2.7 \times 10^{-4}x^2. \tag{D.1}$$

For $M_{med} = 1$ TeV, the fit function is is:

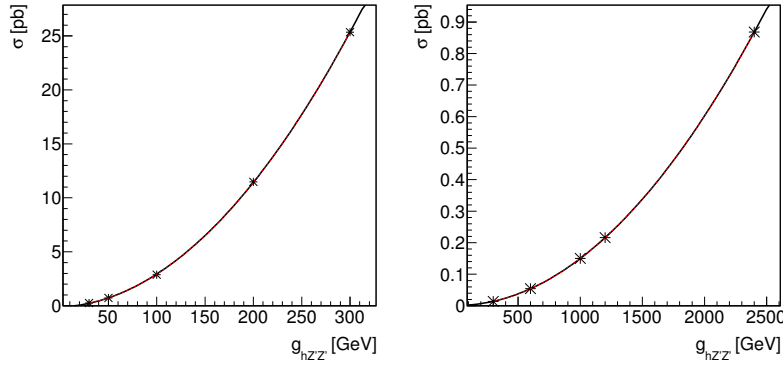$$y = 0.0012 - 2.4 \times 10^{-7}x + 1.5 \times 10^{-7}x^2. \tag{D.2}$$

Figure D.1: Cross section of the $pp \rightarrow H\chi\bar{\chi}$ process as a function of $g_{hZ'Z'}$ for $m_{Z'} = 100$ GeV (left) and $m_{Z'} = 1$ TeV (right). The fit functions are shown in the text.

Bibliography

[A+08]   J. Alwall et al. Comparative study of various algorithms for the merg-
         ing of parton showers and matrix elements in hadronic collisions.
         Eur.Phys.J., C53(2):473–500, 2008.

[A+12]   Daniele Alves et al. Simplified Models for LHC New Physics Searches.
         J.Phys., G39:105005, 2012.

[A+14a] Jalal Abdallah et al. Simplified Models for Dark Matter and Missing
         Energy Searches at the LHC. *arXiv:1409.2893*, 2014.

[A+14b] J. Alwall et al. The automated computation of tree-level and next-to-
         leading order differential cross sections, and their matching to parton
         shower simulations. *JHEP*, 07(2):079, 2014.

[A+15a] Georges Aad et al. Search for new phenomena in events with a photon
         and missing transverse momentum in pp collisions at $\sqrt{s} = 8$ TeV with
         the ATLAS detector. *Phys.Rev.*, D91(1):012008, 2015.

[A+15b] Georges Aad et al. Search for new phenomena in final states with an
         energetic jet and large missing transverse momentum in pp collisions at
         $\sqrt{s} = 8$ TeV with the ATLAS detector. 2015.

[AAB+14] Jean-Laurent Agram, Jeremy Andrea, Michael Buttignol, Eric Conte,
         and Benjamin Fuks. Monotop phenomenology at the Large Hadron
         Collider. *Phys.Rev.*, D89(1):014028, 2014.

[ABG14] Prateek Agrawal, Monika Blanke, and Katrin Gemmler. Flavored dark
         matter beyond Minimal Flavor Violation. *JHEP*, 1410:72, 2014.

[ABHL14] Prateek Agrawal, Brian Batell, Dan Hooper, and Tongyan Lin. Flavored
         Dark Matter and the Galactic Center Gamma-Ray Excess. *Phys.Rev.*,
         D90(6):063512, 2014.

[ADNP15] Chiara Arina, Eugenio Del Nobile, and Paolo Panci. Dark Matter with
         Pseudoscalar-Mediated Interactions Explains the DAMA Signal and the
         Galactic Center Excess. *Phys.Rev.Lett.*, 114:011301, 2015.

[AFM11] J. Andrea, B. Fuks, and F. Maltoni. Monotops at the LHC. *Phys.Rev.*,
         D84:074025, 2011.

[AHM+11] Johan Alwall, Michel Herquet, Fabio Maltoni, Olivier Mattelaer, and
         Tim Stelzer. MadGraph 5 : Going Beyond. *JHEP*, 1106:128, 2011.

[AHT08] Sarah Andreas, Thomas Hambye, and Michel H.G. Tytgat. WIMP dark
         matter, Higgs exchange and DAMA. *JCAP*, 0810:034, 2008.

[AHW13] Haipeng An, Ran Huo, and Lian-Tao Wang. Searching for Low Mass
         Dark Portal at the LHC. *Phys.Dark Univ.*, 2:50–57, 2013.

[AJW12] Haipeng An, Xiangdong Ji, and Lian-Tao Wang. Light Dark Matter and
         Z' Dark Force at Colliders. *JHEP*, 1207:182, 2012.

[AST09] Johan Alwall, Philip Schuster, and Natalia Toro. Simplified Models
         for a First Characterization of New Physics at the LHC. *Phys.Rev.*,
         D79:075020, 2009.

[ATL14] Sensitivity to WIMP Dark Matter in the Final States Containing Jets
         and Missing Transverse Momentum with the ATLAS Detector at 14 TeV
         LHC. Technical Report ATL-PHYS-PUB-2014-007, CERN, Geneva, Jun
         2014.

[ATL15] Search for a single-top quark produced in association with missing energy in proton-proton collisions at $\sqrt{s} = 8$ TeV with the ATLAS detector. *Eur. Phys. J. C*, 75:79, 2015.

[ATYY14] Abdesslam Arhrib, Yue-Lin Sming Tsai, Qiang Yuan, and Tzu-Chiang Yuan. An Updated Analysis of Inert Higgs Doublet Model in light of the Recent Results from LUX, PLANCK, AMS-02 and LHC. *JCAP*, 1406:030, 2014.

[AWZ14] Haipeng An, Lian-Tao Wang, and Hao Zhang. Dark matter with *t*-channel mediator: a simple step beyond contact interaction. *Phys.Rev.*, D89(11):115014, 2014.

[BB13] Yang Bai and Joshua Berger. Fermion Portal Dark Matter. *JHEP*, 1311:171, 2013.

[BB14] Yang Bai and Joshua Berger. Lepton Portal Dark Matter. *JHEP*, 1408:153, 2014.

[BBB+89] Dmitri Yu. Bardin, Mikhail S. Bilenky, W. Beenakker, Frits A. Berends, W.L. van Neerven, et al. Z LINE SHAPE. 1989.

[BBC+15] M. Baak, G.J. Besjes, D. CÃťte, A. Koutsman, J. Lorenz, et al. HistFitter software framework for statistical data analysis. *Eur.Phys.J.*, C75(4):153, 2015.

[BCD+15] Nicole F. Bell, Yi Cai, James B. Dent, Rebecca K. Leane, and Thomas J. Weiler. Dark matter at the LHC: EFTs and gauge invariance. 2015.

[BCDF15] Idir Boucheneb, Giacomo Cacciapaglia, Aldo Deandrea, and Benjamin Fuks. Revisiting monotop production at the LHC. *JHEP*, 1501:017, 2015.

[BCI+] A. Belyaev, G. Cacciapaglia, I. Ivanov, F. Rojas, and M. Thomas. page to appear.

[BDG+12] Nicole F. Bell, James B. Dent, Ahmad J. Galea, Thomas D. Jacques, Lawrence M. Krauss, et al. Searching for Dark Matter at the LHC with a Mono-Z. *Phys.Rev.*, D86:096011, 2012.

[BDM14] O. Buchmueller, Matthew J. Dolan, and Christopher McCabe. Beyond Effective Field Theory for Dark Matter Searches at the LHC. *JHEP*, 1401:025, 2014.

[BDMM15] Oliver Buchmueller, Matthew J. Dolan, Sarah A. Malik, and Christopher McCabe. Characterising dark matter searches at colliders and direct detection experiments: Vector mediators. *JHEP*, 1501:037, 2015.

[BDSG+14] Giorgio Busoni, Andrea De Simone, Johanna Gramling, Enrico Morgante, and Antonio Riotto. On the Validity of the Effective Field Theory for Dark Matter Searches at the LHC, Part II: Complete Analysis for the *s*-channel. *JCAP*, 1406:060, 2014.

[BDSJ+14] Giorgio Busoni, Andrea De Simone, Thomas Jacques, Enrico Morgante, and Antonio Riotto. On the Validity of the Effective Field Theory for Dark Matter Searches at the LHC Part III: Analysis for the *t*-channel. *JCAP*, 1409:022, 2014.

[BDSMR14] Giorgio Busoni, Andrea De Simone, Enrico Morgante, and Antonio Riotto. On the Validity of the Effective Field Theory for Dark Matter Searches at the LHC. *Phys.Lett.*, B728:412–421, 2014.

[BFG15] Matthew R. Buckley, David Feld, and Dorival Goncalves. Scalar Simplified Models for Dark Matter. *Phys.Rev.*, D91(1):015017, 2015.

[BFH10] Yang Bai, Patrick J. Fox, and Roni Harnik. The Tevatron at the Frontier of Dark Matter Direct Detection. *JHEP*, 1012:048, 2010.

[BGG+01] A.J. Buras, P. Gambino, M. Gorbahn, S. Jager, and L. Silvestrini. Universal unitarity triangle and physics beyond the standard model. *Phys.Lett.*, B500:161–167, 2001.

[BHK+10] Maria Beltran, Dan Hooper, Edward W. Kolb, Zosia A.C. Krusberg, and Tim M.P. Tait. Maverick dark matter at colliders. *JHEP*, 1009:037, 2010.

[BLW14]   Asher Berlin, Tongyan Lin, and Lian-Tao Wang. Mono-Higgs Detection of Dark Matter at the LHC. *JHEP*, 1406:078, 2014.

[BPtV01]   C.P. Burgess, Maxim Pospelov, and Tonnis ter Veldhuis. The Minimal model of nonbaryonic dark matter: A Singlet scalar. *Nucl.Phys.*, B619:709–728, 2001.

[BT13]   Yang Bai and Tim M.P. Tait. Searches with Mono-Leptons. *Phys.Lett.*, B723:384–387, 2013.

[C$^+$13]   Serguei Chatrchyan et al. Measurement of the cross section and angular correlations for associated production of a Z boson with b hadrons in pp collisions at $\sqrt{s}$ = 7 TeV. *JHEP*, 1312:039, 2013.

[C$^+$14]   Serguei Chatrchyan et al. Measurement of the production cross sections for a Z boson and one or more b jets in pp collisions at sqrt(s) = 7 TeV. *JHEP*, 1406:120, 2014.

[CCW15]   Francesca Calore, Ilias Cholis, and Christoph Weniger. Background model systematics for the Fermi GeV excess. *JCAP*, 1503:038, 2015.

[CDFW14]   Eric Conte, BÃľranger Dumont, Benjamin Fuks, and Chris Wymant. Designing and recasting LHC analyses with MadAnalysis 5. *Eur.Phys.J.*, C74(10):3103, 2014.

[CDM$^+$14]   Linda Carpenter, Anthony DiFranzo, Michael Mulhearn, Chase Shimmin, Sean Tulin, et al. Mono-Higgs-boson: A new collider probe of dark matter. *Phys.Rev.*, D89(7):075017, 2014.

[CEHL14]   Spencer Chang, Ralph Edezhath, Jeffrey Hutchinson, and Markus Luty. Effective WIMPs. *Phys.Rev.*, D89(1):015011, 2014.

[CEMW04]   John M. Campbell, R. Keith Ellis, F. Maltoni, and S. Willenbrock. Associated production of a Z Boson and a single heavy quark jet. *Phys.Rev.*, D69:074021, 2004.

[CEMW06]   John M. Campbell, R. Keith Ellis, F. Maltoni, and S. Willenbrock. Production of a Z boson and two jets with one heavy-quark tag. *Phys.Rev.*, D73:054007, 2006.

[CG87]   R. Sekhar Chivukula and Howard Georgi. Composite Technicolor Standard Model. *Phys.Lett.*, B188:99, 1987.

[CGT13]   Nathaniel Craig, Jamison Galloway, and Scott Thomas. Searching for Signs of the Second Higgs Doublet. 2013.

[CHH15]   Andreas Crivellin, Ulrich Haisch, and Anthony Hibbs. LHC constraints on gauge boson couplings to dark matter. 2015.

[CHLR13]   R.C. Cotta, J.L. Hewett, M.P. Le, and T.G. Rizzo. Bounds on Dark Matter Interactions with Electroweak Gauge Bosons. *Phys.Rev.*, D88:116009, 2013.

[CMS14]   Search for new physics with monotop final states in pp collisions at $\sqrt{s}$ = 8 TeV. 2014.

[CNS$^+$13]   Linda M. Carpenter, Andrew Nelson, Chase Shimmin, Tim M.P. Tait, and Daniel Whiteson. Collider searches for dark matter in events with a Z boson and missing energy. *Phys.Rev.*, D87(7):074005, 2013.

[Col15]   CMS Collaboration. Search for H/A decaying into Z+A/H, with Z to ll and A/H to fermion pair. 2015.

[CY11]   Kyle Cranmer and Itay Yavin. RECAST: Extending the Impact of Existing Analyses. *JHEP*, 1104:038, 2011.

[DDF$^+$12]   Celine Degrande, Claude Duhr, Benjamin Fuks, David Grellscheid, Olivier Mattelaer, et al. UFO - The Universal FeynRules Output. *Comput.Phys.Commun.*, 183:1201–1214, 2012.

[dF$^+$14]   J. de Favereau et al. DELPHES 3, A modular framework for fast simulation of a generic collider experiment. *JHEP*, 1402:057, 2014.

[DFH+14] Tansu Daylan, Douglas P. Finkbeiner, Dan Hooper, Tim Linden, Stephen K. N. Portillo, et al. The Characterization of the Gamma-Ray Signal from the Central Milky Way: A Compelling Case for Annihilating Dark Matter. 2014.

[DFK+15] B. Dumont, B. Fuks, S. Kraml, S. Bein, G. Chalons, et al. Toward a public analysis database for LHC new physics searches using MAD-ANALYSIS 5. *Eur.Phys.J.*, C75(2):56, 2015.

[DFMQ13] Abdelhak Djouadi, Adam Falkowski, Yann Mambrini, and Jeremie Quevillon. Direct Detection of Higgs-Portal Dark Matter at the LHC. *Eur.Phys.J.*, C73(6):2455, 2013.

[DGIS02] G. D'Ambrosio, G.F. Giudice, G. Isidori, and A. Strumia. Minimal flavor violation: An Effective field theory approach. *Nucl.Phys.*, B645:155–187, 2002.

[DM78] Nilendra G. Deshpande and Ernest Ma. Pattern of Symmetry Breaking with Two Higgs Doublets. *Phys.Rev.*, D18:2574, 1978.

[DNRT13] Anthony DiFranzo, Keiko I. Nagao, Arvind Rajaraman, and Tim M. P. Tait. Simplified Models for Dark Matter Interacting With Quarks. *JHEP*, 1311, 2013.

[DS09] Ethan M. Dolle and Shufang Su. The Inert Dark Matter. *Phys.Rev.*, D80:055012, 2009.

[FHKT11] Patrick J. Fox, Roni Harnik, Joachim Kopp, and Yuhsin Tsai. LEP Shines Light on Dark Matter. *Phys.Rev.*, D84:014028, 2011.

[FHKT12] Patrick J. Fox, Roni Harnik, Joachim Kopp, and Yuhsin Tsai. Missing Energy Signatures of Dark Matter at the LHC. *Phys.Rev.*, D85:056011, 2012.

[For15a] SVN repository for Madgraph input cards for model with s-channel exchange of vector mediator, for electroweak boson final states. https://svnweb.cern.ch/cern/wsvn/LHCDMF/trunk/models/EW_DMV/, 2015. [Online; accessed 15-May-2015].

[For15b] SVN repository for Madgraph inputs for 2HDM model leading to a mono-Higgs signature. https://svnweb.cern.ch/cern/wsvn/LHCDMF/trunk/models/EW_Higgs_2HDM/, 2015. [Online; accessed 12-May-2015].

[For15c] SVN repository for Madgraph inputs for dimension-7 EFT models with direct DM-EW boson couplings. https://svnweb.cern.ch/cern/wsvn/LHCDMF/trunk/models/EW_Fermion_D7/contributed_by_Renjie_Wang/, 2015. [Online; accessed 24-April-2015].

[For15d] SVN repository for Madgraph inputs for model with s-channel exchange of pseudo-scalar mediator, produced in association with top quarks. https://svnweb.cern.ch/cern/wsvn/LHCDMF/trunk/models/HF_S%2BPS/, 2015. [Online; accessed 24-April-2015].

[For15e] SVN repository for Madgraph inputs for mono-top models. https://svnweb.cern.ch/cern/wsvn/LHCDMF/trunk/models/HF_SingleTop/, 2015. [Online; accessed 27-April-2015].

[For15f] SVN repository for Madgraph inputs for simplified model with a colored scalar mediator coupling to DM and b-quarks. https://svnweb.cern.ch/cern/wsvn/LHCDMF/trunk/models/HF_S%2BPS/, 2015. [Online; accessed 24-April-2015].

[For15g] SVN repository for Madgraph inputs for vector and scalar mediator models leading to a mono-Higgs signature. https://svnweb.cern.ch/cern/wsvn/LHCDMF/trunk/models/EW_Higgs_all/, 2015. [Online; accessed 24-April-2015].

[For15h] SVN repository for POWHEG input card for model with s-channel exchange of axial vector mediator. https://svnweb.cern.ch/cern/wsvn/LHCDMF/trunk/models/Monojet_DMA/, 2015. [Online; accessed 24-April-2015].

[For15i] SVN repository for POWHEG input card for model with s-channel
exchange of pseudo-scalar mediator, production through top loop from
gluon-gluon initial state. https://svnweb.cern.ch/cern/wsvn/LHCDMF/
trunk/models/Monojet_DMGG/, 2015. [Online; accessed 24-April-2015].

[For15j] SVN repository for POWHEG input card for model with s-channel
exchange of scalar mediator. https://svnweb.cern.ch/cern/wsvn/
LHCDMF/trunk/models/Monojet_DMS/, 2015. [Online; accessed 24-April-
2015].

[For15k] SVN repository for POWHEG input card for model with s-channel
exchange of scalar mediator, with gluon loop. https://svnweb.cern.
ch/cern/wsvn/LHCDMF/trunk/models/Monojet_DMGG/, 2015. [Online;
accessed 24-April-2015].

[FST06] Jonathan L. Feng, Shufang Su, and Fumihiro Takayama. Lower limit
on dark matter production at the large hadron collider. *Phys.Rev.Lett.*,
96:151802, 2006.

[FW13] Patrick J. Fox and Ciaran Williams. Next-to-Leading Order Predic-
tions for Dark Matter Production at Hadron Colliders. *Phys.Rev.*,
D87(5):054030, 2013.

[GHS13] A. Goudelis, B. Herrmann, and O. StÃĕl. Dark matter in the Inert
Doublet Model after the discovery of a Higgs-like boson at the LHC.
JHEP, 1309:106, 2013.

[GIR+10] Jessica Goodman, Masahiro Ibe, Arvind Rajaraman, William Shep-
herd, Tim M.P. Tait, et al. Constraints on Dark Matter from Colliders.
Phys.Rev., D82:116010, 2010.

[GIR+11] Jessica Goodman, Masahiro Ibe, Arvind Rajaraman, William Shepherd,
Tim M.P. Tait, et al. Constraints on Light Majorana dark Matter from
Colliders. *Phys.Lett.*, B695:185–188, 2011.

[GS11] Jessica Goodman and William Shepherd. LHC Bounds on UV-Complete
Models of Dark Matter. 2011.

[HHR14] Ulrich Haisch, Anthony Hibbs, and Emanuele Re. Determin-
ing the structure of dark-matter couplings at the LHC. *Phys.Rev.*,
D89(3):034009, 2014.

[HKR13] Ulrich Haisch, Felix Kahlhoefer, and Emanuele Re. QCD effects in
mono-jet searches for dark matter. *JHEP*, 1312:007, 2013.

[HKSW15] Philip Harris, Valentin V. Khoze, Michael Spannowsky, and Ciaran
Williams. Constraining Dark Sectors at Colliders: Beyond the Effective
Theory Approach. *Phys.Rev.*, D91(5):055009, 2015.

[HKU13] Ulrich Haisch, Felix Kahlhoefer, and James Unwin. The impact of
heavy-quark loops on LHC dark matter searches. *JHEP*, 1307:125, 2013.

[HR90] L.J. Hall and Lisa Randall. Weak scale effective supersymmetry.
Phys.Rev.Lett., 65:2939–2942, 1990.

[HR15] Ulrich Haisch and Emanuele Re. Simplified dark matter top-quark
interactions at the LHC. 2015.

[K+15] V. Khachatryan et al. Search for Monotop Signatures in Proton-Proton
Collisions at $\sqrt{s}$ = 8 TeV. *Phys.Rev.Lett.*, 114(10):101801, 2015.

[KAM+12] S. Kraml, B.C. Allanach, M. Mangano, H.B. Prosper, S. Sekmen, et al.
Searches for New Physics: Les Houches Recommendations for the
Presentation of LHC Results. *Eur.Phys.J.*, C72:1976, 2012.

[KKL+14a] Sabine Kraml, Suchita Kulkarni, Ursula Laa, Andre Lessa, Veronika
Magerl, et al. SModelS v1.0: a short user guide. 2014.

[KKL+14b] Sabine Kraml, Suchita Kulkarni, Ursula Laa, Andre Lessa, Wolfgang
Magerl, Doris Proschofsky, and Wolfgang Waltenberger. SModelS: a
tool for interpreting simplified-model results from the LHC and its
application to supersymmetry. *Eur.Phys.J.*, C74:2868, 2014.

2760   [Kop11]   Joachim Kopp. Collider Limits on Dark Matter. 2011.

2761   [KPSW]   I.-W. Kim, M. Papucci, K. Sakurai, and A. Weiler. ATOM: Automated
2762   Testing Of Models. *to appear*.

2763   [KSTR15] Jong Soo Kim, Daniel Schmeier, Jamie Tattersall, and Krzysztof Rol-
2764   biecki. A framework to create customised LHC analyses within Check-
2765   MATE. 2015.

2766   [LHNOT07] Laura Lopez Honorez, Emmanuel Nezri, Josep F. Oliver, and
2767   Michel H.G. Tytgat. The Inert Doublet Model: An Archetype for
2768   Dark Matter. *JCAP*, 0702:028, 2007.

2769   [LKW13]   Tongyan Lin, Edward W. Kolb, and Lian-Tao Wang. Probing dark
2770   matter couplings to top and bottom quarks at the LHC. *Phys.Rev.*,
2771   D88(6):063510, 2013.

2772   [LPS14]   Hyun Min Lee, Myeonghun Park, and Veronica Sanz. Gravity-mediated
2773   (or Composite) Dark Matter. *Eur.Phys.J.*, C74:2715, 2014.

2774   [LSWY13] Jia Liu, Brian Shuve, Neal Weiner, and Itay Yavin. Looking for new
2775   charged states at the LHC: Signatures of Magnetic and Rayleigh Dark
2776   Matter. *JHEP*, 1307:144, 2013.

2777   [MMA+14] Sarah Malik, Christopher McCabe, Henrique Araujo, A. Belyaev, Celine
2778   Boehm, et al. Interplay and Characterization of Dark Matter Searches at
2779   Colliders and in Direct Detection Experiments. 2014.

2780   [MMPT07] Michelangelo L. Mangano, Mauro Moretti, Fulvio Piccinini, and
2781   Michele Treccani. Matching matrix elements and shower evolution
2782   for top-quark production in hadronic collisions. *JHEP*, 0701:013, 2007.

2783   [MMW05]   Fabio Maltoni, Thomas McElmurry, and Scott Willenbrock. Inclusive
2784   production of a Higgs or Z boson in association with heavy quarks.
2785   *Phys.Rev.*, D72:074024, 2005.

2786   [NCC+14] Andy Nelson, Linda M. Carpenter, Randel Cotta, Adam Johnstone,
2787   and Daniel Whiteson. Confronting the Fermi Line with LHC data: an
2788   Effective Theory of Dark Matter Interaction with Photons. *Phys.Rev.*,
2789   D89(5):056011, 2014.

2790   [par]   DM@LHC participants. Dm@lhc 2014 proceedings. To appear.

2791   [PS14]   Alexey A. Petrov and William Shepherd. Searching for dark matter at
2792   LHC with Mono-Higgs production. *Phys.Lett.*, B730:178–183, 2014.

2793   [PSWZ14] Michele Papucci, Kazuki Sakurai, Andreas Weiler, and Lisa Zeune.
2794   Fastlim: a fast LHC limit calculator. *Eur.Phys.J.*, C74(11):3163, 2014.

2795   [PVZ14]   Michele Papucci, Alessandro Vichi, and Kathryn M. Zurek. Monojet
2796   versus the rest of the world I: t-channel models. *JHEP*, 1411:024, 2014.

2797   [RWZ15]   Davide Racco, Andrea Wulzer, and Fabio Zwirner. Robust collider
2798   limits on heavy-mediator Dark Matter. 2015.

2799   [SMS06]   Torbjorn Sjostrand, Stephen Mrenna, and Peter Z. Skands. PYTHIA 6.4
2800   Physics and Manual. *JHEP*, 0605:026, 2006.

2801   [SV12]   Ian M. Shoemaker and Luca Vecchi. Unitarity and Monojet Bounds on
2802   Models for DAMA, CoGeNT, and CRESST-II. *Phys.Rev.*, D86:015023,
2803   2012.

2804   [WBG05]   M.R. Whalley, D. Bourilkov, and R.C. Group. The Les Houches accord
2805   PDFs (LHAPDF) and LHAGLUE. 2005.

2806   [WY12]   Neal Weiner and Itay Yavin. How Dark Are Majorana WIMPs? Signals
2807   from MiDM and Rayleigh Dark Matter. *Phys.Rev.*, D86:075021, 2012.

2808   [WY13]   Neal Weiner and Itay Yavin. UV completions of magnetic inelastic and
2809   Rayleigh dark matter for the Fermi Line(s). *Phys.Rev.*, D87(2):023523,
2810   2013.

2811   [ZBW13]   Ning Zhou, David Berge, and Daniel Whiteson. Mono-everything:
2812   combined limits on dark matter production at colliders from multiple
2813   final states. *Phys.Rev.*, D87(9):095013, 2013.